Emergent stability in complex network dynamics

Chandrakala Meena,[1−4,*] Chittaranjan Hens,[5,6] Suman Acharyya,[1,2] Simcha Haber,[1]

Stefano Boccaletti[7−9] & Baruch Barzel[1,2,10,*]

1. Department of Mathematics, Bar-Ilan University, Ramat-Gan, Israel

2. Gonda Multidisciplinary Brain Research Center, Bar-Ilan University, Ramat-Gan, Israel

3. Chemical Engineering and Process Development, CSIR-National Chemical Laboratory, Pune, India

4. Indian Institute of Science Education and Research, Thiruvananthapuram, Maruthamala P. O, Vithura, Kerala 695551

5. Physics and Applied Mathematics Unit, Indian Statistical Institute, Kolkata, India

6. Center for Computational Natural Sciences and Bioinformatics, International Institute of Information Technology, Gachibowli, Hyderabad-500032, Telangana, India

7. CNR - Institute of Complex Systems, Florence, Italy

8. Moscow Institute of Physics and Technology (National Research University), Moscow, Russian Federation

9. Universidad Rey Juan Carlos, calle Tulipán s/n, 28933 Móstoles, Madrid, Spain

10. Network Science Institute, Northeastern University, Boston, MA., USA

 * **Correspondence**. C. Meena: meenachandrakala@gmail.com; B. Barzel: baruchbarzel@gmail.com

In memory of Prof. Robert May

The stable functionality of networked systems is a hallmark of their natural ability to coordinate between their multiple interacting components. Yet, real world networks often appear random and highly irregular, raising the question of what are the naturally emerging organizing principles of complex system stability. The answer is encoded within the system's stability matrix — the Jacobian — but is hard to retrieve, due to the scale and diversity of the relevant systems, their broad parameter space, and their nonlinear interaction dynamics. Here, we introduce the dynamic Jacobian ensemble, which allows us to systematically investigate the fixed-point dynamics of a range of relevant network-based models. Within this ensemble, we find that complex systems exhibit discrete stability classes. These range from asymptotically unstable, where stability is unattainable, to sensitive, in which stability abides within a bounded range of the system's parameters. Alongside these two classes, we uncover a third asymptotically stable class, in which a sufficiently large and heterogeneous network acquires a guaranteed stability, independent of its microscopic parameters and of external perturbation. Hence, in this ensemble, two of the most ubiquitous characteristics of real-world networks - scale and heterogeneity - emerge as natural organizing principles to ensure fixed-point stability in the face of changing environmental conditions.

The study of complex systems is often directed towards dramatic events, such as cascading failures[1−5] or abrupt state transitions.[2,4,6,8,10] In reality, however, these represent the exception rather than the rule. In fact, the truly intriguing phenomenon is that, despite enduring constant perturbations and local obstructions, many systems continue to sustain reliably stable dynamics.[7,11,12,14] This is achieved in the absence of a detailed design, as indeed, the dynamics of the majority of complex systems are mediated by random, often extremely heterogeneous, networks, comprising a large number of interacting components, and driven by a vast space of microscopic parameters. What then are the roots of this observed stability?

1

The answer lies in the system's linear stability matrix, namely its Jacobian J, whose principal eigenvalue λ determines its response to perturbation.[15,16] According to linear stability theory, perturbations may either grow exponentially ($\text{Re}(\lambda) > 0$), capturing instability, or decay exponentially ($\text{Re}(\lambda) < 0$), if the system is stable. The challenge is that the structure of J remains elusive, given the scale, diversity and multiple parameters characterizing real-world complex systems.

To address this we derive the *dynamic Jacobian ensemble*, showing that for a rather broad class of dynamics, stability is determined by a small set of analytically accessible parameters. We further show that this ensemble predicts an emergent stability, asymptoticaly robust in the thermodynamic limit ($N \to \infty$). Therefore, it offers precisely, the desired natural design principles to ensure complex system stability.[17–19]

Results

Fixes-point dynamics. Consider a complex system of N interacting components (nodes), whose dynamic activities $\mathbf{x}(t) = (x_1(t), \ldots, x_N(t))^\top$ are driven by pairwise interactions, potentially nonlinear. The system's fixed-points $\mathbf{x}_\alpha$ capture static states, which, unperturbed, remain independent of time. The dynamics in the vicinity of these fixed-point can be examined through the system's response to small perturbations $\delta\mathbf{x}(t)$, which, in the linear regime, can be approximated by

$$\frac{\mathrm{d}\delta\mathbf{x}}{\mathrm{d}t} = J\delta\mathbf{x} + O(\delta\mathbf{x}^2). \tag{1}$$

Here J, an $N \times N$ matrix, represents the system's Jacobian around $\mathbf{x}_\alpha$, which approximates, through a set of linear equations, the original nonlinear system's dynamics in the perturbative limit, *i.e.* small activity changes $\mathbf{x}(t) = \mathbf{x}_\alpha + \delta\mathbf{x}(t)$. Hence, J's spectral properties, and specifically its principal eigenvalue λ, are crucial for characterizing the system's fixed-point behavior.

Two factors shape J - the system's topology, *i.e.* who interacts with whom, and its internal dynamics, namely what is the nature of these interactions:

Topology. The first ingredient that impacts the structure of J is the network topology A, a binary matrix ($A_{ij} \in (0,1)$, $A_{ii} = 0$), typically sparse and often highly heterogeneous.[3] Designed to capture the linear response between i and j, J's off-diagonal terms vanish if there is no direct i,j link, *i.e.* $A_{ij} = 0 \iff J_{ij} = 0$ for all $i \neq j$. If, however $A_{ij} = 1$, then the relevant term is assigned a *weight* W_{ij} that captures the strength of the i,j linear dependence. Together, this leads to

$$J = (A - I) \circ W, \tag{2}$$

where the Hadamard product $\circ$ represents matrix multiplication element by element, and I is the $N \times N$ identity matrix. In (2) the network structure (A) determines the non-vanishing terms in J, and W determined their weights. The diagonal entries J_{ii} are introduced through the second term, $I \circ W$, where W_{ii} quantifies $x_i(t)$'s self-linear dependence.

Dynamics - the random matrix paradigm. To complete the construction of (2) we must assign all weights W. In many of the traditional analyses these unknown weights are extracted from two pre-selected probability densities, $P_0(w)$ and $P_1(w)$, for the diagonal and off-diagonal terms, respectively. This gives rise to the Jacobian ensemble $\mathbb{E}(A, P_0, P_1)$, in which one first sets

the topology A, then extracts weights from $P_0(w)$ and $P_1(w)$; Fig. 1a-c.

As a classic example for this ensemble, we consider May's[8] construction, in which A is an Erdős-Rényi (ER) network, the off-diagonal weights follow $W_{ij} \sim \mathcal{N}(0, \sigma^2)$, a zero-mean normal distribution, and the diagonal entries are taken uniformly as $W_{ii} = 1$. Hence, the interaction strengths are potentially random, but the self-dynamics are driven by the system's intrinsic relaxation timescales, here normalized to unity. In Methods Section 1 we discuss more detailed constructions, that later built on this random matrix paradigm.

The $\mathbb{E}(A, P_0, P_1)$ ensemble, described above, has two crucial shortcomings: (i) it provides no explicit guidelines on how to connect $P_0(w)$ and $P_1(w)$ with the system's specific nonlinear interactions; (ii) by assigning A and W independently, it ignores the potential interplay between the network structure and J's dynamic weights. This stands in sharp contrast with the frequently observed fact that similar networks potentially exhbit profoundly distinct response patterns.[22–24] How then do we appropriately assign the wights W in (2) to capture this interplay between structure and dynamics?

The dynamic Jacobian ensemble

To construct predictive J matrices we consider each system's specific interaction mechanisms. For example, in epidemic dynamics, individuals interact through infection and recovery,[9,26,27] in biological networks, proteins, genes and metabolites are linked through biochemical processes[11,12,29,31] and in population dynamics, species undergo competitive or symbiotic exchanges.[13,15,33,35] Quite generally, these dynamic mechanisms can be represented by

$$\frac{\mathrm{d}x_i}{\mathrm{d}t} = M_0\big(x_i(t), \mathbf{f}_{0i}\big) + g \sum_{j=1}^{N} A_{ij} M_1\big(x_i(t), \mathbf{f}_{1i}\big) G_{ij} M_2\big(x_j(t), \mathbf{f}_{2j}\big), \tag{3}$$

a dynamic framework recently introduced by Barzel and Barabási.[22] Here $M_0(x_i, \mathbf{f}_{0i})$ captures the self-dynamics of all nodes, and the product function $M_1(x_i, \mathbf{f}_{1i}) \times M_2(x_j, \mathbf{f}_{2j})$ describes the i, j pairwise interaction. Each of these functions, $M_q(x, \mathbf{f}_{qi})$, $q = 0, 1, 2$, is characterized by a set of parameters $\mathbf{f}_{qi}$, or - collectively $\mathbf{f}$, capturing rate constants, that may be potentially distributed across the system's components. Hence, the functional form of $M_q(x)$ is uniform throughout the network, yet the specific rates and coefficients $\mathbf{f}$ are node/link specific. In a similar fashion, the global interaction rate g increases/decreases the strength of *all* interactions, while the specific i, j interaction strength is governed by the potentially diverse weight matrix G_{ij}. Together, (2.1) provides a generic template, allowing, by appropriately selecting $M_q(x)$, to cover a range of frequently used models in social,[9,26] biological[11–13,29,31] and technological[36] systems (Fig. 2; see Methods Section 4 and Supplementary Section 1 for an expanded discussion of Eq. (2.1)).

Dynamic Jacobians (Fig. 1h). To obtain J we relinquish the random matrix construction $\mathbb{E}(A, P_0, P_1)$, and extract the Jacobian directly from Eq. (2.1). In Supplementary Section 2, we show that this leads to a currently unexplored matrix ensemble, in which the Jacobian weights W in (2) are strongly intertwined with the weighted topology A, G via

$$W_{ii} \sim C(\mathbf{f}, g) d_{\mathrm{nn}}^{\eta} d_i^{\mu} \tag{4}$$

for the diagonal weights $J_{ii} = -W_{ii}$, and

$$W_{ij} \sim d_i^{\nu} G_{ij} d_j^{\rho} \tag{5}$$

for the off-diagonal weights $J_{ij} = A_{ij} W_{ij}$ $(i \neq j)$. In (4) and (2.4) $d_i = \sum_{j=1}^{N} A_{ij} G_{ij}$ represents the weighted degree of node i, and

$$d_{\mathrm{nn}} = \frac{1}{N} \sum_{i=1}^{N} \frac{1}{d_i} \sum_{j=1}^{N} A_{ij} G_{ij} d_j \tag{6}$$

represents the average weighted degree of a nearest neighbor node.[2] Together these two parameters, d_i and d_{nn}, capture the role of the weighted network topology (Fig. 1g). The four exponents, $\Omega = (\eta, \mu, \nu, \rho)$ are determined by the dynamics, *i.e.* the functions $M_q(x)$, hence capturing the role of the system's internal driving mechanisms (Fig. 1e). In case of multiple fixed-points, we have Ω_1, Ω_2 etc., a potentially distinct exponent set per each fixed-point. The analytical extraction of Ω from $M_q(x)$ is summarized in Methods Sections 2,3. Finally, the coefficient $C(\mathbf{f}, g) > 0$ is governed by the rate constants $\mathbf{f}$ and g in (2.1), which do not play a role in the scaling exponents Ω (Fig. 1f).

The resulting dynamic Jacobian in (4) and (2.4), our first key result, is fundamentally distinct from the existing random matrix based constructions. On the one hand, the network structure A continues to determine the non-zero entries, similar to the classic ensemble $\mathbb{E}(A, P_0, P_1)$. Also, the typical magnitude of the diagonal entries depends on the system's rates parameters through $C(\mathbf{f}, g)$, once again, analogous, albeit not identical, to the selection of $P_0(w)$ in the existing ensemble. However, the similarity ends there, as (4) and (2.4), in contrast to $\mathbb{E}(A, P_0, P_1)$, also capture the role of the system's nonlinearity. Specifically, they predict emergent patterns in the structure of J, that are rooted in the interplay between topology and dynamics: the degrees $d_{\mathrm{nn}}, d_i, d_j$ are extracted from the weighted network topology $A \circ G$ (Fig. 1g), while the scaling exponents Ω are derived from the dynamic functions $M_q(x)$ (Fig. 1e).

Therefore, we arrive at a new Jacobian ensemble $\mathbb{E}(A, G, \Omega)$, which, unlike the random $\mathbb{E}(A, P_0, P_1)$, accounts for the effect of the system-specific nonlinear interaction dynamics. Consequently, in $\mathbb{E}(A, G, \Omega)$, identical networks may give rise to highly distinctive Jacobian matrices, depending on whether the interactions are, *e.g.*, social, biological or ecological, or even on the specific fixed-point within each type of interaction. This is thanks to the unique set of exponents Ω, characterizing each of these systems/states (Fig. 1h).

Testing $\mathbb{E}(A, G, \Omega)$. To examine predictions (4) and (2.4) we constructed a broad testing ground, including seven relevant dynamic models from different domains: Epidemic - the SIS model[9,26,27] for disease spreading; Regulatory - the Michaelis-Menten model[11] for gene regulation; Inhibitory - growth suppression in pathogen-host interactions;[15] Biochemical - protein-protein interactions[12,29,31] in sub-cellular networks; Population $1, 2$ - two models of mutualistic[13] interactions in population dynamics; and finally, Power - load distribution in electric transmission networks. Applying each of these dynamics to five different model and relevant empirical networks, we arrive at a total of 35 combinations of networks/dynamics, upon which we test our predicted J-ensemble (a detailed description of all models/networks appears in Supplementary Sections 4 and 7; additional dynamics appear in Supplementary Section 5).

In Fig. 2 we present, for each system, its dynamic equation (blue), and the list of relevant networks upon which it was tested (violet). In some cases the system features several fixed-

points, for example, Epidemic (Fig. 2a) exhibits a healthy state (inactive $\mathbf{x}_0$) and a pandemic state (active $\mathbf{x}_1$). These states are presented using a 3D visualization. The network is laid out on the x, y plane, and the activities x_i of all nodes are captured by the vertical z-axis displacement. Hence under $\mathbf{x}_0$ all nodes remain on the x, y plane ($z = 0$), while in the active state $\mathbf{x}_1$ they all have $x_i > 0$. Finally, we display our predicted dynamic exponents $\Omega = (\eta, \mu, \nu, \rho)$ for each system around its active state (orange); see Supplementary Section 4, where we also derive Ω for the inactive states.

Perturbing the system around its active fixed-point, we constructed the Jacobian matrix J for each of our 35 systems (Supplementary Section 7.2). In Fig. 3 we find that, indeed, the diagonal (W_{ii}) and off-diagonal (W_{ij}) weights of our numerically obtained J (blue symbols) follow the predicted scaling of (4) and (2.4) (orange solid lines). For example, in Epidemic we predict $\mu = 1$, while for Regulatory we have $\mu = 0$, both scaling relationships clearly evident in Fig. 3b,d. This means that extracting all diagonal terms independently from $P_0(w)$, as in $\mathbb{E}(A, P_0, P_1)$, misses the distinct patterns that arise from the nonlinear Epidemic/Regulatory dynamics. Similarly, the off-diagonal terms are proportional to $d_i^{-1} G_{ij} d_j^0$ in Epidemic (Fig. 3c) and $d_i^0 G_{ij} d_j^{-2}$ in Regulatory (Fig. 3e) - once again, in striking agreement with our theoretical predictions (orange solid lines). And yet, in stark contrast with the random construction $\mathbb{E}(A, P_0, P_1)$, where W_{ij} are extracted blindly from $P_1(w)$.

Our analysis further predicts that Ω depends only on $M_q(x)$, thus independent of network structure A, weights G, or coefficients $\mathbf{f}$ and g. We examine this in Fig. 3, by testing each of our dynamics on a diverse set of networks, with different degree/weight distributions. As predicted, we find that η, μ, ν and ρ are, indeed, universal, conserved across our diverse model (Erdős-Rényi, Scale-free 1, Scale-free 2) and relevant empirical (Social 1,2, PPI 1,2, etc.) networks. Hence, Ω captures the intrinsic, and most crucially, hitherto overlooked, contribution of the nonlinear dynamics to the structure of J.

Together, our derivation demonstrates that: (i) Actual J are fundamentally distinct from the commonly used random ensembles; (ii) Contrary to these ensembles, they feature non-random scaling patterns in which topology ($d_{\mathrm{nn}}, d_i, d_j$) and dynamics ($\Omega$) are deeply intertwined; (iii) These patterns can be analytically traced to the system's dynamics $M_q(x)$ through Eqs. (4) and (2.4), giving rise to our new *dynamic Jacobian ensemble* $\mathbb{E}(A, G, \Omega)$. Next, we use $\mathbb{E}(A, G, \Omega)$ to derive the conditions for Eq. (2.1)'s dynamic stability.

Dynamic stability

The dynamic stability around a given fixed-point is governed by J's principal eigenvalue λ, requiring that $\mathrm{Re}(\lambda) < 0$. To obtain λ, let us first focus on the role of the network topology A, G. The ingredients of $J \in \mathbb{E}(A, G, \Omega)$, as expressed in Eqs. (4) and (2.4), suggest that λ is strongly linked to the network's weighted degree density function $P(d)$. This is indicated directly through the dependence on d_i and d_j, but also indirectly through the nearest neighbor degree d_{nn}, whose magnitude depends on the system's degree-heterogeneity.[1] For instance, in a randomly wired network we have $d_{\mathrm{nn}} = \langle d^2 \rangle / \langle d \rangle$,[2,38] in which the second moment $\langle d^2 \rangle$ increases with $P(d)$'s variance, and consequently with A, G's heterogeneity. In case $P(d)$ is fat-tailed, we have[1]

$$d_{\mathrm{nn}} \sim N^{\beta}, \tag{7}$$

an asymptotic divergence with system size. Hence, β helps characterize the network's degree-heterogeneity, being $\beta = 0$ for homogeneous networks, in which $P(d)$ is concentrated around its mean, and $\beta > 0$ for heterogeneous A, G, where the variance is unbounded.

The remaining ingredients in (4) and (2.4) that may impact λ are $\Omega = (\eta, \mu, \nu, \rho)$ and $C(\mathbf{f}, g)$. Combining all three contributions together, we show in Supplementary Section 3 that in $\mathbb{E}(A, G, \Omega)$, the principal eigenvalue asymptotically follows

$$\mathrm{Re}(\lambda) \sim N^Q \left(1 - \frac{C(\mathbf{f}, g)}{N^S} \right), \tag{8}$$

where $Q = \beta \left(1 + \nu + \rho - \eta/2 \right)$ and

$$S = \beta(\mathbf{s} + \nu + \rho - \mu - \eta). \tag{9}$$

In (3.30), the parameter $\mathbf{s}$ depends on the sign of the interactions, being $\mathbf{s} = 1$ under cooperative interactions (positive J_{ij}), such as in Epidemic or Regulatory, and $\mathbf{s} = 0$ if the interactions are adversarial (negative J_{ij}), *e.g*, Inhibitory or Biochemical.

Equations (8)-(3.30), our second key result, uncover the asymptotic behavior of λ in the limit of a large complex system $N \to \infty$. Contrary to $\mathbb{E}(A, P_0, P_1)$, in which λ is fully determined by A and G, here the exponents S and Q depend also on dynamics, via Ω. Most importantly, these equations have crucial implications regarding the system's fixed-point stability, giving rise to three potential stability classes, uniquely predicted within our dynamic J-ensemble (Fig. 1i):

Asymptotic instability ($S > 0$, Fig. 1i, red). In case S in (8) is positive, we have, for sufficiently large N, $\mathrm{Re}(\lambda) \sim N^Q > 0$. Therefore, as the system size N is increased, such states inevitably become unstable. **Asymptotic stability** ($S < 0$, Fig. 1i, blue). For $S < 0$ we have $N^S \to 0$, the r.h.s. of (8) is dominated by the negative term, and hence $\mathrm{Re}(\lambda) < 0$. Consequently, here as $N \to \infty$ stability becomes unconditionally guaranteed. **Sensitive stability** ($S = 0$, Fig. 1i, green). Under $S = 0$ the system lacks an asymptotic behavior, and therefore, its stability depends on $C(\mathbf{f}, g)$ in (8). If $C(\mathbf{f}, g) > 1$ the system is stable, otherwise it becomes unstable. Hence, in this class stability is not driven by the system size N, but rather by the coefficient $C(\mathbf{f}, g)$, and consequently by Eq. (2.1)'s rate parameters $\mathbf{f}$ and g.

Stability classifier. The *stability classifier* S in (3.30) helps group all $J \in \mathbb{E}(A, G, \Omega)$ into distinct stability classes. It achieves this by identifying the relevant topological (β) and dynamic (Ω) control parameters that help analytically predict the stability of any system within the form of Eq. (2.1). We can therefore use S to predict *a priori* whether a specific combination of topology and dynamics will exhibit stable functionality or not.

To examine S's predictive power, we tested it extensively against a diverse set of complex networks. Specifically, we used our model and empirical networks to extract $7,387$ Jacobian matrices from the $\mathbb{E}(A, G, \Omega)$ ensemble, with different sets of η, μ, ν and ρ. In Fig. 4a we show the principal eigenvalue $\mathrm{Re}(\lambda)$ vs. S for the entire $7,387$ Jacobian sample. As predicted, we find that the parameter S sharply splits the sample into three classes. The asymptotically unstable class (red, top-right) has $S > 0$ and consequently also $\mathrm{Re}(\lambda) > 0$, a guaranteed instability. The asymptotically stable class (blue, bottom-left) is observed for $S < 0$, and has, in all cases $\mathrm{Re}(\lambda) < 0$, *i.e.* stable dynamics. Finally, for $S = 0$ we observe sensitive stability, with $\mathrm{Re}(\lambda)$ having no asymptotic behavior, positive or negative (green). A small fraction ($\sim 8\%$) of our

sampled J matrices were inaccurately classified by S (grey), an expected consequence of the approximate nature of S's derivation (Supplementary Section 3).

The ingredients of dynamic stability

The parameter S in (3.30) reduces Eq. (2.1)'s dynamic stability into five relevant exponents. The first four $\Omega = (\eta, \mu, \nu, \rho)$ are determined by the system's intrinsic dynamics $M_q(x)$, around each of its fixed-points. The remaining exponent in (3.30), β, is independent of the dynamics, determined solely by A, G, specifically by their weighted degree density function $P(d)$, through (3.1). Therefore, together, S captures the roles of both topology and dynamics, whose interplay determines the system's stability class around a specific fixed-point - stable, unstable or sensitive.

The only remaining factor in (8) is the coefficient $C(\mathbf{f}, g)$, whose value is driven by Eq. (2.1)'s rate parameters $\mathbf{f}, g$. Yet, as our analysis indicates, this factor is sidelined when $N \to \infty$ under $S \neq 0$. We interpret this to mean that under asymptotic stability or instability, the system's countless microscopic parameters turn irrelevant, and the stable/unstable fixed-points of (2.1) become ingrained into the system's intrinsic dynamics, *i.e.* the functional form of $M_q(x)$; see Methods Section 4 and Supplementary Section 1 for an expanded discussion on this distinction.

To gain deeper insight, consider, for example, the factors that drive a system towards the loss of stability. Most often such events result from external stress or changes in environmental conditions.[2] Such forces impact the system by perturbing its dynamic parameters, *e.g.*, changing the rates of specific processes. Seldom, however, do these environmental perturbations affect the system's built-in interaction mechanisms. Indeed, these mechanisms are ingrained in the *physics* of the interacting components, and therefore they are unaffected by external conditions. Hence, asymptotic stability ($S < 0, N \to \infty$) depicts robust dynamic states, that are insensitive to changes in environmental conditions.

The role of degree-heterogeneity. The dependence of S in (3.30) on β highlights the crucial role that $P(d)$ plays in dynamic stability. To understand this, consider a homogeneous network, such as ER with randomly assigned weights. Here $P(d)$ follows a Poisson distribution, having $\beta = 0$. Under these conditions we have $S = 0$ in (3.30), the system has no defined asymptotic behavior, and hence it is sensitively stable - *i.e.* its stability depends on model parameters via $C(\mathbf{f}, g)$. Hence, our predicted asymptotically stable/unstable classes depend on $\beta > 0$, indicating that they emerge as a direct consequence of degree-heterogeneity. This suggests that a fat-tailed $P(d)$, indeed - among the defining features of many real-world complex systems,[3] serves as a dynamically stabilizing structure, locking-in specific fixed-points, in the face of a persistently fluctuating environment.

To further uncover the roots of asymptotic stability/instability, we consider again $\mathbb{E}(A, G, \Omega)$'s principal eigenvalue λ in (8). Its structure portrays stability as a balance between the positive, *i.e.* destabilizing, effect mediated by the network interactions, vs. the negative, stabilizing, feedback, driven by the parameter $C(\mathbf{f}, g)$ in J's diagonal in Eq. (4); Fig. 4b. It is, therefore, natural to enhance stability by increasing $C(\mathbf{f}, g)$, which, in effect, translates to strengthening each node's intrinsic self regulation. Equation (8) predicts that J becomes stable if $C(\mathbf{f}, g)$ exceeds a critical value

$$C_0 \sim N^S, \tag{10}$$

beyond which λ turns negative. For asymptotically stable states ($S < 0$) we have, for sufficiently

large N, $C_0 \to 0$, a guaranteed stability even under arbitrarily small $C(\mathbf{f}, g)$. In contrast, for asymptotically unstable states ($S > 0$) we have $C_0 \to \infty$, hence such systems are impossible to stabilize even under extremely large $C(\mathbf{f}, g)$. We emphasize that $C(\mathbf{f}, g)$ is the only component in (8) that is dependent on the system's tunable parameters, and therefore having an unbounded range of C-values under which the system remains stable (or unstable) guarantees that λ is, indeed, unaffected by parameter perturbation, *e.g.*, changing environmental conditions.

To test Eq. (10), in Fig. 4c-k we extract a set of three specific J matrices from $\mathbb{E}(A, G, \Omega)$, representing systems from our three stability classes: J_{AS}, asymptotically stable with $\Omega = (2, 2, 2, -1)$; J_{SS}, sensitively stable with $\Omega = (0, -1, -2, 0)$; and J_{AU}, asymptotically unstable with $\Omega = (1, -2, -1, 2)$. For each of these we plot C_0 vs. N, capturing the level of negative feedback required to ensure the system's stability. Under ER ($\beta = 0$, Fig. 4i-k) we do not observe a defined asymptotic behavior. The critical C_0 does not scale with N, indicating that sufficient perturbation to the model parameters can, indeed, affect J's stability.

In contrast, the same J matrices on our scale-free network SF1 ($\beta = 0.6$) exhibit a clear asymptotic behavior, congruent with prediction (10). For J_{AS} we have $C_0 \sim N^{-1.2}$, while under J_{AU} we observe $C_0 \sim N^{1.8}$ (Fig. 4f-h, squares), precisely as predicted (solid lines). Finally, in J_{SS}, having $S = 0$, the system, again lacks an asymptotic behavior, and therefore can be stabilized (or destabilized) under finite C_0, independently of system size N (Fig. 4g).

Together, Eq. (10) helps us link the scale N of a complex system with its observed stability. As opposed to the random matrix viewpoint of $\mathbb{E}(A, P_0, P_1)$, in which N has a destabilizing effect, and hence large systems become unstable,[8] our dynamic ensemble uncovers broad conditions where the contrary is true, and $N \to \infty$, is, in fact, what anchors the system's stability (Fig. 5). Next, we return to our testing ground of dynamical systems (Fig. 2) to examine this asymptotic stability, not just on artificially constructed J, but under the full nonlinear setting of Eq. (2.1).

Emergent stability. The stabilizing/destabilizing effect of N and $P(d)$ is especially relevant if (2.1) exhibits multiple fixed-points, for example, an undesirable $\mathbf{x}_0$ and a desirable $\mathbf{x}_1$. In $\mathbb{E}(A, G, \Omega)$ these two states can be potentially characterized by two different exponent sets Ω_0 and Ω_1, and consequently a different stability profile. If *e.g.*, $\mathbf{x}_0$ is asymptotically unstable ($S > 0$) and $\mathbf{x}_1$ is asymptotically stable ($S < 0$), then a large ($N \to \infty$) heterogeneous ($P(d)$ fat-tailed) network will firmly reside only in $\mathbf{x}_1$, unaffected by perturbation to $\mathbf{f}$ or g.

To observe this we return to our testing ground of Fig. 2, this time focusing on dynamic models that have multiple fixed-points. This includes Regulatory, Epidemic and Inhibitory, each of which exhibits on top of its *active* state $\mathbf{x}_1$, in which all $x_i > 0$, an *inactive* state $\mathbf{x}_0 = (0, \ldots, 0)^\top$, where all activities vanish (Population 1,2 also exhibit an inactive $\mathbf{x}_0$, however it is never stable, see Supplementary Section 4.3).

First, we simulated Regulatory on an ER network, and varied the model's two parameters f_i, the individual node degradation rate, and g, the global interaction strength. We find that when the average $\langle f \rangle$ is large or, alternatively, when g is small the system resides in $\mathbf{x}_0$, whereas in the opposite limit, it favors $\mathbf{x}_1$ (Fig. 6c-e, diamonds). This is precisely the *sensitive stability*, in which the system's fixed-point behavior is driven by its microscopic parameters. Repeating the same experiment on our scale-free network SF1, we observe that $\mathbf{x}_1$ is sustained for a broader range of $\langle f \rangle$ and g, hence SF1 is comparably insensitive to changes in these parameters (Fig. 6d-f, triangles). This robustness is a direct outcome of our classifier: $\mathbf{x}_0$ has $\Omega_0 = (0, 0, 0, 0)$, which in (3.30) predicts $S = \beta > 0$, while $\mathbf{x}_1$ has $\Omega_1 = (0, 0, 0, -2)$, and hence $S = -\beta < 0$. Therefore, on a large ($N \to \infty$) scale-free ($\beta > 0$) network, $\mathbf{x}_0$ becomes asymptotically unstable,

and the system is forced to reside in the asymptotically stable $\mathbf{x}_1$.

To observe this systematically we seek the critical global weight g_c, below which $\mathbf{x}_1$ becomes unstable, and the system transitions to $\mathbf{x}_0$. Varying the system size N over 4 orders of magnitude, from 10 to 2×10^4, we observe first hand $\mathbf{x}_1$'s asymptotic stability: while under ER g_c is almost independent of N (Fig. 6g, diamonds), in SF1 it scales negatively with system size, approaching $g_c \to 0$ in the limit $N \to \infty$ (triangles). Hence, as predicted, SF1's $\mathbf{x}_1$ state remains stable even under arbitrarily small g_c, a stability entrenched by system size. This reconfirms prediction (10), but this time, not on theoretically constructed J from $\mathbb{E}(A, G, \Omega)$, as shown in Fig. 4f-k, but rather on the actual numerically simulated dynamics of Eq. (2.1). Similar stability patterns are also observed in Epidemic and Inhibitory (Fig. 6h,i and Supplementary Sections 4.1 and 4.5).

The role of the hub nodes. We, therefore, observe a qualitative difference between homogeneous vs. fat-tailed $P(d)$, in which degree-heterogeneity can potentially afford the network a guaranteed stability, that is asymptotically independent of microscopic parameters. This phenomenon is rooted in the dominance of the hub nodes, whose dynamic behavior forces the entire system towards stability/instability. In that sense, one can think of our classifier S as a mathematical tool to predict precisely what will be the dynamic role of the hubs - whether the hubs serve as stabilizers ($S < 0$), destabilizers ($S > 0$) or neither ($S = 0$).

Discussion and outlook

The linear stability matrix J carries crucial information on the dynamic behavior of complex systems. Here, we exposed distinct patterns in the structure of J that arise from the nature of the system's interaction dynamics. These patterns are expressed through the four dynamic exponents $\Omega = (\eta, \mu, \nu, \rho)$, which we link analytically to the system's dynamic functions, $M_q(x)$, independently of the weighted network topology A, G or parameters $\mathbf{f}, g$. We interpret this to mean that Ω is hardwired into the system's innate interaction dynamics, determined by the dynamic *model*, *e.g.*, Epidemic or Regulatory, but not by the specific model parameters or the system's underlying connectivity patterns. Therefore, our predicted Jacobian ensemble in (4) and (2.4), as well as its associated stability classifier S in (3.30), both capture highly robust and distinctive characteristics of the system's dynamics, that cannot be perturbed or otherwise affected by shifting environmental conditions.

Graph spectral analysis represents a central mathematical tool to translate network structure into dynamic predictions.[39–41] A network's spectrum, *i.e.* its set of eigenvalues and eigenvectors, captures information on its dynamic timescales, potential states, and - in the present context - its dynamic stability. Most often, spectral analysis is applied to the network *topology*, namely we seek the *graph's* eigenvalues, thus overlooking information on the nonlinear dynamics that occur *on* that graph. As an alternative, our $\mathbb{E}(A, G, \Omega)$ ensemble suggests to apply spectral analysis, not to the topology A (or the weighted $A \circ G$), but rather to J, which, thanks to Ω preserves the information of both structure and dynamics.

Strictly speaking, our analysis covers the Barzel-Barabási family of equations in (2.1). With that said, it also shows strong numerical indications for broader relevance beyond this family (Methods Section 5; Supplementary Section 5). Most importantly, it motivates a departure from the decades old random matrix paradigm ($\mathbb{E}(A, P_0, P_1)$), by showing that real-world Jacobians are anything but random. Hence, while the analytically predictable scaling patterns observed here are specific to Eq. (2.1), the notion that such patterns dominate the structure of J is, likely, much more general, and should be pursued as a systematic road map by which to analyze

complex system dynamics.

The random ensemble $\mathbb{E}(A, P_0, P_1)$

(a) Network

(b) Weights
$P_0(w)$
$P_1(w)$

$J = (A - I) \otimes W$

(c) $J \in \mathbb{E}(A, P_0, P_1)$

The dynamic Jacobian ensemble $\mathbb{E}(A, G, \Omega)$

(d)
$$\frac{dx_i}{dt} = M_0(x_i, \mathbf{f}_{0i}) + g \sum_{j=1}^{N} A_{ij} M_1(x_i, \mathbf{f}_{1i}) G_{ij} M_2(x_j, \mathbf{f}_{2i})$$

(e) M_0, M_1, M_2
Dynamics
$\Omega = (\eta, \mu, \nu, \rho)$

(f) $\mathbf{f}, g$
Parameters
2m
$C(\mathbf{f}, g)$

(g) A_{ij}, G_{ij}
Weighted network
$P(d), d_{\mathrm{nn}}, \beta$

(h) $J \in \mathbb{E}(A, G, \Omega)$
d_i^μ
$d_i^\nu d_j^\rho$

(i) Stability classifier
$$S = \beta(s + \nu + \rho - \mu - \eta)$$
$S < 0$ — Stable
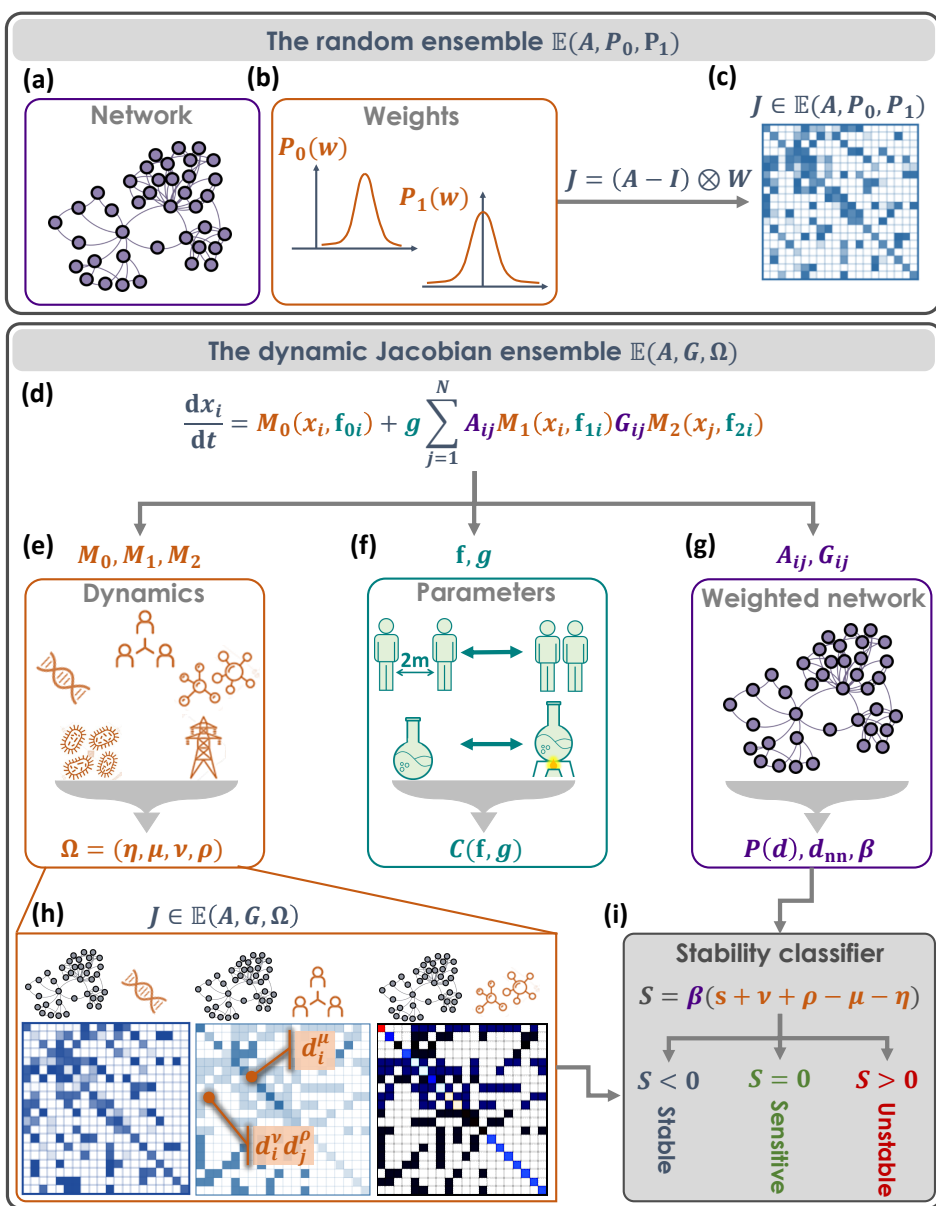$S = 0$ — Sensitive
$S > 0$ — Unstable

Figure 1: **The dynamic Jacobian ensemble**. To predict dynamic stability we seek the system's stability matrix J. (a)-(b) The classic approach is to structure J around the network topology A, with weights extracted from two distributions: $P_0(w)$ for the diagonal entries J_{ii} and $P_1(w)$ for the interactions strengths J_{ij}, $i \neq j$. (c) This provides $J \in \mathbb{E}(A, P_0, P_1)$, a random-matrix based construction, whose stability is determined by the structure A and the random weights W. (d) The dynamic J ensemble features emergent patterns that arise from: (e) The functional form of $M_q(x)$ (orange), capturing the system's ingrained dynamics, *e.g.*, social, biological or technological. We derive Ω in Eqs. (4) and (2.4) directly from these three functions. (f) The microscopic parameters $\mathbf{f}, g$ (turquoise) that provide the specific rate-constants for (2.1)'s dynamic processes. For example, the infection rate in Epidemic (top), or the degradation rate in Biochemical (bottom). These parameters are tunable, following changes in social behavior (Epidemic) or temperature (Biochemical). Their impact on J is encapsulated within the coefficient $C(\mathbf{f}, g)$ in (4). (g) A, G represent the weighted network (purple), expressed in J via the density function $P(d)$, the nearest-neighbor degree d_{nn} in (6) and β in (3.1). (h) The resulting J-ensemble, $\mathbb{E}(A, G, \Omega)$, exhibits non-random scaling patterns. Similar to the random $\mathbb{E}(A, P_0, P_1)$, the non-vanishing terms correspond to the network links, however, in contrast to the random weights of $\mathbb{E}(A, P_0, P_1)$, here the weight of the i, j entry depends on d_i and d_j, as well as on Ω (orange captions). The result is a dynamic ensemble, in which identical networks (A, G) yield highly distinctive J matrices depending on $M_q(x)$, *e.g.*, Regulatory (left), Epidemic (center) or Biochemical (right). (i) The stability of J boils down to the classifier S in (3.30), whose value depends on degree heterogeneity (β, purple) and on Ω (orange terms), but not on the parameters $\mathbf{f}, g$. Therefore, it provides a robust classification into stable (blue) or unstable (red) dynamics, asymptotically insensitive to changes in $\mathbf{f}, g$. Under $S = 0$ the system becomes sensitive (green), and stability is driven precisely by $\mathbf{f}, g$.
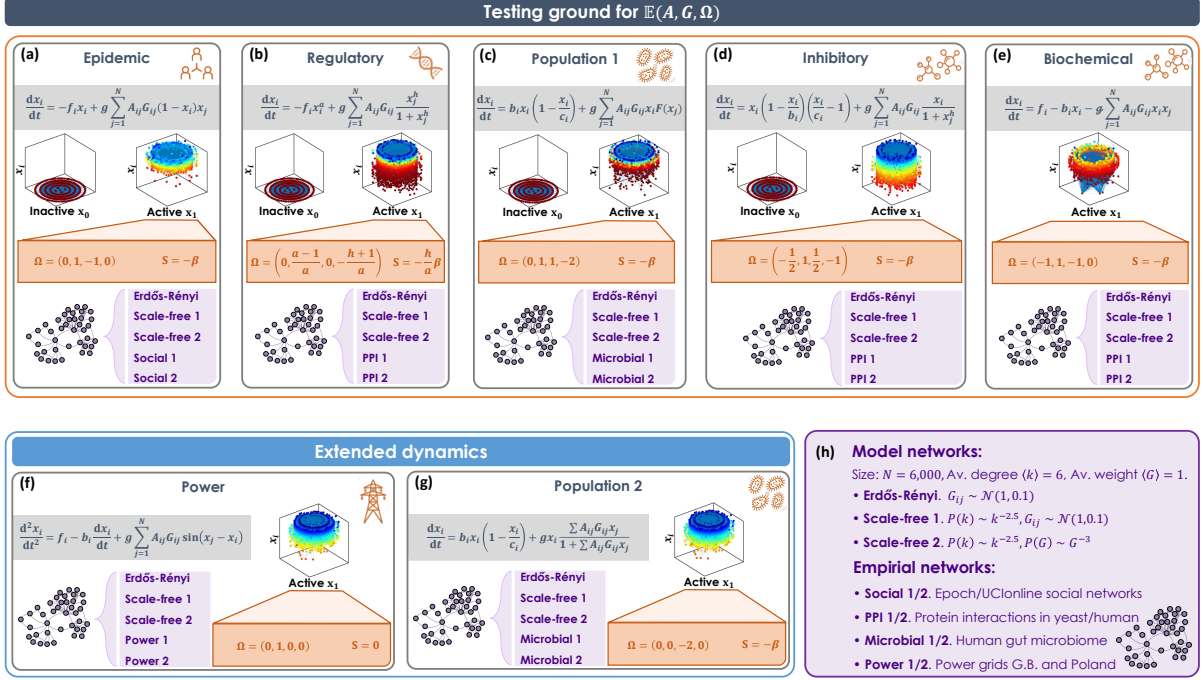
11

Figure 2: **Testing ground for the $\mathbb{E}(A, G, \Omega)$ ensemble**. We constructed different combinations of (weighted) networks A, G and dynamics $M_q(x)$ to examine our J-ensemble. (a) Epidemic. We implemented the susceptible-infected-susceptible (SIS) dynamics (grey box) on a set of model and real-world networks (violet box). This system exhibits two potential fixed-points (3D plots): inactive $\mathbf{x}_0$, in which all activities vanish, *i.e.* healthy, and active $\mathbf{x}_1$, where all $x_i > 0$, namely pandemic. In this 3D visualization the nodes $i = 1, \ldots, N$ are laid out on the x, y plane and their fixed-point activity x_i is represented by color (red - low, blue - high) and vertical displacement (z-axis). Therefore, in $\mathbf{x}_0$ all nodes are on the x, y plane ($z = 0$), and in $\mathbf{x}_1$ they are distributed along $z > 0$ and range from red to blue. In each of these states the system has a different set of exponents Ω and hence a different Jacobian J. Here we present Ω and S for the non-vanishing state $\mathbf{x}_1$ (orange box). The remaining panels follow a similar format. (b) Regulatory. Sub-cellular dynamics following the Michaelis-Menten model. Here Ω, S depend on the model exponents a, h. (c) Population 1. Mutualistic interactions in, *e.g.*, microbial communities. (d) Inhibitory. Suppression dynamics, *e.g.*, between hosts and pathogens. (e) Biochemical. Protein-protein interactions modeled via mass-action kinetics. This system exhibits a single fixed-point. (f) Power. Synchronization dynamics between power system components. (g) Population 2. Mutualistic population dynamics with non-additive interactions, namely replacing the term $\sum_{j=1}^{N} A_{ij} G_{ij} M_2(x_j)$ in Eq. (2.1) by $M_2(\sum_{j=1}^{N} A_{ij} G_{ij} x_j)$. (h) Our networks, including Erdős-Rényi and scale-free with both normally and power-law distributed weights, together with relevant empirical networks. A detailed description of all networks appears in Supplementary Section 7.4. Together we arrive at a set of 35 combinations of networks/dynamics upon which we test our theoretical framework. A detailed analysis of all dynamic models appears in Supplementary Section 4. Note that Population 2 and Power (panels f,g) are not in the form of Eq. (2.1), and hence they expand our testing ground beyond the bounds of our analytical framework (Supplementary Section 5).
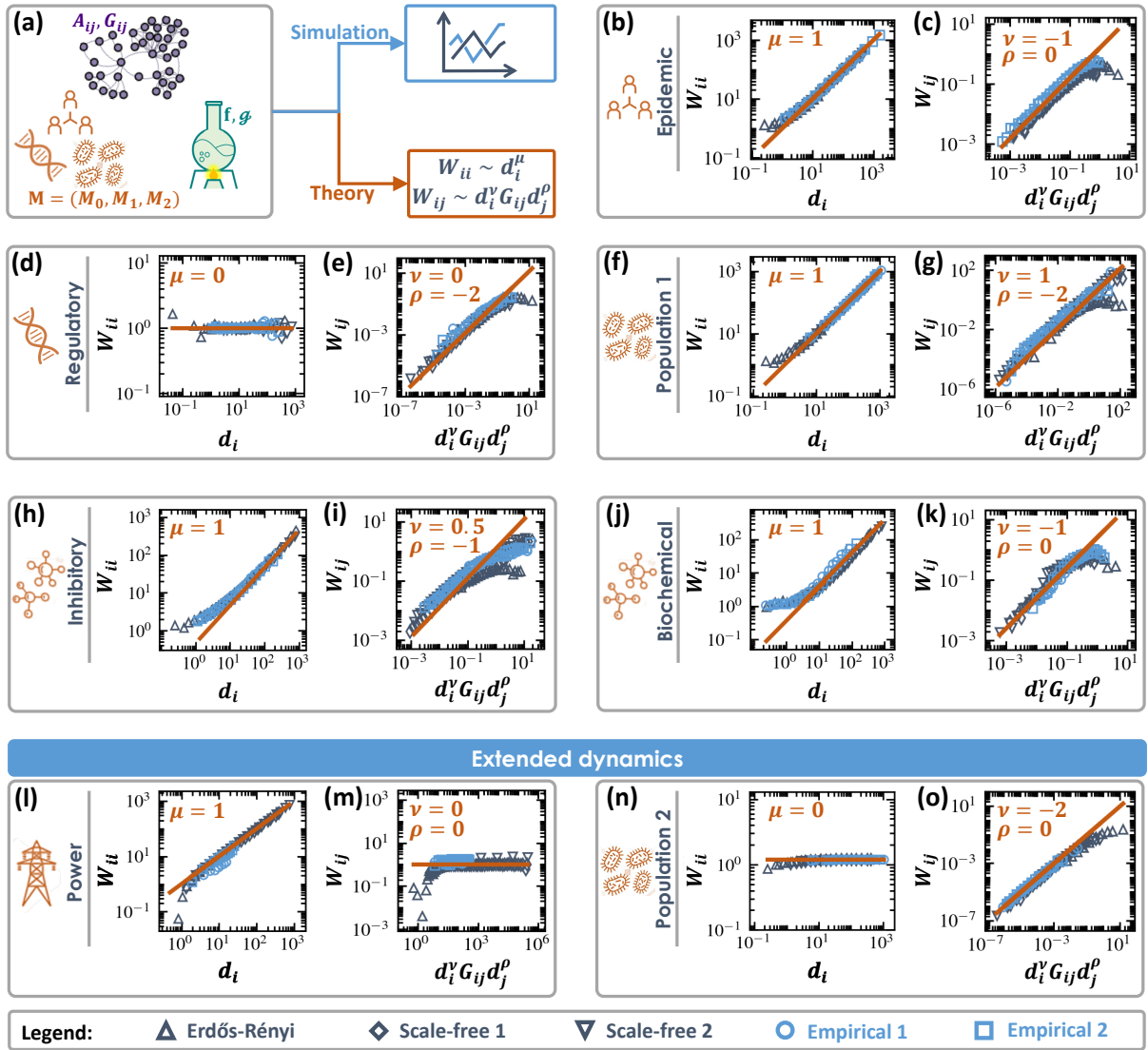
Figure 3: **Emergent patterns in the dynamic ensemble** $\mathbb{E}(A, G, \Omega)$. We implemented our seven dynamic models, Epidemic, Regulatory etc., on relevant model and empirical networks, as detailed in Fig. 2; see legend at bottom. Perturbing all nodes around their numerically obtained fixed-point $(\mathbf{x}_1)$ we constructed the Jacobian J. (a) The numerical simulations incorporate the full complexity of Eq. (2.1): weighted network (purple), diverse parameters (turquoise) and non-linear mechanisms (orange). This provides actual Jacobian matrices, obtained from numerical runs of the nonlinear network models (Simulation, blue, top). We compare our simulation results with our predictions in (4) and (2.4) (Theory, orange, bottom). (b) The diagonal weights W_{ii} vs. d_i as obtained from Epidemic dynamics (symbols). We observe our predicted scaling (4) with $\mu = 1$ (orange solid line). The scaling is independent of A, G, observed consistently on all our model/empirical networks - intrinsic to the Epidemic dynamics, as predicted. (c) The off-diagonal weights W_{ij} vs. our theoretical prediction of (2.4) with $\nu = -1, \rho = 0$ (symbols). Once again, we observe a perfect agreement between simulation (blue symbols) and theory (orange solid line). We also include two relevant empirical networks, Social 1 and Social 2 (light blue circles/squares), capturing online social dynamics. (d)-(e) Similar results are observed under Regulatory ($\mu = \nu = 0, \rho = -2$) on both model and empirical networks (PPI 1 and PPI 2); (f)-(g) Population 1 dynamics ($\mu = \nu = 1, \rho = -2$, empirical networks: Microbial 1 and Microbial 2); (h)-(i) Inhibitory dynamics ($\mu = 1, \nu = 1/2, \rho = -1$, empirical networks: PPI 1 and PPI 2); (j)-(k) Biochemical dynamics ($\mu = 1, \nu = -1, \rho = 0$, empirical networks: PPI 1 and PPI 2). (l)-(m) Power dynamics ($\mu = 1, \nu = \rho = 0$, empirical networks: Power 1 and Power 2); (n)-(o) Population 2 dynamics ($\mu = 0, \nu = -2, \rho = 0$, empirical networks: Microbial 1 and Microbial 2). In all systems, we find that real Jacobian matrices (blue symbols) are well-approximated by our theoretically predicted scaling laws (orange solid lines). Data in all panels are logarithmically binned.[18] Details on numerical calculation of J, log-binning and all networks appear in Supplementary Section 7.
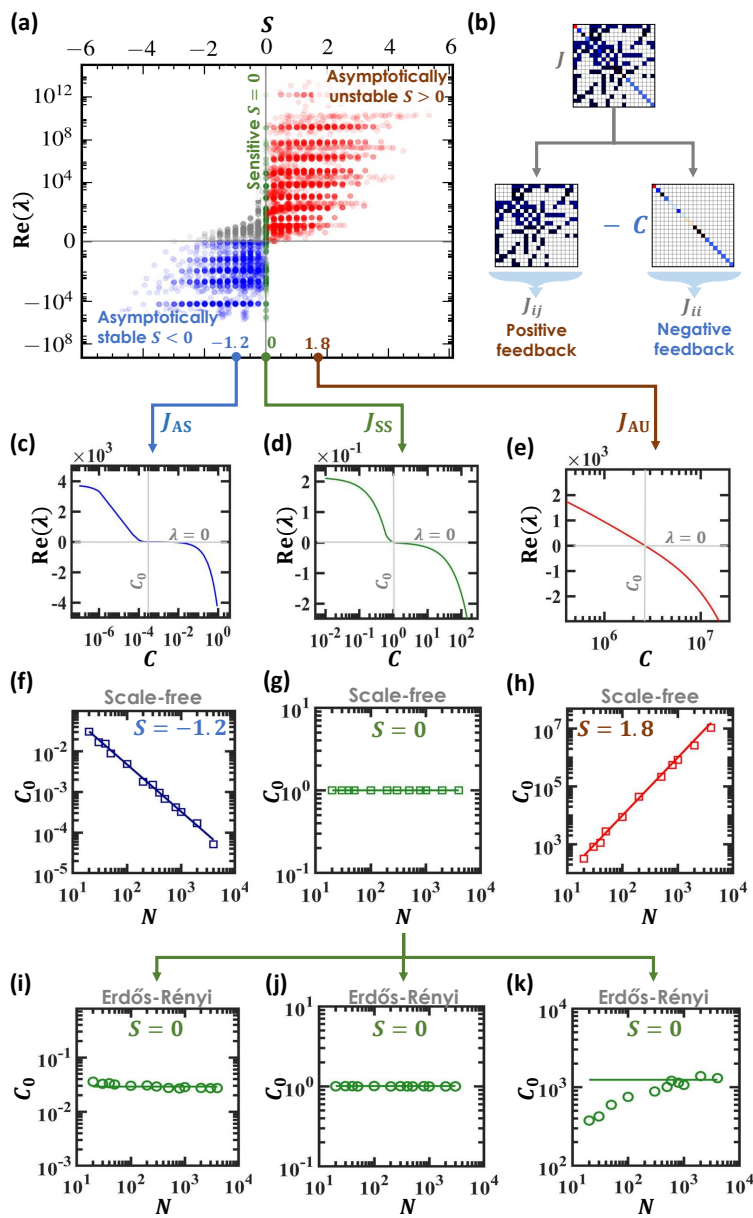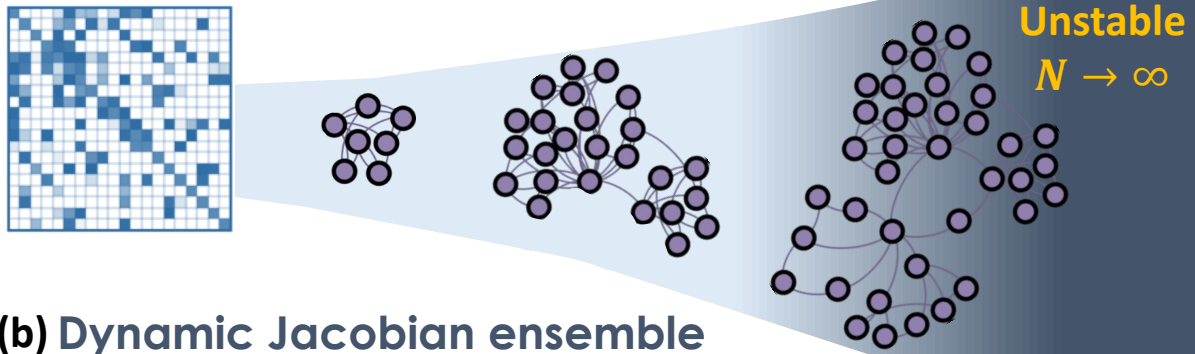
13

Figure 4: **Three classes of dynamic stability**. We extracted $7,387$ Jacobian matrices from the $\mathbb{E}(A, G, \Omega)$ ensemble, using combinations of model/empirical networks with different dynamic exponents Ω. For each J we calculated the principal eigenvalue λ and the stability classifier S in (3.30). (a) $\mathrm{Re}(\lambda)$ vs. S for all $7,387$ J-matrices. We observe the three predicted classes: Asymptotically unstable (red) in which $S > 0$ and hence, as predicted, we have also $\mathrm{Re}(\lambda) > 0$; Sensitively stable (green), where $S = 0$ and $\mathrm{Re}(\lambda$ can be both positive or negative; Asymptotically stable (blue), where $S < 0$ and therefore $\mathrm{Re}(\lambda) < 0$. Our classification showed $\sim 4\%$ inaccuracy on binary networks, $\sim 5\%$ on weighted networks and $\sim 15\%$ on weighted/negative networks - a total discrepancy of $\sim 8\%$ (grey dots) over the entire ensemble. (b) The value of λ emerges from the competition between J's off-diagonal terms, representing positive feedback, and the strength of the diagonal terms J_{ii} (negative feedback). Therefore one can force a system towards stability ($\mathrm{Re}(\lambda) < 0$) by increasing the coefficient C in (4). (c)-(e) Taking three specific J matrices, we plot $\mathrm{Re}(\lambda)$ vs. C, seeking the critical C_0, in which $\mathrm{Re}(\lambda)$ becomes negative (grey lines). This represents the critical C, above which stability is ensured. (f) For the stable J_{AS} ($S = -1.2$) we find that C_0 decreases with N (squares), capturing the asymptotic stability, in which as $N \to \infty$ stability is sustained even under arbitrarily small C. The theoretical scaling predicted in Eq. (10) is also shown (solid line, slope -1.2). (g) For J_{SS} we have $S = 0$, the critical C_0 is independent of N, hence the system's stability can be affected by finite changes to its dynamic parameters. (h) The asymptotically unstable J_{AU} ($S = 1.8$) has $C_0 \to \infty$ in the limit of large N, in perfect agreement with Eq. (10) (solid line). Here, no matter how large is C, the fixed-point associated with J_{AU} is always unstable. (i)-(k) For a homogeneous $P(d)$, e.g., Erdős-Rényi, β vanishes and hence $S = 0$ in (3.30). Under these conditions, regardless of Ω, the system is always sensitively stable and therefore C_0 does not scale with N. This demonstrates the role of degree-heterogeneity for ensuring stability in the face of changing environmental conditions.

14

(a) Random matrix paradigm

Unstable
$N \to \infty$

(b) Dynamic Jacobian ensemble

d_i^{μ}

$d_i^{\nu} d_j^{\rho}$

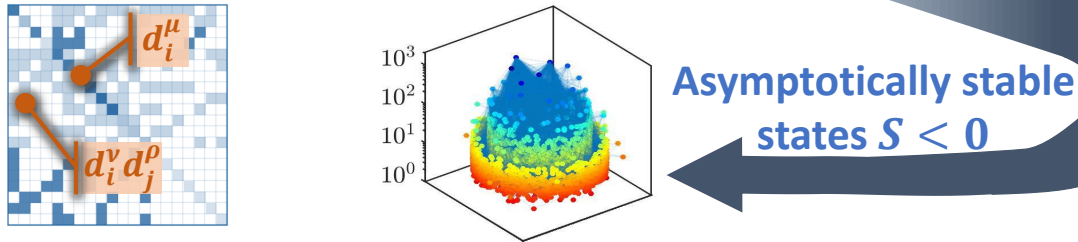**Asymptotically stable states $S < 0$**

Figure 5: **Will a large complex system be stable?** This question, first posed by May in 1972,[8] captures a long standing challenge, fueled by the seeming contradiction between theory and practice. (a) While empirical reality answers with an astounding yes, May's mathematical analysis, based on random matrix theory, suggested the contrary, that large systems are inevitably unstable, giving rise to the well-known *diversity-stability debate*. Here, the series of growing networks (left to right) becomes increasingly unstable as we drift towards $N \to \infty$. In the works that followed it became clear that real-world complex systems are not random. Rather they incorporate unique structural[43–45] and dynamic[18,19,46] constraints - or organizing principles - that can potentially enhance stability. (b) Our dynamic Jacobian ensemble offers such organizing principles, that emerge quite naturally in a variety of real-world systems (Fig. 2). This is expressed through the built-in scaling patterns in J (orange), which, in turn, predict a broad class of asymptotically stable dynamic states (middle). In this class ($S < 0$) system size plays a stabilizing, rather than a destabilizing role. Consequently, we arrive at quite broad conditions where May's original question receives a clear answer: large complex systems not only can, but, often must be stable.
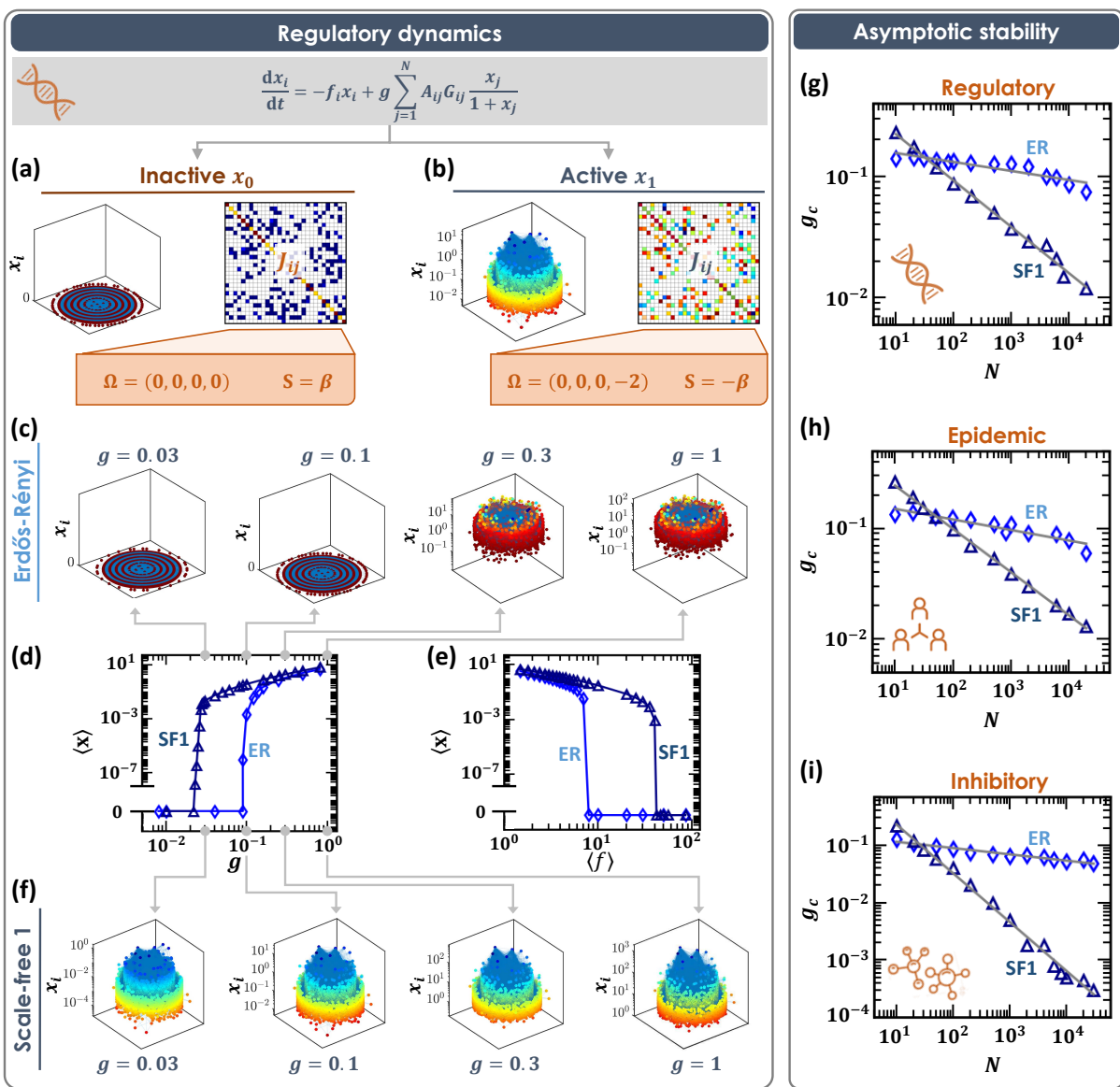
Figure 6: **Emergent stability in large heterogeneous networks**. (a)-(b) Regulatory dynamics exhibit two fixed points (3D plots), each with its own $J \in \mathbb{E}(A, G, \Omega)$, shown to the right of each plot. The inactive $\mathbf{x}_0$ has $\Omega = (0, 0, 0, 0)$ and $S = \beta > 0$ - hence it is asymptotically unstable. The active $\mathbf{x}_1$ has a different J, with $\Omega = (0, 0, 0, -2)$ and $S = -\beta < 0$, asymptotically stable. (c) The state of Regulatory as obtained from numerical simulations on our Erdős-Rényi (ER) network under varying g. The system transitions from $\mathbf{x}_1$ (right) to $\mathbf{x}_0$ (left) under small g. This represents sensitive stability, as indeed predicted for ER, in which parameters, here g, affect the state of the system. (d) To examine this systematically we plot the mean activity $\langle \mathbf{x} \rangle$ vs. g as obtained for ER (diamonds) and for our scale-free network SF1 (triangles). Both systems exhibit a critical g_c, below which $\mathbf{x}_1$ becomes unstable and the system transitions to $\mathbf{x}_0$. The crucial point is, however, that thanks to its heterogeneity SF1 exhibits an increased robustness against g variations, with g_c an order of magnitude lower than that observed for ER. (e) $\langle \mathbf{x} \rangle$ vs. $\langle f \rangle$ shows a similar behavior (here increasing $\langle f \rangle$ causes the system to collapse to $\mathbf{x}_0$). (f) The state of SF1 under the same four conditions shown in panel (c). As predicted, SF1 remains at $\mathbf{x}_1$ even when ER has already collapsed to $\mathbf{x}_0$. (g) g_c vs. the system size N as obtained from numerically simulating Regulatory dynamics. For ER we observe $g_c \sim$ const (diamonds), hence there is a typical g_c below which the system transitions to $\mathbf{x}_0$. Consequently $\mathbf{x}_1$ can be destabilized via parameter perturbation. Note that while N spans over four orders of magnitude, g_c varies by a mere $\sim 40\%$. In contrast, for SF1 we find that g_c exhibits negative scaling with N, approaching $g_c \to 0$ in the limit $N \to \infty$. This captures precisely the predicted asymptotic stability, in which a sufficiently large and heterogeneous network is guaranteed to stably reside in $\mathbf{x}_1$ even under arbitrarily small g (or large $\langle f \rangle$). (h)-(i) Repeating this experiment for Epidemic and Inhibitory, we continue to observe our predicted asymptotic stability: under SF1 we have $g_c \to 0$ as $N \to \infty$, whereas under ER g_c is (almost) independent of N.

16

References

[1] S.V. Buldyrev, R. Parshani, G. Paul, H.E. Stanley and S. Havlin. Catastrophic cascade of failures in interdependent networks. *Nature*, 464:1025–1028, 2010.

[2] I. Dobson, B.A. Carreras, V.E. Lynch and D.E. Newman. Complex systems analysis of series of blackouts: Cascading failure, critical points, and self-organization. *Chaos*, 17:026103, 2007.

[3] D. Duan, C. Lv, S. Si, Z. Wang, D. Li, J. Gao, S. Havlin, H.E. Stanley and S. Boccaletti. Universal behavior of cascading failures in interdependent networks. *Proc. Natl. Acad. Sci. USA*, 116:22452–57, 2019.

[4] A.E. Motter and Y.-C. Lai. Cascade-based attacks on complex networks. *Physical Review E*, 66:065102, 2002.

[5] P. Crucitti, V. Latora and M. Marchiori. Model for cascading failures in complex networks. *Phys. Rev. E*, 69:045104–7, 2004.

[6] D. Achlioptas, R.M. D'Souza and J. Spencer. Explosive percolation in random networks. *Science*, 323:1453–1455, 2009.

[7] J. Gao, B. Barzel and A.-L. Barabási. Universal resilience patterns in complex networks. *Nature*, 530:307–312, 2016.

[8] S. Boccaletti, J.A. Almendral, S. Guana, I. Leyvad, Z. Liua, I.S. Nadal, Z. Wang and Y. Zou. Explosive transitions in complex networks' structure and dynamics: Percolation and synchronization. *Physics Reports*, 660:1–94, 2016.

[9] S. Boccaletti, V. Latora, Y. Moreno, M. Chavez and D.-U. Hwang. Complex networks: Structure and dynamics. *Physics Reports*, 424:175–308, 2006.

[10] Michael M Danziger, Ivan Bonamassa, Stefano Boccaletti, and Shlomo Havlin. Dynamic interdependence and competition in multilayer networks. *Nature Physics*, 15(2):178–185, 2019.

[11] K.Z. Coyte, J. Schluter and K.R. Foster. The ecology of the microbiome: Networks, competition, and stability. *Science*, 350:663–666, 2015.

[12] R.V. Solé and J.M. Montoya. Complexity and fragility in ecological networks. *Proc. R. Soc. London Ser. B*, 268:2039–2045, 2001.

[13] H.I. Schreier, Y. Soen and N. Brenner. Exploratory adaptation in large random networks. *Nature Communications*, 8:14826, 2017.

[14] L.M. Pecora and T.L. Carroll. Master stability functions for synchronized coupled systems. *Phys. Rev. Lett.*, 80:2109, 1998.

[15] V.I. Arnold. *Ordinary Differential Equations*. MIT Press, Cambridge, MA, 1973.

[16] M.W. Hirsch and S. Smale. *Differential Equations, Dynamical Systems and Linear Algebra*. Academic Press, New York, 1974.

[17] K.S. McCann. The diversity–stability debate. *Nature*, 405(6783):228–233, 2000.

[18] J.D. O'Sullivan, R.J. Knell and A.G. Rossberg. Metacommunity-scale biodiversity regulation and the self-organised emergence of macroecological patterns. *Ecology Letters*, 22:1428, 2019.

[19] M. Barbier, C. de Mazancourt, M. Loreau and G. Bunin. Fingerprints of high-dimensional coexistence in complex ecosystems. *Phys. Rev. X*, 11:011009, 2021.

[20] G. Caldarelli. *Scale-free networks: complex webs in nature and technology*. Oxfrod University Press, New York, 2007.

[21] R.M. May. Will a large complex system be stable? *Nature*, 238:413 – 414, 1972.

[22] B. Barzel and A.-L. Barabási. Universality in network dynamics. *Nature Physics*, 9:673 – 681, 2013.

[23] U. Harush and B. Barzel. Dynamic patterns of information flow in complex networks. *Nature Communications*, 8:2181, 2017.

[24] C. Hens, U. Harush, R. Cohen, S. Haber and B. Barzel. Spatiotemporal propagation of signals in complex networks. *Nature Physics*, 15:403, 2019.

[25] R. Pastor-Satorras, C. Castellano, P. Van Mieghem and A. Vespignani. Epidemic processes in complex networks. *Rev. Mod. Phys.*, 87:925–958, 2015.

[26] P.S. Dodds, R. Muhamad and D.J. Watts. An experimental study of search in global social networks. *Science*, 301:827–829, 2003.

[27] D. Brockmann, V. David and A.M. Gallardo. Human mobility and spatial disease dynamics. *Reviews of Nonlinear Dynamics and Complexity*, 2:1, 2009.

[28] G. Karlebach and R. Shamir. Modelling and analysis of gene regulatory networks. *Nature Reviews*, 9:770–780, 2008.

[29] J.D. Murray. *Mathematical Biology*. Springer, Berlin, 1989.

[30] B. Barzel and O. Biham. Binomial moment equations for stochastic reaction systems. *Phys. Rev. Lett.*, 106:150602–5, 2011.

[31] B. Barzel and O. Biham. Stochastic analysis of complex reaction networks using binomial moment equations. *Phys. Rev. E*, 86:031126, 2012.

[32] C.S. Holling. Some characteristics of simple types of predation and parasitism. *The Canadian Entomologist*, 91:385–398, 1959.

[33] J.N. Holland, D.L. DeAngelis and J.L. Bronstein. Population dynamics and mutualism: functional responses of benefits and costs. *American Naturalist*, 159:231–244, 2002.

[34] D. Wodarz, J.P. Christensen and A.R. Thomsen. The importance of lytic and nonlytic immune responses in viral infections. *Trends in Immunology*, 23:194–200, 2002.

[35] E.L. Berlow, J.A. Dunne, N.D. Martinez, P.B. Stark, R.J. Williams and U. Brose. Simple prediction of interaction strengths in complex food webs. *Proceedings of the National Academy of Sciences*, 106:187–191, 2009.

[36] J.F. Hayes and T.V.J. Ganesh Babu. *Modeling and Analysis of Telecommunications Networks*. John Wiley & Sons, Inc., Hoboken, NJ, USA, 2004.

[37] M.E.J. Newman. *Networks - an introduction*. Oxford University Press, New York, 2010.

[38] G. Yan, N.D. Martinez and Y.-Y. Liu. Degree heterogeneity and stability of ecological networks. *Journal of The Royal Society Interface*, 14:131, 2017.

[39] J.A. Almendral and A. Díaz-Guilera. Dynamical and spectral properties of complex networks. *New Journal of Physics*, 9:187–187, 2007.

[40] P. Van Mieghem. Epidemic phase transition of the SIS type in network. *Europhysics Letters*, 97(4):48004, 2012.

[41] P. Van Mieghem. *Graph Spectra for Complex Networks*. Cambridge University Press, Cambridge, UK, 2010.

[42] S. Milojević. Power-law distributions in information science: making the case for logarithmic binning. *Journal of the American Society for Information Science and Technology*, 61:2417–2425, 2010.

[43] S. Allesina and S. Tang. Stability criteria for complex ecosystems. *Nature*, 483:205–208, 2012.

[44] W. Tarnowski, I. Neri and P. Vivo. Universal transient behavior in large dynamical systems on networks. *Phys. Rev. Research*, 2:023333, 2020.

[45] S. Sinha and S. Sinha. Evidence of universality for the May-Wigner stability theorem for random networks with local dynamics. *Phys. Rev. E*, 71(2):020902, 2005.

[46] P. Kirk, D.M.Y. Rolando, A.L. MacLean and M.P.H. Stumpf. Conditional random matrix ensembles and the stability of dynamical systems. *New Journal of Physics*, 17:080325, 2015.

[47] D.J. Watts and S.H. Strogatz. Collective dynamics of 'small-world' networks. *Nature*, 393:440–442, 1998.

[48] L. Schmetterer and K. Sigmund (Eds.). *Hans Hahn Gesammelte Abhandlungen Band 1/Hans Hahn Collected Works Volume 1*. Springer, Vienna, Austria, 1995.

[49] M. Granovetter. Threshold models of collective behavior. *The Americn journal of Sociology*, 83:6, 1420–43, 2002.

[50] Y. Kuramoto. *Chemical oscillations, waves and turbulance*. Springer-Verlag Berlin, Heidelberg, 1984.

[51] P. Kundu, C. Hens, B. Barzel and P. Pal. Perfect synchronization in networks of phase-frustrated oscillators. *Europhysics Letters*, 120:40002, 2018.

[52] D.B. Stouffer, J. Camacho, R. Guimerà, C.A. Ng and L.A. Nunes Amaral. Quantitive patterns in the strcture of model and empirical food webs. *Ecology*, 86:1301–1311, 2005.

Methods

1. Random matrix based Jacobian constructions

The random matrix paradigm was first introduced by May,[8] seeking precisely the question we address here (Fig. 5): will a large complex system be stable? In this original construction all diagonal weights in (2) were set to $W_{ii} = 1$, while the off-diagonal weights were extracted from a zero-mean Gaussian distribution. The rationale is that the self regulation of all components is uniform, driven by the system's intrinsic timescales (normalized to unity), while the interaction strengths vary randomly around zero. Such construction is a particular case of our W_{ii} in (4), setting $C(\mathbf{f}, g) = 1$ and $\eta = \mu = 0$. While the first assumption about $C(\mathbf{f}, g)$ has no significant bearing on our analysis, the second, which ignores the dynamic exponents η, μ, is precisely the crux of our proposed novelty. Indeed, in our framework, it is these two exponents (together with ν and ρ) that capture the role of the nonlinear dynamics, ignored in the random matrix constructions.

In the works that followed May's abstract construction, researchers systematically introduced more realism into J. First, by considering more realistic A_{ij}, for example, small-world[47] or scale-free networks,[38] which have, indeed, been shown to impact (2)'s spectral properties. Other advances tackled $P_0(w)$ and $P_1(w)$, showing that different dynamics may lead to more specific weight distributions, rather than the originally assumed Gaussian distribution. This is achieved by conditioning $P_0(w)$ and $P_1(w)$ to account for specific patterns that arise from known dynamic processes. For example, in predator prey relationships a positive W_{ij} is often matched with a negative W_{ji},[43] capturing the asymmetry in the benefit/loss of the predator and its prey. More complex dynamic constraints may further impact the statistical properties of W, limiting the Jacobian to a selected subset of the random matrix ensemble.[46]

2. Deriving the dynamic Jacobian ensemble

While we provide a complete and rigorous derivation of the $\mathbb{E}(A, G, \Omega)$ ensemble in Supplementary Sections 1-3, below we include a shorthand version of this derivation, tracking the main steps and important mathematical transitions leading to Eqs. (4), (2.4) and (3.30). For simplicity, in this abbreviated analysis, we limit ourselves to systems with uniform weights/parameters. Hence, in Eq. (2.1) we set the global and individual weights to $g = G_{ij} = 1$, and take $\mathbf{f}_{qi} = \mathbf{f}_{qj}$ for all $i, j = 1, \ldots, N$. Under these simplifications, we rewrite Eq. (2.1) as

$$\frac{\mathrm{d}x_i}{\mathrm{d}t} = M_0\big(x_i(t)\big) + M_1\big(x_i(t)\big) \sum_{j=1}^{N} A_{ij} M_2\big(x_j(t)\big), \tag{11}$$

omitting the link weights g, G_{ij} and the parameters $\mathbf{f}_{qi}$, which are now identical for all nodes. We emphasize that in our full derivation, as well as in our reported results and simulations, we do not rely on these simplified assumptions, and only employ them here for brevity and conciseness.

Fixed-point analysis. Starting from (11), we seek the system's potential fixed-points via

$$M_0(x_i) + M_1(x_i) \sum_{j=1}^{N} A_{ij} M_2(x_j) = 0, \tag{12}$$

where we use x_i (omitting the t dependence) to denote the fixed-point $x_i = x_i(t \to \infty)$. To express the summation over j in the l.h.s. we use

$$\langle M_2(x)\rangle_{i\odot} = \frac{1}{d_i}\sum_{j=1}^{N} A_{ij}M_2(x_j), \tag{13}$$

capturing a weighted average over $M_2(x_j)$ across all of i's nearest neighbors. Here, with all link weights set to unity, $d_i = \sum_{j=1}^{N} A_{ij}$ represents i's binary degree. This generalizes to i's weighted degree if we reintroduce our weights g, G_{ij}. In (13) we use the notation $\odot$ to represent a *neighborhood average*, namely an average over i's surrounding nodes $i\odot$. Substituting (13) into (2.6) we obtain

$$M_0(x_i) + d_i M_1(x_i)\langle M_2(x)\rangle_{i\odot} = 0, \tag{14}$$

which we further simplify to

$$R(x_i) = q_i \tag{15}$$

where $R(x) = -M_1(x)/M_0(x)$ and

$$q_i = \frac{1}{\langle M_2(x)\rangle_{i\odot}d_i} \tag{16}$$

is node i's inverse weighted degree. In Eq. (15), the function $R(x)$ is only defined in case $M_0(x) \neq 0$. The treatment of $M_0(x) = 0$ is done separately in Supplementary Section 2.5. We can now extract the fixed-point x_i by inverting $R(x_i)$ to obtain

$$x_i = R^{-1}(q_i), \tag{17}$$

allowing us to express the fixed-point activity of node i in function of its inverse degree q_i. Here, we rely on the implicit assumption that $R(x)$ is invertible, allowing us to write $R^{-1}(q_i)$ in (17). As above, we employ this assumption here only for simplicity; in our complete derivation in Supplementary Section 2, we show how to obtain x_i also under non-invertible $R(x)$.

Jacobian scaling - diagonal weights W_{ii}. We now return to Eq. (11) to extract the Jacobian weights W_{ii} and W_{ij} around the fixed-point obtained in (17). Starting with the diagonal terms, we write

$$W_{ii} = \left.\frac{\partial \dot{x}_i}{\partial x_i}\right|_{x_i=R^{-1}(q_i)} = \left.\left(M_0'(x_i) + M_1'(x_i)\sum_{j=1}^{N} A_{ij}M_2(x_j)\right)\right|_{x_i=R^{-1}(q_i)}, \tag{18}$$

where $M_q'(x) = \partial M_q/\partial x$. Equation (18) represents a derivative of the r.h.s. of (11) taken around the fixed-point x_i, which we express via (17) as $R^{-1}(q_i)$. Next we use $R(x) = -M_1(x)/M_0(x)$ to write $M_0(x) = -M_1(x)/R(x)$, allowing us to express the first derivative on the r.h.s. of (18) as

$$M_0'(x_i) = -\frac{M_1'(x_i)}{R(x_i)} + \frac{M_1(x_i)R'(x_i)}{R^2(x_i)}, \tag{19}$$

which, setting $x_i = R^{-1}(q_i)$, provides

$$M_0'(x) = -\frac{M_1'\big(R^{-1}(q_i)\big)}{q_i} + \frac{M_1\big(R^{-1}(q_i)\big)R'\big(R^{-1}(q_i)\big)}{q_i^2}. \tag{20}$$

To obtain the denominators, q_i and q_i^2 on the r.h.s. of (20) we used the fact that $R(R^{-1}(q_i)) = q_i$. We can now use (13) to express the sum on the r.h.s. of (18) as $\sum_{j=1}^{N} A_{ij} M_2(x_j) = d_i \langle M_2(x) \rangle_{i\odot}$, which, according to (16) is equal to $1/q_i$. Collecting all the terms we arrive at

$$W_{ii} = -\frac{M_1'\big(R^{-1}(q_i)\big)}{q_i} + \frac{M_1\big(R^{-1}(q_i)\big)R'\big(R^{-1}(q_i)\big)}{q_i^2} + \frac{M_1'\big(R^{-1}(q_i)\big)}{q_i}, \tag{21}$$

which in turn provides

$$W_{ii} = \frac{1}{q_i^2} Y\big(R^{-1}(q_i)\big), \tag{22}$$

where $Y(x) = M_1(x)R'(x)$.

Equation (22) expresses the diagonal Jacobian weight W_{ii} in terms of i's inverse degree $q_i \sim d_i^{-1}$. In the asymptotic limit of large d_i (small q_i) we can approximate (22) by expanding $Y(R^{-1}(q_i))$ around $q_i = 0$. We, therefore, express this function as a Hahn[5] power series expansion in the form

$$Y\big(R^{-1}(q_i)\big) = \sum_{n=0}^{\infty} B_n q_i^{\Phi_n}, \tag{23}$$

allowing us below to examine the limit $q_i \to 0$. The Hahn series in (23) represents a generalization of the Taylor expansion to allow for negative and real powers, hence $\Phi_n \in \mathbb{R}$ captures a sequence of real powers in ascending order, i.e. $\Phi_0 < \Phi_1$ and so on. In the limit $q_i \to 0$ we take only the leading term $q_i^{\Phi_0}$, which in (22) provides the scaling relationship

$$W_{ii} \approx B_0 q_i^{-\mu} = B_0 \Big(\langle M_2(x) \rangle_{i\odot} d_i \Big)^{\mu}, \tag{24}$$

where $\mu = 2 - \Phi_0$. In the last step of (24) we reintroduced d_i using the definition of q_i in (16), hence also adding the i neighborhood average $\langle M_2(x) \rangle_{i\odot}$.

Equation (24) describes the weight of the diagonal Jacobian entry associated with a specific node i. It is found to depend on the node's degree d_i, but also on the activity of its neighboring nodes via $\langle M_2(x) \rangle_{i\odot}$. To complete the scaling of W_{ii} with i's degree d_i we must characterize the d_i-dependence of $\langle M_2(x) \rangle_{i\odot}$. The crucial point is that $\langle M_2(x) \rangle_{i\odot}$ captures an average over i's *neighborhood*, not over the node i itself, and hence, on average, it is only indirectly affected by i's degree d_i. To express this more rigorously we write

$$\langle M_2(x) \rangle_{i\odot} \approx \langle M_2(x) \rangle_{\odot} f(d_i), \tag{25}$$

replacing the average over i's neighborhood ($i\odot$) with the *ensemble* average ($\odot$). This ensemble average $\langle M_2(x) \rangle_{\odot} = (1/N) \sum_{i=1}^{N} \langle M_2(x) \rangle_{i\odot}$ represents an aggregation over *all* nodes in the network, and hence it is independent of i or d_i. To account for the potential d_i dependence, we include, on the r.h.s. of (25), the implicit function $f(d_i)$. This function, defined as $f(d_i) = \langle M_2(x) \rangle_{i\odot} / \langle M_2(x) \rangle_{\odot}$, captures the distinction between the conditional i-neighborhood average ($i\odot$) vs. the network's ensemble average ($\odot$). It, therefore, helps quantify potential

statistical dependencies between i and its interacting neighbors $i\odot$. Hence, if the network is randomly wired, *i.e.* lacks degree-correlations,[1] we have $f(d_i) = 1$, independently of i. However, if correlations are present, it will be expressed through a non-trivial $f(d_i)$.

Extracting only the terms that depend on d_i we rewrite Eq. (24) as $W_{ii} \sim f^\mu(d_i)d_i^\mu$, omitting the terms $B_0, \langle M_2(x)\rangle_\odot$, which are independent of d_i. Finally, if $f(d_i)$ is sub-polynomial, it does not contribute to the d_i scaling in the limit of large d_i. This allows us to write

$$W_{ii} \sim d_i^\mu, \tag{26}$$

recovering the asymptotic scaling relationship of Eq. (4). In (26) we eliminated all terms that do not contribute to the polynomial dependence on d_i, thus focusing solely on the obtained *scaling* relationship. These terms may, however, depend on other parameters of (2.1). For example, quite expectedly the term $\langle M_2(x)\rangle_\odot$, an average driven by the activity of all nearest neighbor nodes, is, potentially dependent on the nearest neighbor degree d_{nn} in (6). Similarly, the coefficient B_0 is, most often, a function of the parameters $\mathbf{f}$ and g in (2.1). These additional dependencies are precisely what gives rise the pre-factors $C(\mathbf{f}, g)d_{\mathrm{nn}}^\eta$ in (4), which we ignored in the present derivation (see Supplementary Section 2 for the complete derivation, which covers also these terms).

The substitution leading to Eqs. (25) and (26) represents our first approximation, where we assume that $\langle M_2(x)\rangle_{i\odot}$ is only *weakly* dependent on i's degree d_i. This weak dependence is precisely defined by the assumption that $f(d_i)$ is sub-polynomial, *e.g.*, $f(d_i) \sim \log d_i$. This implies that the neighbors of a node i with degree d_i are, to a sufficient degree, statistically similar to those of j whose degree is d_j. Under this approximation, averaging over a node's neighborhood, conditional on that node's degree, as we do in the r.h.s. of (24) is (almost) the same as averaging over the neighbors of any other node, independently of degree (indeed, up to the sub-polynomial correction $f(d_i)$). In Supplementary Section 1.2 we elaborate on the relevance of this approximation, and in Supplementary Fig. 2 we explicitly measure $f(d_i)$ for our entire testing ground of networks/dynamics. We find that $f(d_i)$ is, indeed, at most logarithmic, supporting the relevance of our approximation for our set of real/model networks.

Off-diagonal weights W_{ij}. To extract the off-diagonal terms $i \neq j$ of $\mathbb{E}(A, G, \Omega)$ we return to Eq. (11), this time writing

$$W_{ij} = \left.\frac{\partial \dot{x}_i}{\partial x_j}\right|_{\substack{x_i=R^{-1}(q_i)\\x_j=R^{-1}(q_j)}} = \left.\frac{\partial}{\partial x_j}\left(M_0(x_i) + M_1(x_i)\sum_{n=1}^{N} A_{in}M_2(x_n)\right)\right|_{\substack{x_i=R^{-1}(q_i)\\x_j=R^{-1}(q_j)}}. \tag{27}$$

Keeping only the terms that explicitly depend on x_j we obtain

$$W_{ij} = M_1(x_i)A_{ij}M_2'(x_j)\Big|_{\substack{x_i=R^{-1}(q_i)\\x_j=R^{-1}(q_j)}} = M_1\big(R^{-1}(q_i)\big)A_{ij}M_2'\big(R^{-1}(q_j)\big), \tag{28}$$

helping us identify the two relevant dynamic functions $M_1\big(R^{-1}(q_i)\big)$ and $M_2'\big(R^{-1}(q_j)\big)$, whose leading powers determine the scaling of W_{ij}. Expressing these functions as Hahn series we write

$$M_1\big(R^{-1}(q_i)\big) = \sum_{n=0}^{\infty} K_n q_i^{\Pi_n} \tag{29}$$

$$M_2'\big(R^{-1}(q_j)\big) = \sum_{n=0}^{\infty} L_n q_j^{\Theta_n}, \tag{30}$$

and in the limit of large d_i and d_j (small q_i, q_j) take only the leading terms $\sim q_i^{\Pi_0}$ and $\sim q_j^{\Theta_0}$. Substituting these terms into (2.56), and using the fact that $q_i \sim d_i^{-1}$, we arrive at

$$W_{ij} \sim d_i^{\nu} A_{ij} d_j^{\rho}, \tag{31}$$

where $\nu = -\Pi_0$ and $\rho = -\Theta_0$, recovering the prediction of Eq. (2.4), under the current setting of $G_{ij} = 1$, *i.e.* unweighted.

The obtained exponents μ, ν and ρ are all extracted from the leading powers of our derived dynamic functions $Y(R^{-1}(x))$ in (23), $M_1(R^{-1}(x))$ in (29) and $M_2'(R^{-1}(x))$ in (30). These functions, in turn, are directly linked to $M_q(x)$ in (2.1), and hence offer a direct procedure by which to extract the $\mathbb{E}(A, G, \Omega)$ Jacobian scaling relationships, as outlined in Fig. 1. The forth and final exponent η in (4) can be extracted in a similar fashion, as we show in Supplementary Section 2.

3. Practical summary - calculating Ω

While the derivation in Methods Section 2 may be elaborate, its practical outcome is rather straightforward, providing a step-by-step recipe by which to construct the exponent set $\Omega = (\eta, \mu, \nu, \rho)$ in Eqs. (4) and (2.4). First, we use the dynamic functions $M_0(x), M_1(x)$ and $M_2(x)$ of Eq. (2.1) to construct the three secondary functions

$$R(x) = -\frac{M_1(x)}{M_0(x)}, \quad Y(x) = M_1(x)R'(x), \quad Z(x) = R(x)M_2(x). \tag{32}$$

The functions $R(x)$ and $Y(x)$ are introduced in Methods Section 1 above; $Z(x)$ is derived in Supplementary Section 2. From (2.66) we extract four additional functions, which we express through a Hahn power-series expansion as

$$M_2\big(Z^{-1}(x)\big) = \sum_{n=0}^{\infty} G_n x^{\Psi_n}, \quad Y\big(R^{-1}(x)\big) = \sum_{n=0}^{\infty} C_n x^{\Phi_n},$$
$$M_1\big(R^{-1}(x)\big) = \sum_{n=0}^{\infty} K_n x^{\Pi_n}, \quad M_2'\big(R^{-1}(x)\big) = \sum_{n=0}^{\infty} L_n x^{\Theta_n} \tag{33}$$

We use $R^{-1}(x)$ and $Z^{-1}(x)$ to denote the inverse functions of $R(x)$ and $Z(x)$. The leading powers $(n = 0)$ in these Hahn series directly provide Ω via

$$\mu = 2 - \Phi_0, \quad \nu = -\Pi_0, \quad \rho = -\Theta_0, \quad \eta = -\Psi_0(\mu - \nu - \rho). \tag{34}$$

Hence, to construct $J \in \mathbb{E}(A, G, \Omega)$ we first generate the weighted network $A \circ G$, then extract the weighted degrees d_i, d_j of all nodes and the nearest neighbor degree d_{nn} of Eq. (6). The

resulting J satisfies

$$J_{ii} \sim -C(\mathbf{f}, g)d_{\mathrm{nn}}^{\eta}d_i^{\mu} \tag{35}$$

$$J_{ij} \sim d_i^{\nu}A_{ij}G_{ij}d_j^{\rho}, \tag{36}$$

where the coefficient $C(\mathbf{f}, g) > 0$ encapsulates the system's specific rate parameters (we do not attempt to predict this coefficient in the current formalism). The detailed derivation of Ω appears in Supplementary Section 2, followed by a step by step application on all our testing ground dynamics (Fig. 2) in Supplementary Section 4.

In the above formulation we have assumed that $R(x)$ and $Z(x)$ are invertible, writing $R^{-1}(x)$ and $Z^{-1}(x)$ in (2.67). In Supplementary Section 2 we explain how to properly treat non-invertible $R(x), Z(x)$. In these sections, we also demonstrate how to extract J for system's with multiple fixed-points, and, specifically, in Supplementary Section 2.5, how to construct J around a trivial fixed-point $\mathbf{x} = (0, \ldots, 0)^{\top}$.

4. The ingredients of $\mathbb{E}(A, G, \Omega)$

In Eq. (2.1) we distinguish between the nonlinear form of the functions $M_q(x)$ and their specific parameters $\mathbf{f}_{qi}$. The former, we argue, are designed to mathematically represent the nodes' intrinsic driving mechanisms, distinguishing between, *e.g.*, Epidemic vs. Biochemical dynamics. The latter, on the other hand, describes the specific rates of these mechanistic processes, which may, potentially change across nodes/links, or under different environmental conditions. To root this distinction on mathematical grounds we refer again to the Hahn expansion, and express each of the functions $M_q(x, \mathbf{f}_{qi})$ via

$$M_q(x_i, \mathbf{f}_{qi}) = \sum_{n=0}^{\infty} C_{qn}(\mathbf{f}_{qi})x_i^{\Gamma_{qn}}. \tag{37}$$

In (1.2) we distinguish between the role of the *powers* Γ_{qn} and that of the *coefficients* C_{qn}. The powers, in most cases, characterize the *functional form* of $M_q(x, \mathbf{f}_{qi})$, differentiating, for example, between $M_q(x, \mathbf{f}_{qi}) \sim x^2$ or $M_q(x, \mathbf{f}_{qi}) \sim x/(1 + x)$. These different functions are designed to represent, mathematically, distinct microscopic mechanisms, *e.g.*, social interactions vs. biological processes. As these mechanisms are ingrained into the *physics* of the interacting components, we take them, in our formulation, to be fixed and uniform across all nodes/links. In contrast, the coefficients C_{qn} are often tunable, depending on the particular rates characterizing each node's dynamics, and hence they depend on the node specific parameters $\mathbf{f}_{qi}$.

To better understand this distinction let us consider a specific example of logistic growth, a common mechanism in population dynamics. Within the dynamic framework of Eq. (2.1) this mechanism is captured by $M_0(x_i) = b_i x_i(1 - x_i/c_i)$, which written in the form (1.2), provides $M_0(x_i) = b_i x_i - (b_i/c_i)x_i^2$. Namely the coefficients are $C_{00} = b_i$ and $C_{01} = -b_i/c_i$, and the corresponding powers are $\Gamma_{00} = 1$ and $\Gamma_{01} = 2$. The crucial point is that while b_i and c_i, *i.e.* the species growth rate and the system's carrying capacity, are node dependent, and potentially affected by environmental conditions, the functional form $M_q(x_i) \sim x_i(1 - x_i)$ is intrinsic to logistic growth, and cannot be easily perturbed. This is precisely captured by the separate role of powers vs. coefficients: the tunable parameters b_i, c_i are expressed only within C_{qn}, whereas the logistic growth functional form is embedded within the powers Γ_{qn} - here describing linear growth ($\Gamma_{00} = 1$) followed by quadratic attenuation due to intra-species competition ($\Gamma_{01} = 2$).

Hence, from a strictly mathematical perspective, we define *parameters* as the factors affecting the coefficients C_{qn} in (1.2), and *functional form* via the set of participating powers Γ_{qn}. Our

interpretation of this mathematical distinction is that the powers are more intrinsic than the coefficients. Indeed, in our logistic growth example, the two powers arise from the system's ingrained driving mechanisms - of growth (linear) vs. competition (quadratic). In contrast, the coefficients depend on the parameters b_i, c_i, which may assume any value within the logistic growth framework, and can even change due to external conditions.

The crucial point is that our Jacobian scaling exponents Ω depend only on the powers Γ_{qn}, and are unrelated to the coefficients C_{qn}. Hence, in our example, all systems driven by logistic growth (and a matching interaction dynamics) will have similar Ω, regardless of the specific parameters b_i, c_i. This portrays Ω and its resulting S, as an innate built-in characteristic of the system's dynamics, detached from its multitude of microscopic parameters. Consequently, our asymptotic stable/unstable classes are intrinsic to the system's dynamics, insensitive to external perturbation or to microscopic discrepancies.

5. Generality and limitations the $\mathbb{E}(A, G, \Omega)$ ensemble

Dynamic limitations. Our ensemble $\mathbb{E}(A, G, \Omega)$ was analytically derived under the conditions defined by the Barzel-Barabási equation (2.1). Despite its general structure, we wish to emphasize that this equation still excludes several families of dynamics. For example, non-additive interactions or threshold models.[49] Similarly, if the system incorporates a mixture of distinct interaction mechanisms, such that every node/link is driven by its own idiosyncratic processes, the dynamics cannot be cast into the form $M_0(x), M_1(x), M_2(x)$.

We note, however, that while our analytical derivations are, indeed, bounded by these restrictions, the family of potential dynamics included within the $\mathbb{E}(A, G, \Omega)$ ensemble may, in fact, be broader. Specifically, in Supplementary Section 5 we consider several expansions to Eq. (2.1) that help us examine the applicability limits of our dynamic Jacobians:

- **Non-factorizable interactions**. Our testing ground includes Power dynamics, in which the interaction term cannot be partitioned into a product $M_1(x_i)M_2(x_j)$, but rather incorporates a diffusive mechanism of the form $M(x_j - x_i)$. Such dynamics, excluded from (2.1), arise in different contexts, from reaction-diffusion to synchronization,[50,51] and despite the fact that they are not covered by our anaytical framework, our analysis of Power indicates that they continue to fall within $\mathbb{E}(A, G, \Omega)$.

- **Non-additive interactions**. Another outlier in Fig. 2 is Population 2, in which the linear sum $\sum_{j=1}^{N} M_2(x_j)$ is replaced by $M_2(\sum_{j=1}^{N} x_j)$, again - outside the bounds of (2.1). Still, as shown, *e.g.*, in Fig. 3n,o, this system also has $J \in \mathbb{E}(A, G, \Omega)$.

- **Mixed dynamics**. The last assumption we challenge is the notion that all components are driven by similar dynamic processes, as expressed by the uniform functional form of $M_q(x)$ across all nodes. In Supplementary Sections 5.4 and 5.5 we examine, numerically, systems with two or three competing self or interaction dynamics. The Jacobians of such systems, we find, exhibit coexisting scaling relationships with exponent sets $\Omega_1, \Omega_2, \ldots$, corresponding to the network's distinct dynamic mechanisms. This captures a natural generalization of $\mathbb{E}(A, G, \Omega)$, that indicates the potential qualitative insight offered by our analysis, even beyond Eq. (2.1)'s technical limits.

Topological limitations. Our predicted asymptotic stability/instability is driven by the limit of large d, *i.e.* the hubs. It is therefore mainly relevant for degree-heterogeneous networks. While extreme heterogeneity is, indeed, common in many biological and social systems, there are areas, such as in ecological systems,[52] were the networks tend to be more homogeneous.

Under such conditions, our theory predicts that the system is in the sensitive class: it *could* be stable, but its stability is not guaranteed in the face of parameter perturbation.

Finally, our asymptotic predictions capture the system's global stability, but have no bearing on the dynamic stability of small motifs or sub-networks, which may be locally unstable. Still in an asymptotically stable system, the global impact of such unstable motifs, vanishes in the limit of large N, and hence the system as a whole remains insensitive to these local discrepancies. We discuss this in detail, including extensive numerical support in Supplementary Section 6.

Data availability. All empirical network data to retrieve the results shown here is available online at: https://gitlab.com/meenachandrakala/Dynamic_Stability/-/tree/master/Dynamic_Stability.

Code availability. All code to reproduce the results shown here is available online at: https://gitlab.com/meenachandrakala/Dynamic_Stability/-/tree/master/Dynamic_Stability.

Emergent stability in complex network dynamics

Supplementary information

April 25, 2023

Contents

1 Analysis framework

Our work is based on two main pillars: (i) Analytical derivations, leading to our Jacobian ensemble; (ii) Numerical simulations, examining the relevance of our theoretical predictions. Naturally, our analytics rest on a set of approximations and clean model assumptions, as we outline below. Our numerical support, on the other hand, incorporates the full complexity of the system, using both model and empirical networks, and implementing the complete nonlinear dynamics of our testing ground illustrated in Fig. 2 of the main text (*i.e.* not linearized or otherwise approximated). This allows us to test the performance of our analytical assumptions in realistic settings. Below we outline the main assumptions upon which we build our *analytical* advances, and also list the extended numerical tests we perform to examine the applicability limits of each of these assumptions.

We begin with Eq. (3) of the main text, which we write here again, for convenience

$$\frac{\mathrm{d}x_i}{\mathrm{d}t} = M_0\big(x_i(t), \mathbf{f}_{0i}\big) + g \sum_{j=1}^{N} A_{ij} M_1\big(x_i(t), \mathbf{f}_{1i}\big) G_{ij} M_2\big(x_j(t), \mathbf{f}_{2i}\big). \tag{1.1}$$

The equation has three components: The weighted network topology A, G; the rate parameters g and $\mathbf{f}_i = (\mathbf{f}_{0i}, \mathbf{f}_{1i}, \mathbf{f}_{2i})$, which we denote collectively by $\mathbf{f}$; and the dynamic functions $M_q(x)$, $q = 0, 1, 2$. We now list the assumptions we make on each of these components.

1.1 Dynamics

Assumption 1. In (1.1) we assume that the dynamic functions can be expressed as a Hahn power series around $x_i = 0$, writing

$$M_q(x_i, \mathbf{f}_{qi}) = \sum_{n=0}^{\infty} C_{qn}(\mathbf{f}_{qi}) x_i^{\Gamma_{qn}} \tag{1.2}$$

for $q = 0, 1, 2$. Here Γ_{qn} represents a sequence of real powers, $\Gamma_{qn} \in \mathbb{R}$, generalizing the classic Taylor expansion to include also negative, rational or irrational powers. This allows us to express via (1.2) practically any relevant nonlinear function including ones that cannot be Taylor expanded around zero.

In (1.2) we distinguish between the coefficients C_{qn} and the powers Γ_{qn}. The former, we assume, depend on $\mathbf{f}_{qi}$, and may therefore be distributed across all nodes. The latter, on the other hand are uniform, capturing the shared dynamic processes across all network components. Hence, our formulation asserts that the powers that participate in (1.2) define the *system's* dynamics, while the coefficients capture each *node's* potentially idiosyncratic rate parameters. This, we emphasize , is our *assumption*, that the dynamics can be expressed in this way, *i.e.*, node/link specific coefficients, but fixed powers. The interpretation and rationale behind this assumption we discuss in the main text, and, in more detail, through the examples below.

Assumption 1's motivation. To get a sense of Assumption 1 in practice we consider three functions that appear in our testing ground - logistic growth (Population), mass-action kinetics (Biochemical) and the Hill function (Regulatory). The first of these three can be expressed via (1.2) as

$$M_q(x_i, \mathbf{f}_{qi}) = b_i x_i \left(1 - \frac{x_i}{c_i}\right) = b_i x_i - \frac{b_i}{c_i} x_i^2 \tag{1.3}$$

having coefficients b_i and $-b_i/c_i$, and powers x_i^1 and x_i^2. This can be cast on the form of (1.2) by setting $C_{00} = b_i, C_{01} = -b_i/c_i$ and $\Gamma_{00} = 1, \Gamma_{01} = 2$. Here, in this context, Assumption 1 is taken to mean that all nodes undergo the same process of logistic growth, following the form $\sim x_i(1-x_i)$, *i.e.* the *powers* 1 and 2. However this logistic process may be characterized by different node-specific *rates*, namely, b_i, the growth rate and c_i, the environment carrying capacity, are potentially i-dependent. This potential diversity is expressed via the *coefficients* C_{00} and C_{01}, which are indeed the only factors in (1.3) that depend on b_i, c_i. This clearly demonstrates the different role of the two factors: the powers capture the defining features of logistic growth - linear reproduction (x_i^1) attenuated by quadratic competition $(-x_i^2)$ and therefore they are identical for all nodes; the coefficients, on the other hand, incorporate the specific rates of these two processes, which may change across nodes or due to shifting environmental conditions.

In mass-action-kinetics we consider interaction processes of the form $aX_i + bX_j \xrightarrow{g} X_{ij}$, in which a copies of X_i and b copies of X_j combine to form the compound molecule X_{ij}. This, in (1.1) leads to an interaction term following $gG_{ij}x_i^a x_j^b$, having the rate constant gG_{ij} (potentially link-specific) and the powers a, b. Here the powers represent the *order* of the interaction, which is determined by stoichiometry, and hence cannot be easily perturbed. On the other hand, the coefficient is the reaction *rate*, which is, indeed, subject to external perturbation by, *e.g.*, changing temperature or chemical affinity.

As our third example, we consider a Hill function, often encountered in regulatory or population dynamics, following

$$M_q(x_i, \mathbf{f}_{qi}) \frac{x_i^h}{1 + (x_i b_i)^h} = \left(\frac{1}{b_i}\right) x_i^h - \left(\frac{1}{b_i}\right)^2 x_i^{2h} + \cdots = \sum_{n=0}^{\infty} (-1)^n \left(\frac{1}{b_i}\right)^{n+1} x_i^{(n+1)h}. \tag{1.4}$$

Here we have $C_{qn}(\mathbf{f}_{qi}) = (-1)^n (1/b_i)^{n+1}$ and $\Gamma_{qn} = (n+1)h$. Therefore, in this example, b_i is considered a *rate parameter*, affecting the *coefficients*, whereas h is *intrinsic*, embedded in the *powers*. Indeed, h here affects the functional form of $M_q(x)$, by controlling the saturation rate of the Hill function, while b_i determines the upper value of the saturation, which, as our formalism indicates, is less intrinsic.

To summarize: we consider all (potentially nonlinear) functions $M_q(x)$ that can be expressed via (1.2); we allow diversity in the coefficients C_{qn}, but assume uniform powers Γ_{qn}. Hence all $M_q(x)$ are of the same *family* or *functional form*, *e.g.*, $\sim b_i x(1 - x/c_i)$, but with distributed *parameters* b_i, c_i. Therefore, *parameters*, in our definition, are factors that affect C_{qn}, but do not feed into the powers Γ_{qn}.

Outcome 1 - derivative functions. Throughout our derivation we apply different mathematical operations on $M_q(x)$, such as multiplication $(M_1 \times M_2)$, division (M_0/M_1), derivation (M_1'), inversion $(M_0^{-1}(x))$ or composition $(M_0(M_1(x)))$. Each of these operations preserves the separation between C_{qn} and Γ_{qn}, and hence our distinction between the node/link dependent coefficients vs. the uniform powers is equally preserved. For example, in case $F(x) = M_1(x) \times M_2(x)$ it yields a new Hahn series, whose coefficients comprise products of the form $C_{1n}C_{2m}$ and whose powers are constructed from sums of the form $\Gamma_{1n} + \Gamma_{2m}$. Therefore, $F(x)$'s expansion continues to have parameter dependent coefficients alongside parameter *in*dependent powers. A similar

separation is preserved for each of the other operations mentioned above.

Testing the limits of Assumption 1. In Supplementary Sections 5.4 and 5.5 we challenge Assumption 1 and analyze systems with mixed-dynamics, in which nodes/links are characterized by two or more different power sets Γ_{qn}, or by a continuum of powers. This helps generalize (1.1) to treat systems with several competing dynamic mechanisms.

Assumption 2. In (1.1) we take the interaction term to be factorizable, writing it in product from $M_1(x) \times M_2(x)$. This is, indeed, a common structure, observed in our range of social, biological and technological systems, as can be observed in Fig. 2 of the main text. It excludes, however, several forms of dynamics, most notably - diffusive dynamics, in which the interaction follows $M(x_j - x_i)$.

Testing the limits of Assumption 2. This assumption, while helping our analytical derivations, is by no means essential, and can, in practice, be relaxed. We demonstrate this by deriving the Jacobian from our Power dynamics (Supplementary Section 5.1, in which the interaction is given by $M(x_i, x_j) \sim \sin(x_j - x_i)$.

Assumption 3. Our final dynamic assumption is that the interactions are additive, allowing us to express them as $\sum_{j=1}^{N} A_{ij} G_{ij} \cdots M_2(x_j)$. More generally, one can also write $M_2(\sum_{j=1}^{N} A_{ij} G_{ij} x_j)$, in which i receives a nonlinear cumulative input from its surrounding neighbors.

Testing the limits of Assumption 3. This assumption is challenged by our application to Population 2 dynamics in Sec. 5.2, which is specifically designed around the form $M_2(\sum_j \cdots)$ rather than $\sum_j \cdots M_2(x_j)$.

Assumption 4. Equation (1.1) exhibits at least one fully positive fixed-point $\mathbf{x}^* = (x_1, \ldots, x_N), x_i \geq 0$, around which we seek to construct J and assess its stability. In this notation we denote the fixed-point by omitting the t dependence, *i.e.* x_i instead of $x_i(t)$, expressing the fact that these are stationary states.

Testing the limits of Assumption 4. In Sec. 5.3 we investigate population dynamics with a mixture of cooperative and adversarial interaction (positive/negative G_{ij}), under which a varying fraction of nodes undergoes extinction. We seek the limits of our framework's applicability under these conditions by observing our predicted J-patterns on the set of surviving nodes.

1.2 Weighted topology

The weighted network topology is given by $A \otimes G$, where the Hadamard product $\otimes$ represents matrix multiplication element-by-element. The $N \times N$ adjacency matrix A is large ($N \to \infty$) sparse ($\sum_{i,j} A_{ij}/N^2 \ll 1$), has no isolated components and binary ($A_{ij} \in \{0, 1\}$) with a vanishing diagonal ($A_{ii} = 0$). The elements of the weight matrix $G \geq 0$ are drawn at random from $P(G)$, capturing the probability density for a random weight to have $G_{ij} \in (G, G + \delta G)$. We categorize all nodes via their binary and weighted degrees

$$ k_i = \sum_{j=1}^{N} A_{ij}, \qquad d_i = \sum_{j=1}^{N} A_{ij} G_{ij} \ , \tag{1.5} $$

the former discrete ($k_i = 1, 2, \ldots$) and the latter continuous ($d_i \in \mathbb{R}$). The network is, therefore, characterized by the degree-distribution $P(k)$, capturing the probability that a randomly selected node i has $k_i = k$, and by the density function $P(d)$, capturing the probability density that $d_i \in (d, d + \delta d)$. For simplicity, we use a loose notation $P(x)$ to denote both discrete probability

functions ($P(X = x)$ and continuous density functions ($P_X(x)$). Therefore, the specific meaning of $P(x)$ should be deduced from context, based on the nature of x, continuous or discrete.

In (1.1) both $P(k)$ and $P(d)$ can take any arbitrary form, including homogeneous (*e.g.*, Poisson, exponential) or fat-tailed distributions (*e.g.*, scale-free). This is clearly observed, for instance, in Fig. 3 of the main text, where we implement our analysis on both Erdős-Rényi (ER) networks and scale-free (SF) networks with different weight distributions, alongside an array of empirical networks. Having said that, we also emphasize that many of our results are linked to degree-heterogeneity, from the scaling of J_{ij} with d_i, d_j to the asymptotic stability that relies on $\beta > 0$ in Eq. (9) of the main text. Therefore, such heterogeneity in $P(k)$ or $P(d)$, while, strictly speaking, is *not* a necessary condition, does, in fact, represent an underlying motivation for parts of our analysis.

In our analysis we encounter several average quantities extracted from $P(k), P(d)$. Most naturally, the average degree $\langle k \rangle$ or the average weighted degree $\langle d \rangle$. Beyond these immediate statistics we also encounter *neighborhood averages*, which we denote by

$$\langle X \rangle_{i,\odot} = \frac{1}{d_i} \sum_{j=1}^{N} A_{ij} G_{ij} X_j. \tag{1.6}$$

This captures the weighted average over observable X_j extracted from node i's direct network neighbors. In (1.6) we use the symbol $\odot$ to represent a *neighborhood*, hence $i, \odot$ is the group of i's direct neighbors. For example, $\langle d \rangle_{i,\odot}$ represents the average weighted degree of all nodes surrounding i. This allows us to express the average neighbor node d_{nn}, appearing in main text Eq. (6), via

$$d_{\mathrm{nn}} = \langle d \rangle_{\odot} = \frac{1}{N} \sum_{i=1}^{N} \langle d \rangle_{i,\odot}. \tag{1.7}$$

Here, in addition to our paper's notation d_{nn}, we also used our currently introduced $\odot$ to express the *neighborhood* average. This form of neighborhood averaging is, in fact, naturally ingrained in our dynamic equation (1.1), where we can use (1.6) to express the summation on the r.h.s. as

$$\sum_{j=1}^{N} A_{ij} G_{ij} M_2(x_j, \mathbf{f}_{2j}) = d_i \langle M_2(x) \rangle_{i,\odot} \equiv d_i \langle M \rangle_{i,\odot}. \tag{1.8}$$

This represents a direct application of (1.6) over the observable

$$M_j = M_2(x_j, \mathbf{f}_{2j}). \tag{1.9}$$

Therefore, $\langle M \rangle_{i,\odot}$ denotes the (weighted) average value of $M_2(x_j, \mathbf{f}_{2j})$ within i's direct neighborhood.

Finally, another form of averaging we encounter during our analysis is the degree-conditional averages $\langle X | d \rangle$ and $\langle X | d \rangle_{\odot}$. First we define the set

$$Q(d) = \left\{ i \in \{1, \ldots, N\} \,\middle|\, d_i \in (d, d + \delta d) \right\}, \tag{1.10}$$

comprising all nodes whose weighted degree is in the range $(d, d + \delta d)$. Such binning within the interval $(d, d + \delta d)$ is required since d is a continuous variable, and hence writing $d_i = d$ yields a group of measure zero. The conditional averages are then defined as

$$X(d) \quad = \quad \langle X | d \rangle = \frac{1}{|Q(d)|} \sum_{i \in Q(d)} X_i \qquad (1.11)$$

$$X_{\mathrm{nn}}(d) \quad = \quad \langle X | d \rangle_{\odot} = \frac{1}{Q(d)} \sum_{i \in Q(d)} \langle X \rangle_{i,\odot} = \frac{1}{|Q(d)|} \sum_{i \in Q(d)} \frac{1}{d_i} \sum_{j=1}^{N} A_{ij} G_{ij} X_j, \qquad (1.12)$$

where $|Q(d)|$ is the number of nodes in $Q(d)$. Here $X(d)$ is the average observable X_i for nodes $i \in Q(d)$, thus, for example, $x(d)$ represents the average activity of nodes with weighted degree d. Similarly, when plotting W_{ii} vs. d_i in Fig. 3 of the main text, then, formally speaking, we measured $W_{\mathrm{Diag}}(d)$, *i.e.* the average diagonal term of W over all nodes $i \in Q(d)$.

The second average, $X_{\mathrm{nn}}(d)$ in (1.12), is constructed from the neighborhood average taken over all nodes in $Q(d)$. It is, therefore, designed to characterize *neighbors* of nodes in $Q(d)$, not the $Q(d)$ nodes themselves. For example, $x_{\mathrm{nn}}(d)$ is the average activity of a randomly selected node j, given that this node is a neighbor of $i \in Q(d)$. Hence (1.11) averages over i, conditional on i's degree, while (1.12) averages over i's *neighbors* conditional on i's degree. The former, we emphasize, captures a direct dependence on the node's degree, while the latter is indirect, since the conditionality is on the neighbor's degree.

To express these conditional averages we use

$$X(d) \quad = \quad \langle X | d \rangle = \langle X \rangle f_X(d) \qquad (1.13)$$

$$X_{\mathrm{nn}}(d) \quad = \quad \langle X | d \rangle_{\odot} = \langle X \rangle_{\odot} f_{X,\odot}(d) \qquad (1.14)$$

where the functions $f_X(d)$ and $f_{X,\odot}(d)$ help link between the ensemble averages $\langle X \rangle, \langle X \rangle_{\odot}$ and and the d-conditioned averages $\langle X | d \rangle$ and $\langle X | d \rangle_{\odot}$. We, therefore arrive at four distinct forms of averaging: (i) $\langle X \rangle$ - the typical value of observable X of a randomly selected node; (ii) $\langle X \rangle_{\odot}$ - the typical value of observable X of a randomly selected neighbor; (iii) $\langle X | d \rangle$ - the typical value of X of a randomly selected node within $Q(d)$; (iv) $\langle X | d \rangle_{\odot}$ - the typical value of X of a randomly selected node, who has a neighbor within $Q(d)$.

Averages (i) and (ii) above represent *ensemble averages* and (iii) captures the direct dependence of observable X_i on d_i. To evaluate (iv) via (1.14) we list below several approaches by which to approximate $f_{X,\odot}(d)$:

Mean-field. The classic mean-field approximation assumes that all components have a statistically similar surrounding. This translates to $f_{X,\odot}(d) \approx 1$ in (1.14), namely that $X_{\mathrm{nn}}(d)$ is approximately independent of d. Under this approximation, individual nodes may be diverse, and hence $X(d)$ may be strongly dependent on d, yielding a potentially broadly distributed X across all nodes. However, the neighborhoods are assumed to be statistically uniform, and hence all nodes are, on average, exposed to a similar set of neighbors. In simple terms, consider $i \in Q(d)$ and $j \in Q(d')$, where $d \neq d'$. Node i's observable X_i is, on average $X(d)$, potentially distinct from j's $X(d')$. Yet, i's k_i neighbors and j's k_j neighbors are both extracted from the same statistical pool, and therefore, regardless of the individual differences between X_i and X_j, their *neighborhoods* are, on average, the same, *i.e.* $X_{\mathrm{nn}}(d) \approx X_{\mathrm{nn}}(d')$.

This approximation is exact in the limit where degree-correlations vanish, *e.g.*, the configuration model[1] framework, where, indeed, the information about i's degree has no bearing on the statistical properties of its neighbor j. It thus allows us to replace conditional averages $X_{nn}(d)$ by the relevant ensemble average $\langle X \rangle_{\odot} = X_{nn}$. We emphasize that this approximation only neglects the indirect dependencies ($\odot$), but continues to enable the individual node diversity via $f_X(d)$, which may depend quite strongly on d.

Assumption 5. In our derivation we employ a significantly weaker assumption than the mean-field above. While mean-field implied $f_{X,\odot}(d) \approx 1$, we, instead, assume that

$$f_{X,\odot}(d) \sim F(d) d^{\alpha}, \tag{1.15}$$

where $F(d)$ is sub-polynomial, *e.g.*, $F(d) \sim \log(d)$, complemented by a polynomial dependence with a leading exponent α. The exact structure of (1.15) depends on the specific observable X and on the detailed weighted network topology, which determines the level of degree-correlations in the system, *i.e.* how much it deviates from *mean-field*. Specifically, in case $alpha = 0$, we have $f_{X,\odot}(d) \sim F(d)$, sub-polynomial. This represent *weak degree-correlations*, in which $f_{X,\odot}(d) \neq 1$ (as in the mean-field approximation), but still, in the limit of large d, it does not *scale* with d.

Our derivation in the following sections can treat both strong ($\alpha \neq 0$) and weak ($\alpha = 0$) degree-correlations by introducing α where relevant. The specific value of α, however, for any given observable X can only be extracted from numerical/empirical data, as we have no analytical basis for *a priori predicting* α. Therefore, where relevant, we measure $f_{X,\odot}(d)$ explicitly, from each of our networks/dynamics to assess the weak/strong degree-correlations.

1.3 Parameters

Assumption 6. The parameters $\mathbf{f}_i$ may be, potentially, distributed across all nodes. In our derivation we assume that the assignment of these parameters is done at random. Therefore, we expect negligible correlations between $\mathbf{f}_i$ and A, G. As a result, i's parameters $\mathbf{f}_i$ are statistically independent of i's degree d_i. Consequently, if we consider the conditional average $\langle \mathbf{f}_i | d \rangle$, carried out over nodes with an assigned degree d, it is, statistically, the same as $\langle \mathbf{f}_i \rangle$, *i.e.* the *ensemble average*. As an example, which will become useful below, we can, specifically apply this to the coefficients of the Hahn expansion in (1.2), writing

$$\langle C_{qn}(\mathbf{f}_{qi}) | d \rangle = \langle C_{qn}(\mathbf{f}) \rangle, \tag{1.16}$$

taken to mean that if we average any of (1.2)'s coefficients associated specifically with nodes in $Q(d)$ we obtain the same outcome as averaging over the entire node ensemble. In simple terms *parameter*-wise nodes sampled from $Q(d)$ are statistically similar to those from $Q(d')$.

1.4 Additional approximations

While the above description outlines our fundamental *model assumptions*, in some instances we also use approximations to these assumptions that help us (i) advance analytically where we cannot analyze the exact system; (ii) offer a more concise derivation, avoiding overly complicated and cumbersome calculations:

Mean-field. In few specific steps during our derivation we approximate $\langle M_q(x) \rangle \approx M_q(\langle x \rangle)$ (see Sec. 2.2.1). This is exact in case $M_q(x)$ is linear, and justified if x is narrowly distributed.

Another option, which occurs quite frequently in many relevant models, is that $M_q(x)$ is sublinear, for example, the saturating function $M_2(x \to \infty) \to 1$ observed in many interactions. In this latter case, even if x is broadly distributed, $M_q(x)$ is still bounded, and hence $\langle M_q(x) \rangle$ can be evaluated via mean-field. We discuss the validity of this approximation in the relevant locations, and emphasize that, in most cases, it helps us avoid overly sophisticated notations and derivations, but, as our results indicate, it has little impact on the accuracy of our predictions.

Star-approximation. In Sec. 3 we employ a star-approximation, simplifying A into a single hub and spoke network. This is, of course, a crude simplification, needed only to extract the principal eigenvalue λ (Eq. (8) of the main text), but unrelated to our derivation of the Jacobian J itself. Hence the ensemble $\mathbb{E}(A, G, \Omega)$ is derived under Assumptions 1 - 6 above, and only λ requires the star simplification. Due to the approximate nature of Sec. 3's derivation, we accompany is by extensive numerical support, covering $\sim 10^4$ independently sampled Jacobian matrices.

2 The Jacobian ensemble $\mathbb{E}(A, G, \Omega)$

To analyze stability we seek the structure of the Jacobian matrix J, as extracted from the system's specific nonlinear interaction mechanisms. We first rewrite Eq. (1.1) as

$$\frac{\mathrm{d}x_i}{\mathrm{d}t} = F_i\big(\mathbf{x}(t)\big), \tag{2.1}$$

where

$$F_i\big(\mathbf{x}(t)\big) = M_0\big(x_i(t), \mathbf{f}_{0i}\big) + g \sum_{j=1}^{N} A_{ij} M_1\big(x_i(t), \mathbf{f}_{1i}\big) G_{ij} M_2\big(x_j(t), \mathbf{f}_{2j}\big), \tag{2.2}$$

and denote its fixed-point(s) by $\mathbf{x}^* = (x_1, \ldots x_N)^\top$, omitting the t-dependence to capture their stationary state. These fixed-points are obtained by solving the equilibrium equation

$$F_i(\mathbf{x}^*) = 0. \tag{2.3}$$

To assess the dynamic stability of each of Eq. (2.3)'s solutions we track their response to small perturbations, via the Jacobian

$$J_{ij} = \frac{\partial F_i(\mathbf{x})}{\partial x_j}\bigg|_{\mathbf{x}=\mathbf{x}^*}, \tag{2.4}$$

whose structure we obtain below. Writing

$$J = (A - I) \otimes W \tag{2.5}$$

we treat separately the diagonal terms $J_{ii} = -W_{ii}$ and the off-diagonal terms $J_{ij} = A_{ij}W_{ij}$ (I represents the identity matrix).

2.1 The fixed-points $\mathbf{x}^*$

We consider systems of the form (2.1) that exhibit at least one fully positive fixed-point $\mathbf{x}^*$. First, using Eq. (2.2) we write

$$M_0(x_i, \mathbf{f}_{0i}) + g\sum_{j=1}^{N} A_{ij} M_1(x_i, \mathbf{f}_{1i}) G_{ij} M_2(x_j, \mathbf{f}_{2j}) = 0, \tag{2.6}$$

seeking the potentially multiple equilibrium solutions of the system. Next, we use (1.8) to express the sum on the r.h.s. of the equation, obtaining

$$M_0(x_i, \mathbf{f}_{0i}) + M_1(x_i, \mathbf{f}_{1i}) g d_i \langle M \rangle_{i,\odot} = 0, \tag{2.7}$$

a direct equation for i's fixed-point value x_i. For certain dynamics Eq. (2.7) has a *trivial* solution in which $M_0(x_i) = M_1(x_i) = 0$. Most often this solution captures an inactive state in which all $x_i = 0$. Such solutions are treated separately in Sec. 2.5. Here we focus on the Jacobian around the non-trivial states of the system, where $M_0(x_i, \mathbf{f}_{0i}) \neq 0$.

For these non-trivial cases we rewrite (2.7) as

$$R_i(x_i) = \frac{1}{\langle M \rangle_{i,\odot} g d_i} \equiv q_i, \tag{2.8}$$

where

$$R_i(x_i) = R_i(x_i, \mathbf{f}_{0i}, \mathbf{f}_{1i}) = -\frac{M_1(x_i, \mathbf{f}_{1i})}{M_0(x_i, \mathbf{f}_{0i})} \tag{2.9}$$

and q_i defined in (2.8) is node i's *inverse degree*, whose value scales as $q_i \sim d_i^{-1}$. The function $R_i(x_i)$ is directly attainable from the system's dynamics, through $M_0(x_i, \mathbf{f}_{0i})$ and $M_1(x_i, \mathbf{f}_{1i})$. This function depends on i through the parameters $\mathbf{f}_{0i}, \mathbf{f}_{1i}$, and hence $R_i(x_i)$ is potentially distinct from $R_j(x_j)$.

We can now extract x_i by inverting the function $R_i(x_i)$ in (2.8), providing us with

$$x_i = R_i^{-1}(q_i), \tag{2.10}$$

in which i's fixed-point activity is described in terms of its inverse degree. In certain cases $R_i(x_i)$ in non-monotonic, and hence $R_i^{-1}(q_i)$ is ill-defined. This indicates that Eq. (2.6) has several solutions, capturing multiple fixed-points of the system. For example, in Fig. 7a we illustrate a function $R(x)$ in which $R(x) = q$ has three distinct solutions, represented by the red, yellow and green dots. Therefore, $R^{-1}(x)$ assumes three separate values at $x = q$, formally, an undefined function (Fig. 7b). To observe each of these solutions via (2.10) we focus on the different *branches* of $R(x)$ separately: first we plot $R(x)$. Then if it is non-monotonous, we identify its extremum points. This allows us to construct the different invertible branches of $R(x)$, for instance the one including only the maximum point (Branch 1, Fig. 7c,d), the one including only the minimum point (Branch 2, Fig. 7e,f) or the branch traversing through the intermediate points between these two extrema (Branch 3, Fig. 7g,h). Each of these constructions *is* invertible, and allows us to analyze all fixed-points independently using Eq. (2.10).
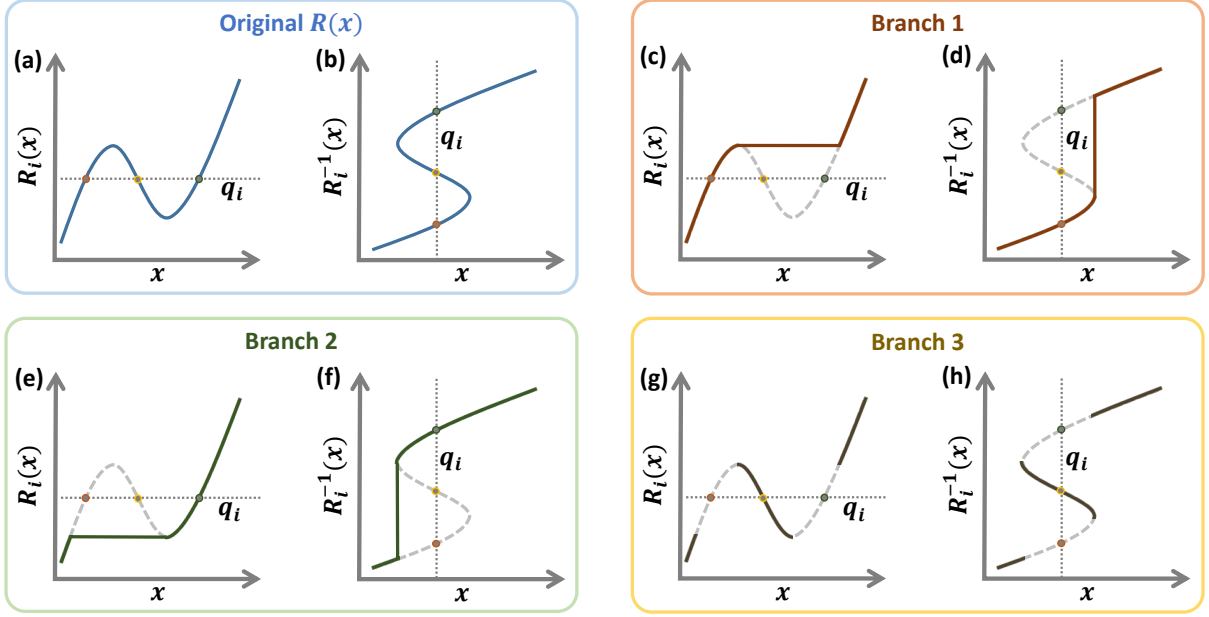
Figure 7: **Inverting a non-monotonic** $R(x)$. (a) In case $R(x)$ in (2.8) is non-monotonic its inverse function is ill-defined. (b) This leads in Eq. (2.10) to multiple solutions (orange, yellow, green), describing a potentially multi-stable system. To treat this we construct three functions, corresponding to the different branches of $R(x)$: (c)-(d) Branch 1, in which the only solution to (2.10) is the orange fixed-point; (e)-(f) Branch 2, providing the green fixed-point; (g)-(h) Branch 3, for the intermediate yellow fixed-point.

2.2 Diagonal terms W_{ii} and $W(d)$

Using (2.2) and (2.4) we can now write the diagonal Jacobian terms as

$$W_{ii} = \frac{\partial F_i(\mathbf{x})}{\partial x_i}\bigg|_{\mathbf{x}=\mathbf{x}^*} = \left(M_0'(x_i, \mathbf{f}_{0i}) + M_1'(x_i, \mathbf{f}_{1i})g\sum_{j=1}^{N} A_{ij}G_{ij}M_2(x_j, \mathbf{f}_{2j})\right)\bigg|_{\mathbf{x}=\mathbf{x}^*}, \qquad (2.11)$$

where $M_0'(x) = \partial M_0/\partial x$ and $M_1'(x) = \partial M_1/\partial x$. Once again, we use (1.8) to express the sum on the r.h.s., obtaining

$$W_{ii} = M_0'(x_i, \mathbf{f}_{0i})\bigg|_{\mathbf{x}=\mathbf{x}^*} + gd_i M_1'(x_i, \mathbf{f}_{1i})\bigg|_{\mathbf{x}=\mathbf{x}^*}\langle M\rangle_{i,\odot}, \qquad (2.12)$$

in which we condense the summation over $M_2(x_j, \mathbf{f}_{2j})$ into the neighborhood average $\langle M\rangle_{i,\odot}$. Finally, expressing the fixed-point $\mathbf{x}^*$ via (2.10) and substituting the inverse degree q_i in place of $(g\langle M\rangle_{i,\odot}d_i)^{-1}$, as per Eq. (2.8), we write

$$W_{ii} = M_0'\big(R_i^{-1}(q_i), \mathbf{f}_{0i}\big) + \frac{1}{q_i}M_1'\big(R_i^{-1}(q_i), \mathbf{f}_{1i}\big). \qquad (2.13)$$

Next we use the definition of $R_i(x_i)$ in (2.9) to write $M_0(x_i, \mathbf{f}_{0i}) = -M_1(x_i, \mathbf{f}_{1i})/R_i(x_i)$, which provides

$$M_0'(x_i, \mathbf{f}_{0i}) = -\frac{M_1'(x_i, \mathbf{f}_{1i})}{R_i(x_i)} + \frac{M_1(x_i, \mathbf{f}_{1i})R_i'(x_i)}{R_i^2(x_i)}. \qquad (2.14)$$

Substituting (2.14) into (2.13) and replacing x_i by $R_i^{-1}(q_i)$ we obtain

$$W_{ii} = -\frac{M_1'\big(R_i^{-1}(q_i), \mathbf{f}_{1i}\big)}{q_i} + \frac{M_1\big(R_i^{-1}(q_i), \mathbf{f}_{1i}\big) R_i'\big(R_i^{-1}(q_i)\big)}{q_i^2} + \frac{M_1'\big(R_i^{-1}(q_i), \mathbf{f}_{1i}\big)}{q_i}, \qquad (2.15)$$

where we used the fact that $R_i(R_i^{-1}(q_i)) = q_i$ to obtain the q_i and q_i^2 terms in the denominators. Collecting all terms, we arrive at

$$W_{ii} = \frac{1}{q_i^2} Y_i\big(R_i^{-1}(q_i), \mathbf{f}_{0i}, \mathbf{f}_{1i}\big), \qquad (2.16)$$

where $Y_i(x) = M_1(x, \mathbf{f}_{1i}) R_i'(x)$.

To obtain the asymptotic scaling of W_{ii} with d_i we use the Hahn expansion to express $Y_i(x)$ in the form of a power series, as shown in (1.2). Seeking the asymptotic limit $d_i \to \infty$, we derive our Hahn expansion around $q_i \sim d_i^{-1} \to 0$. Hence, we write

$$Y_i\big(R_i^{-1}(q_i), \mathbf{f}_{0i}, \mathbf{f}_{1i}\big) = \sum_{n=0}^{\infty} B_n(\mathbf{f}_{0i}, \mathbf{f}_{1i}) q_i^{\Phi_n}, \qquad (2.17)$$

and below, examine the leading terms only.

Following Outcome 1 in Sec. 1.1 we assert that in (2.17) the coefficients $B_n = B_n(\mathbf{f}_{0i}, \mathbf{f}_{1i})$, *i.e.* depending on the specific system parameters $\mathbf{f}$. These coefficients are therefore node-specific, since generally $\mathbf{f}_{qi} \neq \mathbf{f}_{qj}$. The powers Φ_n, however, are independent of $\mathbf{f}$, and are therefore uniform for all nodes. Indeed, $Y_i(x)$ is directly constructed from $M_q(x_i, \mathbf{f}_{qi})$ through basic function operations: multiplication ($M_1 R'$), division (M_1/M_0), inversion (R^{-1}) and derivation (R'). As explained in Outcome 1, each of these operations preserves the separation between coefficients and powers. Hence Φ_n are determined by Γ_{qn} in (1.2), but remain independent of the coefficients C_{qn}. Consequently, since Γ_{qn} are node independent, so are Φ_n.

Taking the limit $q_i \to 0$ we keep only the leading power Φ_0 in (2.17), *i.e.* $Y_i(R_i^{-1}(q_i), \mathbf{f}_{0i}, \mathbf{f}_{1i}) \approx B_0(\mathbf{f}_{0i}, \mathbf{f}_{1i}) q_i^{\Phi_0}$. This in Eq. (2.16) predicts

$$W_{ii} = B_0(\mathbf{f}_{0i}, \mathbf{f}_{1i}) q_i^{-\mu}, \qquad (2.18)$$

where

$$\mu = 2 - \Phi_0. \qquad (2.19)$$

Equation (2.18) provides the dependence of the diagonal Jacobian weight W_{ii} on i's inverse degree q_i; it is exact up to higher powers $q_i^{\Phi_1}, q_i^{\Phi_2}, \ldots$, which vanish under $q_i \to 0$. To complete our derivation we seek $W(d) = \langle W_{ii}|d \rangle$, namely the conditional average over W_{ii} given that $i \in Q(d)$. Using (1.11) we express this average as

$$W(d) = \frac{1}{|Q(d)|} \sum_{i \in Q(d)} W_{ii} = \frac{1}{|Q(d)|} \sum_{i \in Q(d)} B_0(\mathbf{f}_{0i}, \mathbf{f}_{1i}) q_i^{-\mu}, \qquad (2.20)$$

where in the last step, we expressed W_{ii} via Eq. (2.18). Next we recall Assumption 6, stating that the parameters, here $\mathbf{f}_{0i}$ and $\mathbf{f}_{1i}$, are randomly assigned, independently of d_i. This allows us, following Eq. (1.16), to extract the coefficient $B_0(\mathbf{f}_{0i}, \mathbf{f}_{1i})$ from the summation in (2.20), and

replace it by the ensemble average $\langle B_0(\mathbf{f}) \rangle$. We also reintroduce the complete expression for q_i in (2.8), thus rewriting $W(d)$ as

$$W(d) = \langle B_0(\mathbf{f}) \rangle \frac{1}{|Q(d)|} \sum_{i \in Q(d)} \left(g \langle M \rangle_{i,\odot} d_i \right)^{\mu}. \tag{2.21}$$

To advance further we note that: (i) g is a constant, and (ii) by definition, all $i \in Q(d)$ have $d_i = d$ (or more accurately $d_i \in (d, d + \delta d)$). This allows us to extract these two factors out of the summation, and further simplify (2.21) into the form

$$W(d) = \langle B_0(\mathbf{f}) \rangle g^{\mu} d^{\mu} \frac{1}{|Q(d)|} \sum_{i \in Q(d)} \langle M \rangle_{i,\odot}^{\mu} = \left(\langle B_0(\mathbf{f}) \rangle g^{\mu} \langle M^{\mu} | d \rangle_{\odot} \right) d^{\mu}, \tag{2.22}$$

where, in the final step, we used the neighborhood conditional average defined in (1.12), to express the sum over $\langle M \rangle_{i,\odot}$. We can now use Eq. (1.14) to write this conditional average as

$$\langle M^{\mu} | d \rangle_{\odot} = \langle M^{\mu} \rangle_{\odot} f_{M,\odot}(d), \tag{2.23}$$

where $\langle M^{\mu} \rangle_{\odot}$ is the network ensemble average, and $f_{M,\odot}(d) = \langle M^{\mu} | d \rangle_{\odot} / \langle M^{\mu} \rangle_{\odot}$ accounts for $\langle M^{\mu} | d \rangle_{\odot}$'s degree conditionality. Collecting all terms we arrive at

$$W(d) = \left(\langle B_0(\mathbf{f}) \rangle g^{\mu} \langle M^{\mu} \rangle_{\odot} \right) f_{M,\odot}(d) d^{\mu}, \tag{2.24}$$

in which the prefactor (in parenthesis) comprises all terms that do not contribute to the degree dependence. Next, to complete our derivation, we seek the value of $\langle M^{\mu} \rangle_{\odot}$, which we recall is equal to $\langle M_2^{\mu}(x) \rangle_{\odot}$, the average of $M_2^{\mu}(x_j, \mathbf{f}_{2j})$ over all *neighbor* nodes j.

2.2.1 Evaluating $\langle M_2^{\mu}(x) \rangle_{\odot}$

Our derivation of $W(d)$ indicates the importance of the neighborhood average

$$\langle M^{\mu} \rangle_{\odot} = \frac{1}{N} \sum_{i=1}^{N} \langle M_2^{\mu}(x) \rangle_{i,\odot} = \frac{1}{N} \sum_{i=1}^{N} \frac{1}{d_i} \sum_{j=1}^{N} A_{ij} G_{ij} M_2^{\mu}(x_j), \tag{2.25}$$

capturing the mean value of $M_2^{\mu}(x)$ over all neighborhoods. To link (2.25) to the weighted network topology A, G we use the mean-field approximation of Sec. 1.4. We note that throughout our derivation this is the only component where we employ this approximation. Indeed, $\langle M^{\mu} \rangle_{\odot}$, as opposed to, *e.g.*, x_i or $W(d)$, that were calculated above, is an aggregated function, capturing an ensemble average. It is therefore natural to evaluate this function using a mean-field approach that builds on averaging the behavior of Eq. (2.1).

We first define the weighted nearest neighbor activity as

$$x_{\text{nn}} = \langle x \rangle_{\odot} = \frac{1}{N} \sum_{i=1}^{N} \frac{1}{d_i} \sum_{j=1}^{N} A_{ij} G_{ij} x_j, \tag{2.26}$$

and its corresponding nearest neighbor weighted degree as

$$d_{\text{nn}} = \langle d \rangle_\odot = \frac{1}{N} \sum_{i=1}^{N} \frac{1}{d_i} \sum_{j=1}^{N} A_{ij} G_{ij} d_j. \tag{2.27}$$

Hence, the average nearest neighbor node is characterized by activity x_{nn} and degree d_{nn}. While x_{nn} depends on the system's dynamics (2.1), d_{nn} is fully determined by the weighted topology $A \otimes G$ through the network's weighted degree density $P(d)$. In the absence of degree correlations and under a symmetric A, G we have[2]

$$d_{\text{nn}} = \frac{\langle d^2 \rangle}{\langle d \rangle}, \tag{2.28}$$

where $\langle d^n \rangle$ is the nth moment of $P(d)$. For a homogeneous network in which $P(d)$ is bounded this predicts $d_{\text{nn}} \approx \langle d \rangle$, however, if the network is highly heterogeneous, $i.e.$ $P(d)$ is fat-tailed, we have $d_{\text{nn}} \gg \langle d \rangle$. In case the network is not symmetrical, $i.e.$ a directed A_{ij} or asymmetric weights $G_{ij} \neq G_{ji}$, we distinguish between the in/out degrees of all nodes as

$$d_{i,\text{in}} = \sum_{j=1}^{N} A_{ij} G_{ij}; \quad d_{i,\text{out}} = \sum_{j=1}^{N} A_{ji} G_{ji} \, , \tag{2.29}$$

obtaining[2]

$$d_{\text{nn}} = \frac{\langle d_{\text{in}} d_{\text{out}} \rangle}{\langle d \rangle}, \tag{2.30}$$

incorporating a mixed moment - the average over the product $d_{i,\text{in}} d_{i,\text{out}}$.

More generally, in case the network also features measurable degree-correlations we use the conditional density function $P(d|d')$ to express the probability density to observe $d_i \in (d, d+\delta d)$, given that i's neighbor has degree d'. This allows us to write[4]

$$d_{\text{nn}} = \int_{d_{\text{min}}}^{\infty} \int_{d_{\text{min}}}^{\infty} dP(d|d') P(d') \, \mathrm{d}d \, \mathrm{d}d', \tag{2.31}$$

accounting for the potential degree dependence between neighboring nodes. In all cases, from (2.28) to the more general (2.31), under extreme degree-heterogeneity, d_{nn} may diverge with system size as[1]

$$d_{\text{nn}} \sim N^\beta, \tag{2.32}$$

with β determined by the network/weight heterogeneity.

To link $\langle M^\mu \rangle_\odot$ to d_{nn} and x_{nn} we use the mean-field formalism presented in Ref.[2], allowing to use to write a direct equation for a *nearest neighbor* node. While the precise derivation and validity limits of this formalism are detailed therein, here, for conciseness, we use a brief, shorthand, derivation, outlining all the crucial approximations along the path. We begin by writing our fixed-point condition in the form of (2.3), namely

$$F_i(\mathbf{x}^*) = 0. \tag{2.33}$$

12

We then apply our nearest neighbor averaging to write

$$\langle F_i(\mathbf{x}^*)\rangle_\odot = 0, \tag{2.34}$$

which taking $F_i(\mathbf{x}^*)$ from Eq. (2.7), provides

$$\langle M_0(x_i)\rangle_\odot + g\langle M_1(x_i)d_i\langle M\rangle_{i,\odot}\rangle_\odot = 0 \tag{2.35}$$

We can employ the mean-field approximation to break down the second average on the l.h.s. and write it as a product of three separate averages, *i.e.* we neglect correlations between the terms. This brings us to

$$\langle M_0(x_i)\rangle_\odot + g\langle M_1(x_i)\rangle_\odot\langle d_i\rangle_\odot\langle\langle M\rangle_{i,\odot}\rangle_\odot = 0, \tag{2.36}$$

which we can simplify term by term: first we use, again, the mean-field approximation of Sec. 1.4 to write $\langle M_0(x_i)\rangle_\odot \approx M_0(\langle x\rangle_\odot) = M_0(x_{\mathrm{nn}})$ and, analogously $\langle M_1(x_i)\rangle_\odot \approx M_1(x_{\mathrm{nn}})$. Next, we note that $\langle d_i\rangle_\odot$ is, by definition equal to d_{nn}. Finally if we write $\langle\langle M\rangle_{i,\odot}\rangle_\odot$ explicitly we obtain

$$\langle\langle M\rangle_{i,\odot}\rangle_\odot = \frac{1}{N}\sum_{m=1}^{N}\frac{1}{d_m}\sum_{j=1}^{N}A_{mj}G_{mj}\langle M_2(x_j)\rangle_{j,\odot}, \tag{2.37}$$

an average over all neighbors' neighbors, which, under our mean-field assumption is identical to averaging over all neighbors. Hence, for the last term we write $\langle\langle M\rangle_{i,\odot}\rangle_\odot = \langle M_2(x_j)\rangle_\odot \approx M_2(x_{\mathrm{nn}})$, again employing Sec. 1.4's mean-field assumption. Collecting all terms this brings us to

$$M_0(x_{\mathrm{nn}}) + gd_{\mathrm{nn}}M_1(x_{\mathrm{nn}})M_2(x_{\mathrm{nn}}) = 0, \tag{2.38}$$

a self-consistent equation for the average neighbor (degree d_{nn}) activity x_{nn}; we once again refer the reader to Ref.[2] for a more formal derivation of (2.38). Using $R(x_{\mathrm{nn}}) = -M_1(x_{\mathrm{nn}})/M_0(x_{\mathrm{nn}})$ as in (2.8) we arrive at

$$Z(x_{\mathrm{nn}}) = \frac{1}{gd_{\mathrm{nn}}} \equiv q_{\mathrm{nn}}, \tag{2.39}$$

where $Z(x) = R(x)M_2(x)$ is a dynamic function, fully determined by $M_0(x), M_1(x), M_2(x)$ in (1.1), and q_{nn} is the inverse nearest neighbor degree.

By inversion we obtain

$$x_{\mathrm{nn}} = Z^{-1}(q_{\mathrm{nn}}), \tag{2.40}$$

and hence

$$M_2(x_{\mathrm{nn}}) = M_2\big(Z^{-1}(q_{\mathrm{nn}})\big). \tag{2.41}$$

Similarly to $R_i(x_i)$ in (2.8) the dynamic function $Z(x)$ may also be non-invertible in case the

system has multiple fixed-points. We treat this by considering the different branches of $Z(x)$, following a similar analysis to the one shown in Fig. 7. Below, in Sec. 4.2 we show in detail how we treat such non-ivertibility, which arises naturally during our analysis of Regulatory dynamics.

To obtain the asymptotic scaling of $M_2(x_{nn})$ on d_{nn} we use the Hahn expansion to express (2.41) in the form of a power series around $q_{nn} \to 0$, *i.e.* large d_{nn}. Hence we write

$$M_2\big(Z^{-1}(q_{nn})\big) = \sum_{n=0}^{\infty} G_n q_{nn}^{\Psi_n}, \tag{2.42}$$

where Ψ_n, once again, is a set of real powers in ascending order with n. In the limit of large d_{nn} (small q_{nn}) the expansion in (2.42) is dominated by the leading power Ψ_0, predicting that

$$M_2(x_{nn}) \sim d_{nn}^{\xi}, \tag{2.43}$$

where

$$\xi = -\Psi_0. \tag{2.44}$$

As in the case of $Y_i(R^{-1}(q_i))$ in (2.17), also here, thanks to Outcome 1 of Sec. 1.1 the powers Ψ_n are directly linked to the powers Γ_{qn} of the dynamic functions $M_q(x)$ in (1.2). Indeed, to arrive at the composite function $M_2(Z^{-1}(x))$, we used standard operations of division ($R = -M_1/M_0$), multiplication ($Z = RM_2$), inversion ($Z^{-1}(x)$) and finally composition ($M_2(Z^{-1}(x))$) - all maintaining the separation of powers and coefficients.

To complete our derivation we refer back to $\langle M^\mu \rangle_\odot = \langle M_2^\mu(x) \rangle_\odot$. Through our mean-field approximation we write $\langle M^\mu \rangle_\odot \approx M_2^\mu(x_{nn})$, which using (2.43) provides $\langle M^\mu \rangle_\odot \sim d_{nn}^{\xi\mu}$. With this at hand we now return to $W(d)$ in (2.24) and replace the term $\langle M^\mu \rangle_\odot$ with $d_{nn}^{\xi\mu}$, obtaining

$$W(d) \sim \Big(\langle B_0(\mathbf{f}) \rangle g^\mu \Big) d_{nn}^{\xi\mu} f_{M,\odot}(d) d^\mu. \tag{2.45}$$

One more step remains to fully characterize $W(d)$, extracting the unknown function $f_{M,\odot}(d)$. Therefore, to complete our analysis we seek to evaluate $f_{M,\odot}(d)$, which, according to Eq. (2.23), represents the ratio

$$f_{M,\odot}(d) = \frac{\langle M^\mu | d \rangle_\odot}{\langle M^\mu \rangle_\odot} \tag{2.46}$$

between the degree conditional average $\langle M^\mu | d \rangle_\odot$ and the ensemble average $\langle M^\mu \rangle_\odot$. In accordance with Assumption 5 (Eq. (1.15) of Sec. 1.2) we examine whether we observe a polynomial dependence of the form $f_{M,\odot}(d) \sim F(d) d^\alpha$ or, alternatively, only the sub-polynomial $F(d)$ with $\alpha = 0$. Therefore, in Fig. 8 we extract $f_{M,\odot}(d)$ numerically, by simulating each of our dynamical systems, and calculating both $\langle M^\mu | d \rangle_\odot$ and $\langle M^\mu \rangle_\odot$ - the first by averaging the value of $M_2^\mu(x_i)$ over all neighborhoods surrounding a degree d node, and the second by averaging over *all* neighborhoods, independently of degree. Taking the ratio $\langle M^\mu | d \rangle_\odot / \langle M^\mu \rangle_\odot$ we obtain, numerically, the precise form of $f_{M,\odot}(d)$, for our seven models, each with its five underlying networks (35 systems altogether). Quite consistently, we find that $f_{M,\odot}(d)$ is sub-polynomial, *i.e.* $\alpha = 0$, and, in fact, can be well-approximated by $f_{M,\odot}(d) \approx 1$. This indicates that with respect to $\langle M^\mu \rangle_\odot$ our weak-dependency assumption (sub-polynomial $f_{M,\odot}(d)$), and, in fact, even the stronger
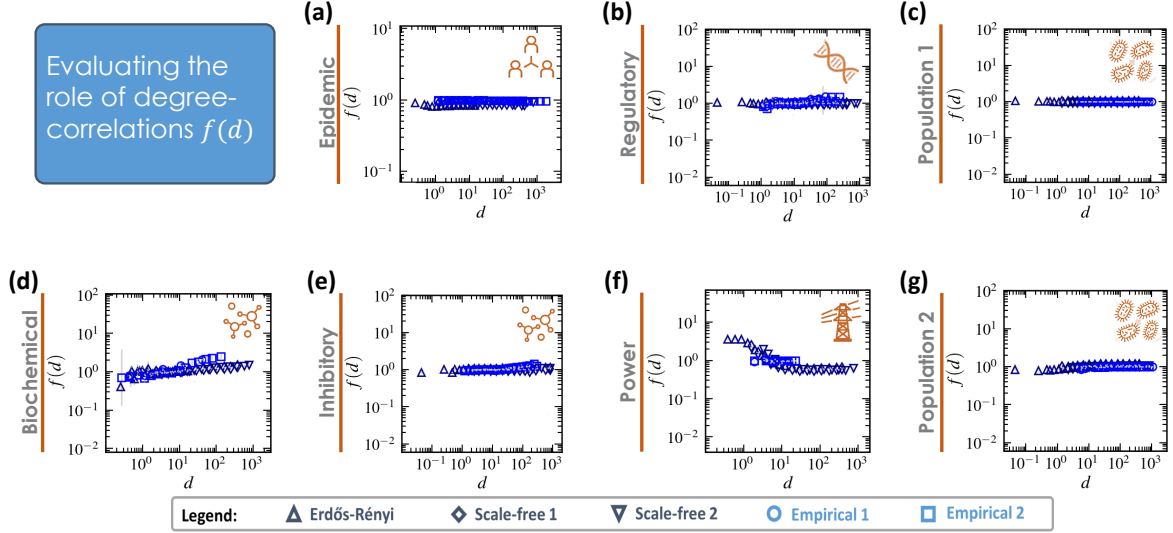
Figure 8: **Evaluating the degree correction function** $f_{M,\odot}(d)$. We used Eq. (2.46) to numerically evaluate $f_{M,\odot}(d) = \langle M^\mu|d\rangle_\odot / \langle M^\mu\rangle_\odot$, capturing the role of degree-correlations on the average neighbor activity. Results were obtained for each of our dynamic models implemented on both model and relevant empirical networks. In all cases we find that $f_{M,\odot}(d)$ is largely independent of d, roughly following $f_{M,\odot}(d) \sim 1$. Consequently, this correction to the mean-filed assumption $\langle X|d\rangle_\odot \approx \langle X\rangle_\odot$ has a negligible impact on our predicted scaling patterns.

mean-field approximation ($f_{X,\odot}(d) \approx 1$) can capture, quite accurately, the system's dynamics.

This outcome, we emphasize, is not at all surprising. Indeed, the meaning of $\langle X|d\rangle_\odot$, as defined in (1.12), is the average of X_j carried our over the *neighbors* of i ($A_{ij} = 1$), under the condition that i's weighted degree is around d ($i \in Q(d)$). The crucial point is that this condition is on i, while the averaging is on i's neighborhood, not on i itself. Therefore, the information that $i \in Q(d)$ has only an indirect influence on the value of X_j, when averaged over i's k_i nearest neighbors. This indirect effect underlies the observed weak (sub-polynomial) dependence of $\langle X|d\rangle_\odot$ on d.

We can now characterize the different factors that shape $W(d)$ in (2.45). The first terms in the parenthesis depend on the global parameters $\mathbf{f}, g$, and hence we can express it implicitly via the coefficient $C(\mathbf{f}, g)$. Following is the scaling with d_{nn}, which is a global *network* parameter, determined by $A \otimes G$, multiplying all diagonal terms, irrespective of d. This brings us to the last two terms that explicitly depend on d: $f_{M,\odot}(d)$ which we found to have a negligible effect, and d^μ, which, in the limit of large d dominates the scaling of $W(d)$. Taken together this provides

$$W(d) \sim C(\mathbf{f}, g) d_{\mathrm{nn}}^{\xi\mu} d^\mu, \qquad (2.47)$$

where μ and ξ are taken from (2.19) and (2.44), respectively. Using our Jacobian structure $J = (A - I) \otimes W$, we construct the diagonal of J as

$$J_{ii} = -W(d_i), \qquad (2.48)$$

precisely recovering Eq. (5) of the main text; see our more detailed discussion of this and other related points in Sec. 2.4.

Equation (2.48) describes our ensemble approximation: the *real* Jacobian diagonal terms are provided by (2.11), which is exact, and may be potentially distinct even for nodes with identical degrees. These *exact* terms are measured numerically and represented by symbols in Fig. 3

15

of the main text. Our *analytically predicted* Jacobians, on the other hand, approximate these exact terms by estimating each diagonal entry via (2.48). This evaluates J_{ii} by substituting i's weighted degree d_i into (2.47), yielding an identical entry for all nodes of similar degree. Such approximation is designed to capture J_{ii}'s ensemble average, namely

$$-W(d) = \frac{1}{|Q(d)|} \sum_{i \in Q(d)} J_{ii}, \tag{2.49}$$

the average diagonal Jacobian entry for nodes of degree $d_i \in (d, d+\delta d)$. This analytical construction is represented by the orange solid lines in Fig. 3 of the main text, and shown to accurately capture the exact J (blue symbols).

2.3 The off-diagonal terms W_{ij} and $W(d_1, d_2)$

The off-diagonal Jacobian terms are given by

$$W_{ij} = \frac{\partial F_i(\mathbf{x})}{\partial x_j}\bigg|_{\mathbf{x}=\mathbf{x}^*} = \frac{\partial}{\partial x_j} \left(M_0(x_i, \mathbf{f}_{0i}) + M_1(x_i, \mathbf{f}_{1i}) g \sum_{j=1}^{N} A_{ij} G_{ij} M_2(x_j, \mathbf{f}_{2j}) \right)\bigg|_{\mathbf{x}=\mathbf{x}^*}, \tag{2.50}$$

which after collecting only the terms that explicitly depend on x_j reduces to

$$W_{ij} = M_1(x_i, \mathbf{f}_{1i}) g A_{ij} G_{ij} M_2'(x_j, \mathbf{f}_{2j})\big|_{\mathbf{x}=\mathbf{x}^*}. \tag{2.51}$$

Expressing the fixed-point activities via (2.10) we write (2.51) in the form

$$\widetilde{W}_{ij} = M_1\big(R_i^{-1}(q_i), \mathbf{f}_{1i}\big) g A_{ij} M_2'\big(R_j^{-1}(q_j), \mathbf{f}_{2j}\big), \tag{2.52}$$

where $\widetilde{W}_{ij} = W_{ij}/G_{ij}$ is the *weight-less* off-diagonal Jacobian entry. This naturally giver rise to two dynamic functions

$$M_1\big(R_i^{-1}(q_i), \mathbf{f}_{1i}\big) = \sum_{n=0}^{\infty} K_n(\mathbf{f}_{1i}) q_i^{\Pi_n} \tag{2.53}$$

$$M_2'\big(R_j^{-1}(q_j), \mathbf{f}_{2j}\big) = \sum_{n=0}^{\infty} L_n(\mathbf{f}_{2j}) q_j^{\Theta_n}, \tag{2.54}$$

both constructed directly from $M_q(x)$. Once again, thanks to Outcome 1 (Sec. 1.1) the powers Π_n, Θ_n are parameter independent, and hence uniform for all nodes pairs i, j. Taking the limit of small q_i, q_j (large d_i, d_j) we keep only the leading powers of (2.53) and (2.54), which in (2.52) provides

$$\widetilde{W}_{ij} = g A_{ij} K_0(\mathbf{f}_{1i}) L_0(\mathbf{f}_{2j}) q_i^{\Pi_0} q_j^{\Theta_0} + \cdots, \tag{2.55}$$

exact upto higher order terms $q_i^{\Pi_1}, q_j^{\Theta_1}, \dots$. Using $q_i = (\langle M \rangle_{i,\odot} g d_i)^{-1}$ as per Eq. (2.8), we arrive at

16

$$\widetilde{W}_{ij} = gA_{ij}K_0(\mathbf{f}_{1i})L_0(\mathbf{f}_{2j})\left(\frac{1}{\langle M\rangle_{i,\odot}gd_i}\right)^{\Pi_0}\left(\frac{1}{\langle M\rangle_{j,\odot}gd_j}\right)^{\Theta_0}, \tag{2.56}$$

in which the dependence on d_i, d_j is made explicit.

Similar to our calculation of $W(d)$ from W_{ii}, also here we seek to average $\widetilde{W}_{ij}$ over the set $Q(d_1, d_2) = \{i, j = 1, \ldots, N | A_{ij} = 1, i \in Q(d_1), j \in Q(d_2)\}$, namely the set of all interacting node pairs ($A_{ij} = 1$) whose degrees are $d_i \in (d_1 + \delta d_1), d_j \in (d_2 + \delta d_2)$. Hence we write

$$W(d_1, d_2) = \frac{1}{|Q(d_1, d_2)|}\sum_{(i,j)\in Q(d_1,d_2)}\widetilde{W}_{ij}, \tag{2.57}$$

providing the average magnitude of the (weight-less) Jacobian entry linked to i, j pairs within $Q(d_1, d_2)$. Carrying out this average we reconstruct the steps that have already led us to $W(d)$ in (2.45). Hence, to avoid a lengthy repetition, we simply follow the analysis along the already established path from (2.20) to (2.45): (i) The coefficients $K_0(\mathbf{f}_{1i}), L_0(\mathbf{f}_{2j})$ are replaced by their ensemble averages (Assumption 6); (ii) The parameter g can be extracted out from the average (it is constant); (iii) d_i and d_j are replaced by d_1 and d_2, respectively, since all nodes in the summation are in $Q(d_1, d_2)$; (iv) The neighborhood averages $\langle M\rangle_{i,\odot}$ and $\langle M\rangle_{j,\odot}$ translate to the degree conditioned averages $\langle M|d_1\rangle_\odot$ and $\langle M|d_2\rangle_\odot$. These d-averages can be expressed via (2.23) as

$$\langle M|d_1\rangle_\odot = \langle M\rangle_\odot f_{M,\odot}(d_1) \qquad \langle M|d_2\rangle_\odot = \langle M\rangle_\odot f_{M,\odot}(d_2) , \tag{2.58}$$

in which $\langle M\rangle_\odot$ is the ensemble average (independent of d) and $f_{M,\odot}(d)$ has been already shown to have a negligible contribution to the degree-scaling (Fig. 8). Substitutions (i) - (iv) leave us with

$$W(d_1, d_2) = \left(g^{1-\Pi_0-\Theta_0}\langle K_0(\mathbf{f})\rangle\langle L_0(\mathbf{f})\rangle\right)\langle M\rangle_\odot^{-\Pi_0-\Theta_0}d_1^{-\Pi_0}d_2^{-\Theta_0}, \tag{2.59}$$

where we have, indeed, neglected the terms associated with $f_{M,\odot}(d)$.

As we are only interested in the asymptotic scaling with d_1, d_2 we neglect all terms that do not contribute the scaling, namely all terms in the parenthesis. We also use our analysis in Sec. 2.2.1, where we have shown that $\langle M\rangle_\odot \sim d_{\mathrm{nn}}^\xi$ to express the relevant term in (2.59). This leads us to our final result

$$W(d_1, d_2) \sim d_{\mathrm{nn}}^{\xi(\nu+\rho)}d_1^\nu d_2^\rho \tag{2.60}$$

where

$$\nu = -\Pi_0, \quad \rho = -\Theta_0, \tag{2.61}$$

and ξ is taken from (2.44).

2.4 Piecing together the J_{ij} puzzle

We now refer back to Eq. (2.5) to bring together the diagonal J_{ii} in (2.48) and the off-diagonal W_{ij} derived above. First, we recall that for the off-diagonal terms our derivation provided us with $W(d_1, d_2)$, which is aggregated from the weight-less $\widetilde{W}_{ij}$ of (2.52). To obtain the actual off-diagonal terms of J we must reintroduce the weights as $W_{ij} = G_{ij}W(d_i, d_j)$, namely multiply (2.60) by G_{ij} and replace d_1, d_2 by d_i, d_j (this substitution $d_1 \rightarrow d_i, d_2 \rightarrow d_j$ is similar to the substitution $d \rightarrow d_i$ conducted in (2.48), see discussion that followed therein). Next, we piece all our results together to construct the complete Jacobian as appears in Eq. (2.5), *i.e.* $J = (A - I) \otimes W$, obtaining

$$J_{ij} = A_{ij}W_{ij} - I_{ij}W_{ii} = -I_{ij}C(\mathbf{f}, g)d_{\mathrm{nn}}^{\xi\mu}d_i^{\mu} + A_{ij}G_{ij}d_{\mathrm{nn}}^{\xi(\nu+\rho)}d_i^{\nu}d_j^{\rho}. \qquad (2.62)$$

The first term on the r.h.s. represents the (negative) diagonal entries, and second term captures the off-diagonal entries, which are non-zero only if $A_{ij} = 1$. As we are only interested in the sign of the principle eigenvalue, but not in its specific magnitude, we have the degree of freedom to multiply J by an arbitrary constant. We therefore normalize J by $d_{\mathrm{nn}}^{-\xi(\nu+\rho)}$, providing

$$J_{ii} \quad \sim \quad -C(\mathbf{f}, g)d_{\mathrm{nn}}^{\eta}d_i^{\mu} \qquad (2.63)$$

$$J_{ij} \quad \sim \quad d_i^{\nu}A_{ij}G_{ij}d_j^{\rho} \qquad (2.64)$$

for the diagonal and off-diagonal terms respectively, with $\eta = \xi(\mu - \nu - \rho)$ - recovering Eqs. (4) and (5) of the main text.

Equations (2.63) and (2.64) describe the asymptotic structure of the diagonal and off-diagonal Jacobian terms, as extracted from the dynamics of Eq. (2.1). The resulting J is characterized by several distinct structural and dynamic inputs: A, the network topology, which determines the non-vanishing off-diagonal elements. Together with the link weights G it also determines the degrees d_i, d_j and the average neighbor degree d_{nn}. The exponents

$$\Omega = (\eta, \mu, \nu, \rho) \qquad (2.65)$$

are independent of the network topology, extracted from the dynamic functions $M_q(x)$. These exponents are universal in the sense that they do not depend of the specific model *parameters* $g, \mathbf{f}$, but rather on the powers Γ_{qn} in (1.2), grouping together all systems which follow the same *model*, *i.e.* Epidemic, Regulatory etc. The coefficient C, in contrast, is non-universal, and its value is determined by the specific rate-constants and time-scales driving Eq. (2.1), for example, the distribution of $\mathbf{f}$ or the value of g; here we do not attempt to predict the magnitude of this coefficient. In the limit of sufficiently large d_i and d_j, and, where applicable - in the limit of large d_{nn}, the specific finite value of C has negligible impact on the principal eigenvalue of J as we explicitly show in Sec. 3. Hence, in this limit, stability is asymptotically determined by the exponents Ω, irrespective of C. The meaning is that the *model* can be asymptotically stable or unstable, regardless of its specific *parameters*.

2.4.1 Impact of $P(d)$ and d_{nn}

In this derivation we considered the scaling of J on the weighted degrees d_i, d_j, and on the nearest neighbor degree d_{nn}. Valid under the general assumptions listed in Sec. 1, the discussion

The ensemble $\mathbb{E}(A, G, \Omega)$ summary. Staring from Eq. (2.1) we use $M_0(x)$, $M_1(x)$ and $M_2(x)$ to construct the functions

$$R(x) = -\frac{M_1(x)}{M_0(x)}, \quad Y(x) = M_1(x)R'(x), \quad Z(x) = R(x)M_2(x). \tag{2.66}$$

For each of these functions, we set the parameters $\mathbf{f}_{qi}$ to their ensemble averages. The powers we extract below are, in any case, independnet of these parameters. From (2.66) we extract the four relevant power-series expansions

$$M_2\big(Z^{-1}(x)\big) = \sum_{n=0}^{\infty} G_n x^{\Psi_n}, \quad Y\big(R^{-1}(x)\big) = \sum_{n=0}^{\infty} B_n x^{\Phi_n},$$

$$M_1\big(R^{-1}(x)\big) = \sum_{n=0}^{\infty} K_n x^{\Pi_n}, \quad M_2'\big(R^{-1}(x)\big) = \sum_{n=0}^{\infty} L_n x^{\Theta_n} \tag{2.67}$$

whose leading powers determine the dynamic exponents $\Omega = (\eta, \mu, \nu, \rho)$ as

$$\mu = 2 - \Phi_0, \quad \nu = -\Pi_0, \quad \rho = -\Theta_0, \quad \eta = -\Psi_0(\mu - \nu - \rho). \tag{2.68}$$

To construct $J \in \mathbb{E}(A, G, \Omega)$ (around a non-trivial fixed-point) we first assign the network/weights A, G, then extract the weighted degrees d_i of all nodes and the nearest neighbor degree d_{nn} from Eq. (2.27). The resulting J satisfies

$$J_{ii} \quad \sim \quad -C d_{\mathrm{nn}}^{\eta} d_i^{\mu} \tag{2.69}$$

$$J_{ij} \quad \sim \quad d_i^{\nu} A_{ij} G_{ij} d_j^{\rho}, \tag{2.70}$$

where the constant $C > 0$ is arbitrary.

becomes especially relevant when $P(d)$ is fat-tailed, *e.g.*, scale-free, where degrees, indeed, span orders of magnitude, and the scaling relationships reach their asymptotic limit. Specifically, as the hub-degrees and the nearest neighbor degree can potentially diverge with N, we can obtain our predicted asymptotic classes.

The role of d_{nn}. While d_i is a node specific attribute, that captures a specific dependency between the ith diagonal term and i's weighted degree, the pre-factor d_{nn}^{η} in (2.63) represents a network aggregated parameter, indeed - a *constant*, whose impact is often negligible in the asymptotic limit of large d. We include it in our analysis, however, because under extreme degree-heterogeneity, we may observe that d_{nn} diverges as $d_{\mathrm{nn}} \sim N^{\beta}$ (2.32), and therefore *can* potentially impact the system's stability in the limit $N \to \infty$. For example, in a random scale-free network where $P(d) \sim d^{-\gamma}$, we can use $d_{\mathrm{nn}} = \langle d^2 \rangle / \langle d \rangle$ in (2.28) to obtain

$$d_{\mathrm{nn}} \sim \begin{cases} N & \gamma < 2 \\ N^{3-\gamma} & 2 \leq \gamma < 3 \\ \log(N) & \gamma \geq 3 \end{cases}, \tag{2.71}$$

which scales with N as long as $\gamma < 3$. There are, however, broad conditions, that arise quite naturally in many real systems, in which the d_{nn} term in (2.63) can be neglected, helping us simplify the stability analysis:

Finite d_{nn}. In case $\gamma \geq 3$, d_{nn} no longer scales with N, it behaves as a constant and has

no impact in the asymptotic limit. Under these conditions it suffices to write Eq. (2.63) as $J_{ii} \sim -C d_i^{\mu}$, with d_{nn} effectively encapsulated within C.

Bounded activities. In some models the activities x_i are bounded. For example, in spreading processes, from epidemics to cascading failures, the activities satisfy $0 \le x_i \le 1$. Under these conditions the leading power in the power-series expansion of (2.10) is zero, and hence $x(d \to \infty) \sim 1$. The result is that the nearest neighbor activity x_{nn}, associated with degree d_{nn} is itself bounded, and even if $d_{\mathrm{nn}} \to \infty$ as in Eq. (2.71), we still have $x_{\mathrm{nn}} \sim 1$. Consequently $M_2(x_{\mathrm{nn}})$ in (2.41) also approaches a constant value, and therefore the leading power in the expansion (2.42) is $\Psi_0 = 0$. This provides, based on Eq. (2.44), $\xi = 0$, which in turn leads to $\eta = 0$ in (2.63), again resulting in $J_{ii} \sim -C d_i^{\mu}$, independent of d_{nn}.

Saturating $M_2(x)$. Another common feature in many relevant models is that $M_2(x_j \to \infty) \to 1$. This represents the saturating impact of node j on its nearest neighbor i, as frequently observed in regulatory processes or in population dynamics. Once again, we have $M_2(x_{\mathrm{nn}}) \sim 1$ in the limit of large x_{nn}, providing $\xi = 0$, and consequently $\eta = 0$ in (2.63).

These rather frequent scenarios, observed, *e.g.*, in our Epidemic, Regulatory, Population and Power dynamics provide a simplifies J, in which $\eta = 0$, omitting d_{nn} from the stability analysis. In Biochemical and Inhibitory, on the other hand, we have $\eta \ne 0$, and hence the d_{nn} term cannot be neglected.

2.5 J around a trivial fixed-point

Our derivation up to this point relied on the function $R_i(x_i) = -M_1(x_i, \mathbf{f}_{1i})/M_0(x_i, \mathbf{f}_{0i})$, which becomes undefined in case $M_0(x_i, \mathbf{f}_{0i}) = 0$. This represents a *trivial* fixed-point, in which the activities satisfy

$$x_i = M_0^{-1}(0, \mathbf{f}_{0i}). \tag{2.72}$$

Returning to Eq. (2.6), we write

$$M_0(x_i, \mathbf{f}_{0i}) + g \sum_{j=1}^{N} A_{ij} G_{ij} M_1(x_i, \mathbf{f}_{1i}) M_2(x_j, \mathbf{f}_{2j}) = 0, \tag{2.73}$$

which, if $M_0(x_i, \mathbf{f}_{0i}) = 0$, can only be solved by setting either $M_1(x_i, \mathbf{f}_{1i}) = 0$ for all i or $M_2(x_j, \mathbf{f}_{2j}) = 0$ for all j. In the first case we write

$$x_i = M_1^{-1}(0, \mathbf{f}_{1i}), \tag{2.74}$$

and in the second case we have

$$x_j = M_2^{-1}(0, \mathbf{f}_{2j}). \tag{2.75}$$

In principle such conditions may arise under a general x_i, including $x_i \ne 0$. However, having *all* x_i satisfy at least two of the conditions (2.72), (2.74) and (2.75) is extremely unlikely under a *natural* selection of $M_0(x), M_1(x)$ and $M_2(x)$, unless one specifically designs these functions to sustain such solutions. Indeed, one must sets all links A_{ij}, weights G_{ij} and rate constants $\mathbf{f}, g$, together with the functional form of $M_0(x), M_1(x)$ and $M_2(x)$ to have a non-zero $\mathbf{x}^*$ that

simultaneously solves all N equations of (2.73). Such *fine-tuning*, indeed a specific and highly non-random design, is excluded from our derivation, which is centered around complex, typically random, and most often heterogeneous systems. In simple terms, the probability for such solution to exist within our dynamic ensemble is practically zero.

The natural exception to the above fine-tuned solution is the trivial solution $x_i = 0$ for all i, which, indeed, arises in many real-world systems, including ones examined in the present analysis. For example, in Epidemic dynamics, the healthy state $x_i = 0$ has $M_0(x_i, \mathbf{f}_{0i}) = -f_i x_i = 0$, and $M_2(x_j) = x_j = 0$, hence satisfying (2.72) and (2.75). In Population 1, the null-state has $M_0(x_i, \mathbf{f}_{0i}) = b_i x_i (1 - x_1/c_i) = 0$, $M_1(x_i, \mathbf{f}_{1i}) = x_i = 0$ and $M_2(x_j, \mathbf{f}_{2j}) = F(x_j) = 0$, satisfying all three conditions simultaneously. Finally, in Inhibitory and Regulatory, the null-state has $M_0(x_i = 0, \mathbf{f}_{0i}) = M_1(x_i = 0, \mathbf{f}_{1i}) = 0$ and $M_0(x_i = 0, \mathbf{f}_{0i}) = M_2(x_j = 0, \mathbf{f}_{2j}) = 0$, respectively, once again satisfying two of the conditions (2.72) - (2.75). This specific state - the null state $\mathbf{x}^* = (0, \ldots, 0)^\top$ - cannot be analyzed via the above derivation, and requires a dedicated treatment.

To obtain J around the null state we use (2.13) and (2.51) to write

$$W_{ii} = M_0'(0) + g M_1'(0) d_i M_2(0) \tag{2.76}$$

$$W_{ij} = g M_1(0) A_{ij} G_{ij} M_2'(0), \tag{2.77}$$

omitting, for simplicity, the parameter terms $\mathbf{f}_{qi}$. Several distinct cases arise (Table 1):

Stability of the null-state $x^* = (\mathbf{0}, \ldots, \mathbf{0})^\top$			
Case I	**Case II**	**Case III**	**Case IV**
$M_1'(0) \neq 0, M_2(0) \neq 0$	$M_2(0) = 0$	$M_1(0) = M_2(0) = 0$	$M_q'(0) = 0, q = 0,1,2$
$J \sim \begin{pmatrix} Cd_1 & 0 & 0 \\ 0 & \ddots & 0 \\ 0 & 0 & Cd_N \end{pmatrix}$	$\Omega = (0,0,0,0)$	$J \sim \begin{pmatrix} M_0'(0) & 0 & 0 \\ 0 & \ddots & 0 \\ 0 & 0 & M_0'(0) \end{pmatrix}$	$J \sim \begin{pmatrix} 0 & 0 & 0 \\ 0 & \ddots & 0 \\ 0 & 0 & 0 \end{pmatrix}$
Stable in case $M_1'(0) < 0$, unstable otherwise.	Asymptotically unstable.	Stable in case $M_0'(0) < 0$, unstable otherwise, independently of A, G.	Linear approximation irrelevant, higher order derivatives needed.

Table 1: **Stability of the null-state $\mathbf{x}^* = (0, \ldots, 0)^\top$.** The null-state cannot be treated via our general formalism, and hence we analyze it separately. Our analysis distinguishes between four cases, depending on the values of $M_q(0)$ and $M_q'(0)$.

Case I. In case $M_1'(0)$ and $M_2(0)$ are both non zero, we have the diagonal terms scaling as $W_{ii} \sim d_i$, corresponding to $\mu = 1$. Here, since $M_2(0) \neq 0$, the null-solution of (2.73) inevitably requires that $M_1(0) = 0$, *i.e.* condition (2.74). Consequently, the off-diagonal terms in (2.77) all vanish, indicating that the interactions, in this case, have no linear contribution, and are only expressed via higher order nonlinear terms. In $\mathbb{E}(A, G, \Omega)$ this is captured by taking the limit $\nu, \rho \to -\infty$, deep within the asymptotically stable regime in case J_{ii} is negative ($M_1'(0) < 0$), or the unstable regime if it is positive ($M_1'(0) > 0$). As an example, we consider the dynamics $\mathrm{d}x_i/\mathrm{d}t = -f_i x_i - g \sum_{j=1}^N A_{ij} G_{ij} x_i / (1 + x_j)$, in which the interaction is of deactivating nature. Using (2.76) we write $J_{ii} = -1 - g d_i$, which, indeed, under large d_i, scales as $J_{ii} \sim -d_i^\mu$ with $\mu = 1$. The off-diagonal terms, in this dynamics vanish as per Eq. (2.77).

Case II. If, however $M_2(0) = 0$, *i.e.* condition (2.75), we have both W_{ii} and W_{ij} independent of

d_i, d_j, predicting $J \in \mathbb{E}(A, G, \Omega)$ with $\Omega = (0, 0, 0, 0)$. This captures an asymptotically unstable fixed point. We observe this, for example, in the healthy state of Epidemic dynamics. There we have $M_0'(0) = f_i$, $M_2(0) = 0$ and $M_1(0)M_2'(0) = 1$. Together this leads to $W_{ii}, W_{ij} \sim \text{const}$, *i.e.* lacking any scaling with d_i and d_j. Indeed, we show in the Sec. 4.1 that the healthy state of the Epidemic model is asymptotically unstable, recovering a well-established result on the spread of epidemics on scale-free networks[6].

Case III. A third scenario is when both conditions (2.74) and (2.75) are satisfied, *i.e.* $M_1(0) = M_2(0) = 0$. The off-diagonal terms in (2.77) vanish in this case, indicating that the interactions are super-linear, having no linear component. The diagonal terms become $W_{ii} = M_0'(0)$, independent of the network structure. Therefore, in such dynamics stability is fully determined by the sign of W_{ii}, unstable in case $M_0'(0) \geq 0$ and stable otherwise. We encounter such conditions in Population 1, where $M_1(x) = x$ and $M_2(x) = x/(1 + x)$, both zero when $x = 0$. The self-dynamics in this case has $M_0(x) = b_i x(1 - x/c_i)$, whose derivative around $x = 0$ provides $W_{ii} = b_i > 0$. This dynamics is, therefore, always unstable around the trivial fixed-point.

Note that Cases II and III are of different nature. While Case II is a specific member of $\mathbb{E}(A, G, \Omega)$, with all exponents being zero, Case III's instability is unrelated to $\mathbb{E}(A, G, \Omega)$. To understand this consider Epidemic's trivial state, which is in Case II, vs. that of Population 1, which is in Case III. The former can potentially be stable, if, for instance the recovery rate f_i is large enough. Its instability only emerges asymptotically in the limit of large and heterogeneous networks, *i.e.* our asymptotically unstable class. Therefore it is an integral system within out ensemble $\mathbb{E}(A, G, \Omega)$. Indeed, this form of asymptotic instability emerges from the interplay between topology $(P(d), N)$ and dynamics (Ω), representing a direct outcome of our theoretical framework. Case III dynamics, in contrast, have an intrinsically unstable null state, even under low dimension (small N) or non-heterogeneous degrees ($P(d)$ homogeneous). Their null state instability, is, therefore, not driven by the topology/dynamics interplay, ingrained in our J-ensemble, but rather it is independent of topology. Indeed, as we discuss in Sec. 4.3, in Population 1 the null state is always unstable, even in a one-dimensional system.

Case IV. The final case is where $M_0'(0) = M_1'(0) = M_2'(0) = 0$, which occurs when these functions are super-linear around $x = 0$. Under these conditions the linear approximation becomes irrelevant and higher order terms must be included to capture the fixed-point dynamics. As an example, we consider our Regulatory dynamics, having $M_0(x, \mathbf{f}_i) = -f_i x^a$, $M_1(x) = 1$ and $M_2(x) = x^h/(1 + x^h)$. For $a, h > 1$ the first derivatives vanish around $x = 0$, and J is void. Consequently, under these conditions the null state Jacobian vanishes, and hence cannot be used to assess the system's stability. Such cases, where J is irrelevant require specific treatment, independent of our formalism, which is specifically focused on J. Fortunately, this treatment under Case IV, is quite straightforward, as we demonstrate in our analysis of the Regulatory dynamics in Sec. 4.2.

To summarize, our analytical framework of (2.66) - (2.70) is designed to treat the non-trivial fixed-points of (2.1). If, however, the system exhibits also a null $\mathbf{x}^* = (0, \ldots, 0)^\top$ state, we must treat this state specifically, following the case by case analysis presented above. Fortunately, these null state Jacobians are straightforward to analyze, and can be done alongside our general analytical derivation.

3 Principle eigenvalue of $J \in \mathbb{E}(A, G, \Omega)$

While the principal eigenvalue λ of $J \in \mathbb{E}(A, G, \Omega)$ is difficult to obtain analytically, we find that simplifying A into a *star-network* can provide a rather reliable prediction, especially since we are only focused on whether λ is positive/negative, not on its specific value. We first distinguish between two families of dynamics: the first has $\mathbf{s} = 1$, describing cooperative interactions, in which the off-diagonal terms $J_{ij} > 0$. This is observed, for example, in Regulatory or in Epidemic, where j positively contributes to its neighbor i's activity. The second option, $\mathbf{s} = 0$, describes adversarial interactions, where j' activity has a negative impact on x_i. This can be indirect, such as in Inhibitory, where x_j decreases i's *growth rate*, or direct, such as in Biochemical, where j directly depletes the i population via chemical binding.

The star-construction. The structure of J in (2.69) - (2.70) depends strongly on the network degrees through d_i, d_j and d_{nn}. Recalling the mean-field approximation of Sec. 1.2, we can capture the stability of the system by examining the dynamics of a typical neighborhood. We therefore consider a single node, with weighted degree d_{nn}, *i.e.* a typical neighbor. Since weights G_{ij} are randomly distributed, uncorrelated with degree (Sec. 1.2), we can extract our neighbor's unweighted degree k from its weighted d_{nn} via $d_{\mathrm{nn}} \approx \langle G \rangle k$, which using Eq. (7) of the main text provides

$$k \propto d_{\mathrm{nn}} \sim N^{\beta} \tag{3.1}$$

a potential divergence with system size in case $P(k)$ is fat-tailed.

This construction captures the environment of a typical hub in, *e.g.*, a scale-free network. Indeed, such hubs in a scale-free environment can be viewed as a collection of weakly coupled *stars*, that are only sparsely linked to each other[7]. Under these conditions we have the $(k+1) \times (k+1)$ network

$$A = \begin{bmatrix} 0 & 1 & 1 & \ldots & 1 \\ 1 & 0 & 0 & \ldots & 0 \\ \vdots & & \ddots & & \vdots \\ 1 & 0 & 0 & \ldots & 0 \end{bmatrix}, \tag{3.2}$$

capturing a single, highly connected node, surrounded by k small nodes.

3.1 Jacobians with positive weights $\mathbf{s} = 1$

We now use (2.69) and (2.70), to construct the Jacobian of the star-network (3.2), which under cooperative interactions takes the form

$$J = -C \tilde{d}_{\mathrm{nn}}^{\eta} \begin{bmatrix} k^{\mu} & 0 & \ldots & 0 \\ 0 & 1 & \ldots & 0 \\ \vdots & & \ddots & \vdots \\ 0 & 0 & \ldots & 1 \end{bmatrix} + \begin{bmatrix} 0 & k^{\nu} & \ldots & k^{\nu} \\ k^{\rho} & 0 & \ldots & 0 \\ \vdots & & \ddots & \vdots \\ k^{\rho} & 0 & \ldots & 0 \end{bmatrix}, \tag{3.3}$$

where $C > 0$ and the off-diagonal terms are all positive. In (3.3) we used $\tilde{d}_{\mathrm{nn}}$ to express the nearest neighbor degree in our star construction, which is potentially distinct from d_{nn} of the originally approximated scale-free network. Lacking an *a priori* estimate for this parameter we

express is as

$$\tilde{d}_{\mathrm{nn}} \sim N^{\alpha}, \tag{3.4}$$

leaving us a degree of freedom to later tune α such that the prediction from our star construction best captures the observed results from the actual complete networks (note: α in (3.4) is unrelated to that of (1.15) in Sec. 1.2). Hence, β, characterizing the star-hub (k), is extracted from A via (1.7) and α is a tunable parameter, which we select for the star-model to best fit the complete network results.

> We emphasize that the star approximation in (3.2) by no means captures the complete behavior of an actual network, as indeed it represents but a crude representation of an isolated single node environment. However, our goal here is to examine stability vs. instability - a feature that only depends on the *sign* of the principal eigenvalue, not on its specific value, and is, therefore, insensitive to the detailed structure of A. As we show in Fig. 4 of the main text, the star approximation, while highly stylized, is, indeed, sufficient to capture this J characteristic.

To obtain the principal eigenvalue we solve the linear equation

$$J\mathbf{v} = \lambda\mathbf{v}. \tag{3.5}$$

Using the symmetry of (3.3), we seek a solution of the form $\mathbf{v} = (a, b, b, \ldots, b)^{\top}$, allowing us to reduce (3.5) into

$$-C\tilde{d}_{\mathrm{nn}}^{\eta}k^{\mu}a + kk^{\nu}b = \lambda a \tag{3.6}$$

$$k^{\rho}a - C\tilde{d}_{\mathrm{nn}}^{\eta}b = \lambda b. \tag{3.7}$$

Note that in $\mathbf{v}$ the specific values of a, b have no significance, only the ratio a/b, as we are only interested in the *direction* of the eigenvector, not its magnitude. We therefore arbitrarily set $a = 1$, allowing us to solve (3.6) - (3.7) and obtain

$$\lambda = \frac{1}{2}\left(-C\tilde{d}_{\mathrm{nn}}^{\eta}(k^{\mu}+1) + \sqrt{C^2\tilde{d}_{\mathrm{nn}}^{2\eta}(k^{\mu}+1)^2 - 4C^2\tilde{d}_{\mathrm{nn}}^{2\eta}k^{\mu} + 4k^{1+\nu+\rho}}\right), \tag{3.8}$$

where, of the two solutions, we selected only the one in which the square-root is added (rather than subtracted), as we seek the *largest* eigenvalue. Focusing on the limit

$$\lim_{N\to\infty}(\lambda), \tag{3.9}$$

we use (3.1) and (3.4) to rewrite (3.8) as

$$\lambda \sim \frac{1}{2}\Big(-CN^{\alpha\eta}(N^{\beta\mu}+1)$$
$$+ \sqrt{C^2N^{2\alpha\eta}(N^{\beta\mu}+1)^2 + 4\left[-C^2N^{2\alpha\eta+\beta\mu} + N^{\beta(1+\nu+\rho)}\right]}\Big), \tag{3.10}$$

in which we replace $\tilde{d}_{\mathrm{nn}}$ and k by N^{α} and N^{β}, respectively. In (3.10) we ignore the pre-factors of the N-scaling, focusing only on the powers (α, β), hence substituting the equality sign $=$ with

the asymptotic scaling operator $\sim$.

The case where $\mu > 0$. First we analyze λ under $\mu > 0$. Here, we write $N^{\beta\mu} \gg 1$, simplifying (3.10) in the limit $N \to \infty$ into

$$\lambda \sim \frac{1}{2}\left(-CN^{\alpha\eta+\beta\mu} + \sqrt{C^2 N^{2(\alpha\eta+\beta\mu)} + 4\left[-C^2 N^{2\alpha\eta+\beta\mu} + N^{\beta(1+\nu+\rho)}\right]}\right). \tag{3.11}$$

Extracting the common terms out of the product we rewrite (3.11) as

$$\lambda \sim \frac{1}{2}CN^{\alpha\eta+\beta\mu}\left(-1 + \sqrt{1 + 4\left(-N^{-\beta\mu} + \frac{1}{C^2}N^\sigma\right)}\right), \tag{3.12}$$

where

$$\sigma = \beta\left(1 + \nu + \rho - 2\mu - 2\frac{\alpha}{\beta}\eta\right). \tag{3.13}$$

Note that in (3.12) the term $N^{-\beta\mu} \leq 1$, as $\mu > 0$. Therefore, in case $\sigma \geq 0$, the N^σ term dominates the r.h.s. of the equation, providing, under $N \to \infty$,

$$\lambda \sim \frac{C}{\sqrt{C^2}}N^{\frac{1}{2}\sigma+\alpha\eta+\beta\mu}. \tag{3.14}$$

Using the fact that $C > 0$ it becomes guaranteed that λ in (3.14) is positive, *i.e.* the system is *unstable*.

Next we consider the case $\sigma < 0$. Under these conditions $N^\sigma \ll 1$, allowing us to expand the square-root in (3.12) to first order, providing

$$\lambda \sim \frac{1}{2}CN^{\alpha\eta+\beta\mu}\left(-1 + 1 + 2\left(-N^{-\beta\mu} + \frac{1}{C^2}N^\sigma\right)\right) = -CN^{\alpha\eta} + \frac{1}{C}N^{\sigma+\alpha\eta+\beta\mu}. \tag{3.15}$$

We can rewrite this in the form of Eq. (8) of the main text, obtaining

$$\lambda \sim N^Q\left(1 - \frac{C}{N^S}\right), \tag{3.16}$$

where

$$Q = \sigma + \alpha\eta + \beta\mu \tag{3.17}$$

$$S = \sigma + \beta\mu. \tag{3.18}$$

As N^Q is guaranteed to be positive, the sign of λ depends on S: in case $S > 0$ the negative term in (3.16) satisfies $CN^{-S} \ll 1$, and hence we have $\lambda \sim N^Q > 0$, an unstable dynamics. If however $S < 0$, we have $-CN^{-S} \to -\infty$, predicting $\lambda < 0$, regardless of C, an asymptotically stable system. Consequently the system is stable as long as $S < 0$, which, using (3.18), and taking σ from (3.13), predicts the stability condition

$$\beta \left(1 + \nu + \rho - \mu - 2\frac{\alpha}{\beta}\eta \right) < 0. \tag{3.19}$$

This condition reduces stability into a small set of *relevant* parameters: β, characterizing the network topology A, and $\Omega = (\eta, \mu, \nu, \rho)$, associated with the dynamics through powers in the expansion of $M_q(x)$ in (1.2). The non-universal parameter $C = C(\mathbf{f}, g)$ becomes irrelevant in the limit of sufficiently large N. Finally, α represents a degree of freedom to help tune the star approximation to best fit our ensemble of actual networks, as we do below. Note that condition (3.19) can also be expressed as $\sigma + \beta\mu < 0$. This implies that if $\sigma > \beta\mu$ the system is unstable. This instability condition already contains the previously obtained condition of $\sigma > 0$, that led to Eq. (3.14). Therefore, Eq. (3.19) is sufficient to characterize the system's stability, covering both the σ positive and the σ negative cases.

Finally, the case $S = 0$ in (3.16) represents sensitive stability, in which λ's value is not asymptotically defined, and rather it depends on the coefficient C. In this class, stability in no longer a characteristic of the dynamic *model*, but rather of its specific rate constants $\mathbf{f}$ and g, as encapsulated within C. A trivial example is when $\beta = 0$, *i.e.* a non fat-tailed $P(d)$, for example - Erdős-Rényi. Indeed, as we discuss in the main text, in such networks, stability can be tuned by the model parameters, lacking a defined asymptotic behavior.

The case where $\mu \leq 0$. Here, we have $N^{\beta\mu} \leq 1$, and hence Eq. (3.10) can be approximated by

$$\lambda \sim \frac{1}{2}\left(-CN^{\alpha\eta} + \sqrt{C^2 N^{2\alpha\eta} + 4\left[-C^2 N^{2\alpha\eta+\beta\mu} + N^{\beta(1+\nu+\rho)} \right]} \right), \tag{3.20}$$

leading to

$$\lambda \sim \frac{1}{2}CN^{\alpha\eta}\left(-1 + \sqrt{1 + 4\left(-N^{\beta\mu} + \frac{1}{C^2}N^\omega \right)} \right), \tag{3.21}$$

where

$$\omega = \beta \left(1 + \nu + \rho - 2\frac{\alpha}{\beta}\eta \right). \tag{3.22}$$

Equation (3.21) features a summation of $N^{\beta\mu} \leq 1$ with N^ω, whose value depends on ω. Therefore, as before, if $\omega > 0$, λ becomes dominated by the N^ω term, following

$$\lambda \sim \frac{C}{\sqrt{C^2}}N^{\frac{1}{2}\omega + \alpha\eta}, \tag{3.23}$$

which is always positive, *i.e. unstable*. If, however, $\omega < 0$, we use a linear approximation to write

$$\lambda \sim \frac{1}{2}CN^{\alpha\eta}\left(-1 + 1 + 2\left(-N^{\beta\mu} + \frac{1}{C^2}N^\omega \right) \right) = -CN^{\alpha\eta+\beta\mu} + \frac{1}{C}N^{\omega+\alpha\eta}, \tag{3.24}$$

as before - a competition between a positive vs. a negative term. Collecting the powers we, once again, rewrite (3.24) in the form

$$\lambda \sim N^Q \left(1 - \frac{C}{N^S} \right), \qquad (3.25)$$

where this time

$$Q = \omega + \alpha\eta \qquad (3.26)$$

$$S = \omega - \beta\mu. \qquad (3.27)$$

Stability is ensured if, for $N \to \infty$, the negative term dominates, namely if $S < 0$. Using (3.22) to express ω this provides

$$\beta \left(1 + \nu + \rho - \mu - 2\frac{\alpha}{\beta}\eta \right) < 0, \qquad (3.28)$$

recovering precisely the condition in (3.19).

Tuning α. The parameter α represents a degree of freedom, rooted in the fact that the star approximation is a simplification, which can be optimized if we select this parameter such that the star best captures the complete network environment. We find that setting

$$\alpha = \frac{\beta}{2} \qquad (3.29)$$

provides the optimal approximation, accurately predicting stability $\sim 96\%$ of the time for our $2,881$ unweighted networks, $\sim 94\%$ for our $2,290$ networks with distributed weights, and $\sim 85\%$ in our $2,216$ networks with negative links weights (Fig. 9). This completes the stability analysis, providing the stability classifier

$$S = \beta \left(1 + \nu + \rho - \mu - \eta \right), \qquad (3.30)$$

as appears in Eq. (9) of the main text under $\mathsf{s} = 1$.

3.2 Jacobians with negative weights $\mathsf{s} = 0$

Adversarial interactions, in which J's off-diagonal terms are negative confront us with more complex behaviors. Here, for example, i's direct neighbor j has a negative impact on x_i, but its second neighbor m has an indirect positive effect, as it reduces x_j, and by that positively contributes to x_i. Our star approximation of (3.2), including only nearest neighbors, overlooks these indirect effects - and hence yields an identical outcome whether the interactions are cooperative, $\mathsf{s} = 1$, or adversarial, $\mathsf{s} = 0$. Therefore, to evaluate S under negative J_{ij} we consider a fully connected network of

$$k \sim N^\beta \qquad (3.31)$$

nodes, *à la* May's original formulation[8]. This, once again, we emphasize, is but a crude approximation, whose relevance we support via our extensive numerical testing (Fig. 9). With *all* nodes now having degree k, the resulting Jacobian takes the form
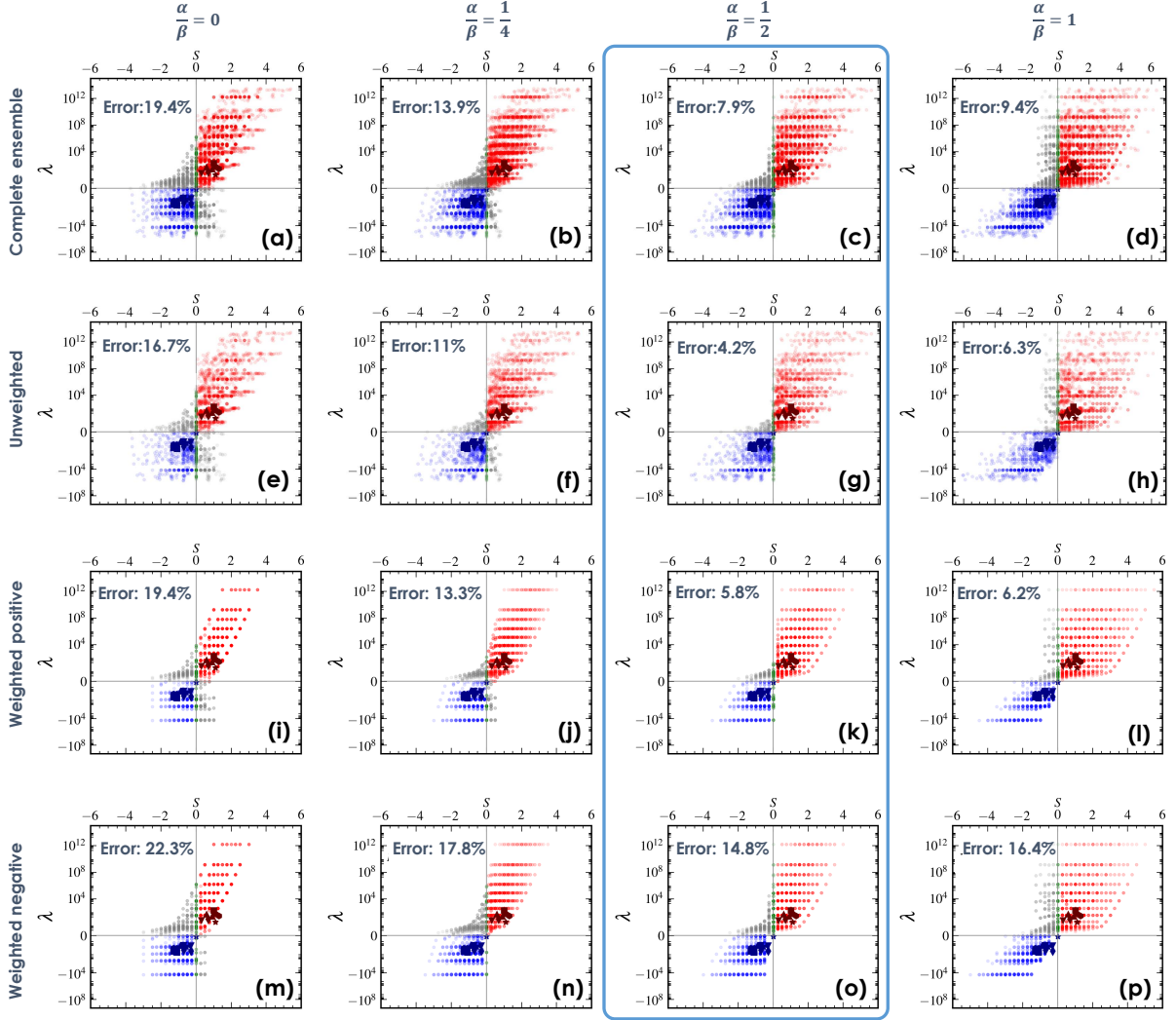
Figure 9: **Tuning the parameter** α. In Eqs. (3.19) and (3.28) we have the degree of freedom to set α/β for the star approximation to best predict the stability of actual networks. We used our ensemble of $7,387$ J matrices (Fig. 4a of main text) to predict stability using different values of α/β. Quantifying the Error by the fraction of mis-classified J matrices (grey dots), we find that setting $\alpha/\beta = 1/2$ (blue frame) provides the optimal fit: securing a $\sim 96\%$ correct classification (Error= 4.2%) for unweighted networks, $\sim 94\%$ (Error= 5.8%) for weighted networks and $\sim 85\%$ (Error= 14.8%) for weighted networks with negative J_{ij}. Here the empirical networks (Social 1,2; PPI 1,2; Power 1,2; Microbial 1/2) are highlighted in bold red/blue symbols

$$J = -Ck^{\eta} \begin{bmatrix} k^{\mu} & 0 & \dots & 0 \\ 0 & k^{\mu} & \dots & 0 \\ \vdots & & \ddots & \vdots \\ 0 & 0 & \dots & k^{\mu} \end{bmatrix} - \begin{bmatrix} 0 & k^{\nu+\rho} & \dots & k^{\nu+\rho} \\ k^{\nu+\rho} & 0 & \dots & k^{\nu+\rho} \\ \vdots & & \ddots & \vdots \\ k^{\nu+\rho} & k^{\nu+\rho} & \dots & 0 \end{bmatrix}, \tag{3.32}$$

in which both the diagonal and the off-diagonal terms are preceded by a minus sign.

For a matrix of the form (3.32) the principal eigenvector is $\mathbf{v} = (1, -1, 0, \dots, 0)^{\top}$, whose associated eigenvalue is

$$\lambda = -Ck^{\eta+\mu} + k^{\nu+\rho}. \tag{3.33}$$

Using (3.31) we rewrite (3.33) in the form

$$\lambda = N^{Q}\left(1 - \frac{C}{N^{S}}\right), \tag{3.34}$$

where now

$$Q = \beta(\nu + \rho) \tag{3.35}$$

$$S = \beta(\nu + \rho - \mu - \eta). \tag{3.36}$$

Hence under adversarial interactions the stability classifier is different from (3.30), providing the stability condition

$$S = \beta\left(\nu + \rho - \mu - \eta\right) < 0, \tag{3.37}$$

namely Eq. (9) of the main text, only this time, with $\mathbf{s} = 0$.

The role of topology vs. dynamics. The stability conditions (3.30) or (3.37) are driven by five distinct exponents. The first four exponents $\Omega = (\eta, \mu, \nu, \rho)$ are determined by the dynamic model - Social, Regulatory, Population etc. - intrinsic to the system's inherent interaction mechanisms. These exponents are independent of the topology A or of microscopic model parameters, encapsulated within C, and are therefore *hardwired* into the system's dynamic behavior. For example, our formalism predicts that the SIS model (Epidemic) has $\Omega = (0, 1, -1, 0)$ (Sec. 4.1). This prediction is characteristic of the SIS model, namely it is an intrinsic feature of the SIS interaction mechanisms of infection and recovery. It is, therefore, insensitive to the specific rates of the model - predicting that Ω remains unchanged if, *e.g.*, a disease has a high or low infection rate, or if it is transmitted via physical contact or aerosols. These will impact the constant C in (2.69), but will have no impact on the universal scaling. Similarly, Ω is unaffected by A. Therefore, regardless of whether the disease spreads along the standard social network (Flu) or via sexual transmission (AIDS), as long as the *mechanism* is SIS (or any other mechanism for that matter) Ω remains the same. The remaining exponent in our classifier, β, on the other hand, is independent of the dynamics, and determined solely by A, G, specifically by the weighted degree distribution $P(d)$, which characterizes the divergence of d_{nn} in the limit of large N. Hence, together, S captures the emergence of stability/instability as driven by the interplay of topology (β), microscopic parameters (C) and dynamics (Ω).

4 Analyzing the dynamic models

To demonstrate our formalism we examined several commonly used dynamic models, as listed in Fig. 2 of the main text. Below we extract the exponents Ω and the stability classifier S for each of these models. The first five models are treated in this section, while the last two, Power and Population 2, which extend our application beyond the analytical framework of Sec. 1, are analyzes separately in Sec. 5.

4.1 Epidemic dynamics

As our first demonstration we model epidemic spreading via the Susceptible-Infected-Susceptible (SIS) model[9], in which $x_i(t)$ captures the probability of infection of node i. Denoting the susceptible state by $\mathcal{S}$ and the infected state by $\mathcal{I}$, the model includes the following transitions

$$\mathcal{I} \quad \xrightarrow{f_i} \quad \mathcal{S} \tag{4.1}$$

$$\mathcal{I} + \mathcal{S} \quad \xrightarrow{G_{ij}} \quad 2\mathcal{I}, \tag{4.2}$$
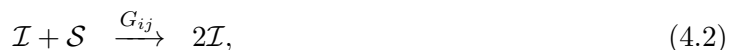
capturing the processes of recovery at a rate f_i, and infection at the pairwise interaction rate G_{ij}. This gives rise to the dynamic equation[10]

$$\frac{\mathrm{d}x_i}{\mathrm{d}t} = -f_i x_i(t) + g \sum_{j=1}^{N} A_{ij} G_{ij} \big(1 - x_i(t) \big) x_j(t), \tag{4.3}$$

in which $M_0(x_i, \mathbf{f}_{0i}) = -f_i x_i$, characterized by the single parameter $\mathbf{f}_{0i} = \{f_i\}$, $M_1(x_i) = 1 - x_i$ and $M_2(x_j) = x_j$, both having no free parameters. The link weights G_{ij} capture the infection rate between all interacting individuals, and g is the average infection rate.

Null state. First, we note that the SIS model exhibits a trivial fixed-point $\mathbf{x}^* = 0$, the *healthy* state, in which $M_0(0) = M_2(0) = 0$. Together this classifies the SIS model into Case II of Table 1, hence predicting the null-state Jacobian to follow $J \in \mathbb{E}(A, G, \Omega)$ with

$$\Omega = (0, 0, 0, 0). \tag{4.4}$$

Using Eq. (3.30) this provides $S = \beta$, which for a fat-tailed $P(d)$, in which $\beta > 0$, predicts asymptotic instability.

With this prediction our formalism retrieves an already well-established result, that the epidemic threshold of the SIS model vanishes under a scale-free topology[6]. Therefore, regardless of the specific parameters, f_i, g, the pandemic state is always the only stable fixed-point of this model under degree-heterogeneous A. This is precisely the meaning of our observation here that $\mathbf{x}^* = (0, \dots, 0)^\top$ is asymptotically unstable. However, while the original result was reported specifically for the Epidemic dynamics, using a dedicated analysis, in our formalism, this observation is but a special case of a broad class of potentially stable/unstable dynamics, all predictable via the $\mathbb{E}(A, G, \Omega)$ ensemble.

Pandemic state. To obtain the relevant J ensemble for the non-zero fixed-point/s, we seek the

exponents $\Omega = (\eta, \mu, \nu, \rho)$. We begin by translating $M_q(x)$ into the relevant functions shown in (2.66), providing

$$R(x) = -\frac{M_1(x)}{M_0(x)} = \frac{1 - x}{fx} \tag{4.5}$$

$$Y(x) = M_1(x)R'(x) = \frac{x - 1}{fx^2} \tag{4.6}$$

$$Z(x) = R(x)M_2(x) = \frac{1}{f} - \frac{1}{f}x, \tag{4.7}$$

where we used $f = \langle f \rangle$ to denote the average recovery rate. Inverting $R(x)$ and $Z(x)$, we write

$$R^{-1}(x) = \frac{1}{fx + 1}, \tag{4.8}$$

$$Z^{-1}(x) = 1 - fx, \tag{4.9}$$

allowing us to construct the Hahn expansions of (2.67) as

$$M_2\big(Z^{-1}(x)\big) = Z^{-1}(x) = 1 - fx \tag{4.10}$$

$$Y\big(R^{-1}(x)\big) = \frac{R^{-1}(x) - 1}{f \times \big(R^{-1}(x)\big)^2} = -x - fx^2 \tag{4.11}$$

$$M_1\big(R^{-1}(x)\big) = 1 - R^{-1}(x) = \frac{fx}{fx + 1} = fx - f^2 x^2 + f^3 x^3 - \cdots \tag{4.12}$$

$$M_2'\big(R^{-1}(x)\big) = 1. \tag{4.13}$$

Here both $R(x)$ and $Z(x)$ are invertible, and therefore, the system exhibits only a single fixed-point apart from $\mathbf{x}^* = (0, \ldots, 0)^\top$. Each of the functions in (4.10) - (4.13) is expressed as a Hahn power-series, in some cases a finite polynomial, *e.g.*, (4.10) or (4.11), and in others an infinite series, where we only write the leading terms around $x \to 0$. Here, coincidentally, the last function (4.13) is a constant, *i.e.* a trivial power-series in which the only participating power is x^0. We can list the relevant powers in these Hahn expansions as $\Psi_0 = 0, \Phi_0 = 1, \Pi_0 = 1$ and $\Theta_0 = 0$, which, using (2.68) provides

$$\mu = 2 - \Phi_0 = 1; \quad \nu = -\Pi_0 = -1; \quad \rho = -\Theta_0 = 0; \quad \eta = -\Psi_0(\mu - \nu - \rho) = 0. \tag{4.14}$$

Consequently the stability classifier in (3.30) is $S = \beta(1 - 1 + 0 - 1 - 0) = -\beta$, which under $\beta > 0$ (*i.e.* fat-tailed $P(d)$) predicts the asymptotic stability of the pandemic state, indeed, reconfirming Ref.[6].

4.2 Regulatory dynamics

We used the Michaelis-Menten model to capture gene regulation in sub-cellular networks[11]. Here, Eq. (2.1) tracks the level of gene expression $x_i(t)$, as regulated via its interacting genes, providing

$$\frac{\mathrm{d}x_i}{\mathrm{d}t} = -f_i x_i^a(t) + g \sum_{j=1}^{N} A_{ij} G_{ij} \frac{x_j^h(t)}{1 + x_j^h(t)}. \tag{4.15}$$

The self-dynamic term $M_0(x_i, \mathbf{f}_{0i}) = -f_i x_i^a$ captures biochemical processes[12], such as degradation ($a = 1$) or dimerization ($a = 2$). The interaction terms $M_1(x_i) = 1$, $M_2(x_j) = x_j^h/(1 + x_j^h)$ describe genetic activation, a *switch-like* dynamics, which ranges from $M_2(0) = 0$ to $M_2(x_j \to \infty) = 1$, capturing the activation of gene i by gene j. The Hill coefficient h governs the rate of saturation of $M_2(x)$, often associated with the level of cooperation in gene regulation[11]. The exponents a and h, are, in this case, expressed in the *powers* Γ_{qn} of (1.2), and are hence rendered *intrinsic*, thus taken to be uniform for all nodes/links (see Secs. 5.4 and 5.5, where we break this assumption). The parameters f_i, G_{ij}, on the other hand, capture the specific rates of all processes, which are potentially diverse across all nodes/links. Similarly, the average interaction rate g is also subject to external perturbation by the cell's environmental conditions.

Null state. Regulatory dynamics exhibit a trivial solution $\mathbf{x}^* = (0, \ldots, 0)^\top$, capturing cell-death. Following (2.76) and (2.77) we write

$$W_{ii} = \left. a f_i x^{a-1} \right|_{x=0} \tag{4.16}$$

$$W_{ij} = \left. A_{ij} w_{ij} \frac{h x^{h-1}}{(1 + x^h)^2} \right|_{x=0}. \tag{4.17}$$

Both terms vanish in case $a, h > 1$. This represents Case IV of Sec. 2.5 (Table 1), in which the linear regime is void. Under these conditions, the stability of the null state must be treated by resorting to higher orders, which are not within the scope of our formalism. Fortunately, thanks to the fact that the higher order expansion is around the trivial point $\mathbf{x}^* = (0, \ldots, 0)^\top$, the analysis becomes straightforward. Indeed, for $x_i \to 0$, Eq. (4.15) approaches

$$\frac{\mathrm{d}x_i}{\mathrm{d}t} = -f_i x_i^a + g \sum_{j=1}^{N} A_{ij} G_{ij} x_j^h \longrightarrow \begin{cases} -f_i x_i^a & a < h \\ g \sum_{j=1}^{N} A_{ij} G_{ij} x_j^h & a \geq h \end{cases}, \tag{4.18}$$

being dominated by the negative term if $a < h$, and by the positive term otherwise. For the specific case of $a = h$, both terms have similar dependence on x_i. However, since the positive interaction term scales with d_i ($g \sum_{j=1}^{N} A_{ij} G_{ij} = g d_i$), it will asymptotically dominate the dynamics ($d_i \gg f_i/g$ for sufficiently large hubs), predicting instability also under $a = h$. As a consequence the null state is stable if $a < h$ and unstable otherwise.

The remaining scenario is the specific case where $a = h = 1$, precisely the dynamics we analyze in the main text under Regulatory. Here (4.16) and (4.17) provide $W_{ii} = f_i$ and $W_{ij} = A_{ij} G_{ij}$, both independent of d_i, d_j. This corresponds to $J \in \mathbb{E}(A, G, \Omega)$, with

$$\Omega = (0, 0, 0, 0), \tag{4.19}$$

an asymptotically unstable fixed-point, as per Case II of Sec. 2.5. Therefore, while $\mathbf{x}^* = (0, \ldots, 0)^\top$ may generally be stable, if the system is large and heterogeneous it will inevitably

avoid this undesired state.

Active fixed-points. We now return to our formalism to analyze the stability of the non-vanishing states. First, we construct the three functions summarized in (2.66):

$$R(x) = -\frac{M_1(x)}{M_0(x)} = \frac{1}{fx^a} \tag{4.20}$$

$$Y(x) = M_1(x)R'(x) = -\frac{a}{fx^{a+1}} \tag{4.21}$$

$$Z(x) = R(x)M_2(x) = \frac{x^h}{f(x^a + x^{a+h})}, \tag{4.22}$$

where, once again, we use $f = \langle f \rangle$ to represent ensemble average over f_i. Inverting $R(x)$, we write

$$R^{-1}(x) = f^{-\frac{1}{a}} x^{-\frac{1}{a}}, \tag{4.23}$$

allowing us to construct the Hahn expansions (2.67)

$$Y\left(R^{-1}(x)\right) = -\frac{a}{f}\left(\frac{1}{fx}\right)^{-\frac{a+1}{a}} = af^{\frac{1}{a}} x^{\frac{a+1}{a}} \tag{4.24}$$

$$M_1\left(R^{-1}(x)\right) = 1 = x^0 \tag{4.25}$$

$$M_2'\left(R^{-1}(x)\right) = \frac{hf^{-\frac{h-1}{a}} x^{-\frac{h-1}{a}}}{\left(1 + f^{-\frac{h}{a}} x^{-\frac{h}{a}}\right)^2} = hf^{\frac{h+1}{a}} x^{\frac{h+1}{a}} - 2hf^{\frac{2h+1}{a}} x^{\frac{2h+1}{a}} + \cdots . \tag{4.26}$$

In each of these expansions we write the leading terms in the $x \to 0$ limit: in (4.24) and (4.25) the expansion features a single term, *i.e.* a pure monomial, and in (4.26) we show the first two terms of the relevant Hahn expansion. To obtain Ω we extract only the leading *powers* $\Phi_0 = (a+1)/a, \Pi_0 = 0, \Theta_0 = (h+1)/a$, ignoring the *coefficients*, *e.g.*, $af^{1/a}$ or $hf^{(h+1)/a}$. We can now use (2.68) to extract the dynamic exponents as

$$\mu = 2 - \Phi_0 = \frac{a-1}{a}; \quad \nu = -\Pi_0 = 0; \quad \rho = -\Theta_0 = -\frac{h+1}{a}. \tag{4.27}$$

To obtain the final exponent η we must calculate $M_2(Z^{-1}(x))$, requiring us to invert the function $Z(x)$ in (4.22). This becomes prohibitively complicated under a general a and h, however, as we are only focused on the leading powers of $M_2(Z^{-1}(x))$, we can advance using an asymptotic analysis. Similar to the trivial fixed-point analysis, we once again, distinguish between $a \geq h$ and $a < h$.

Regulatory dynamics under $a \geq h$. Under these conditions $Z(x)$ is monotonous and therefore invertible. For $x \to \infty$ we have $Z(x) \sim x^{-a}$, which approaches zero (Fig. 10a, red). Therefore, the inverse $Z^{-1}(x)$ tends to infinity as $x \to 0$ (blue). The form of this divergence can be obtained by mirroring the large x behavior of $Z(x)$, providing $Z^{-1}(x) \sim x^{-1/a}$. This enables us to construct the final Hahn expansion to leading order as
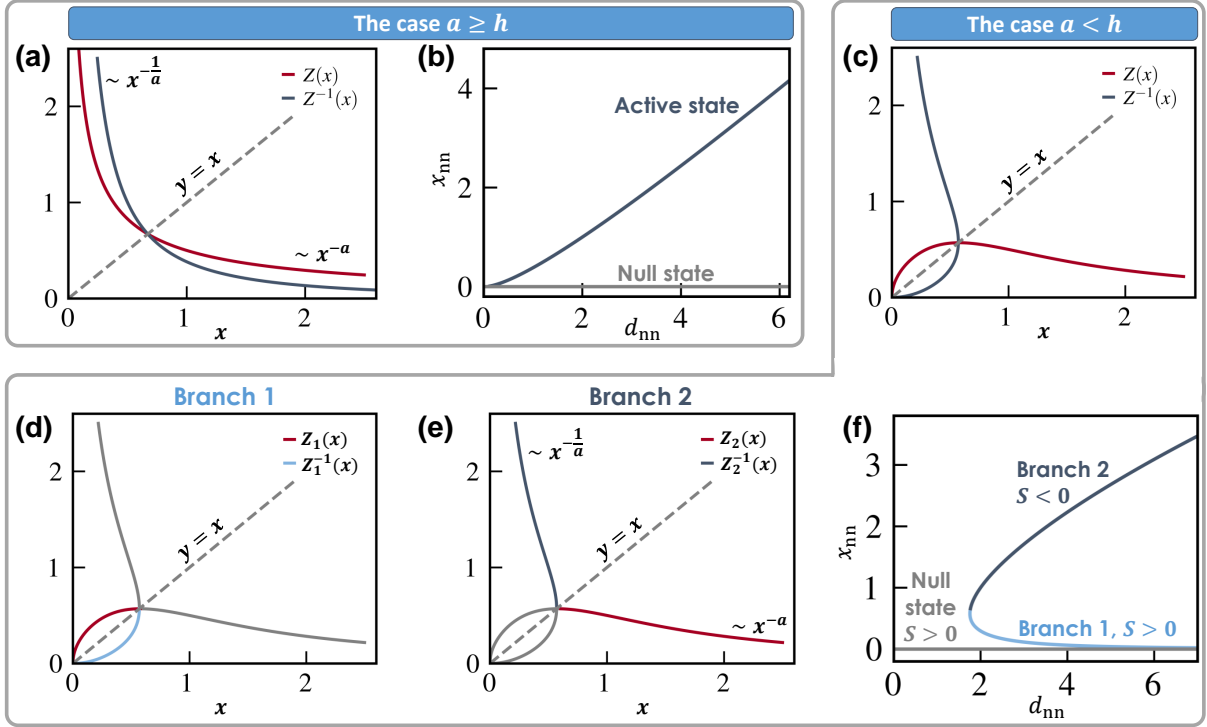
Figure 10: **Analyzing $Z(x)$ in Regulatory dynamics**. (a) $Z(x)$ in (4.22) vs. x (red) for $a \geq h$, set here to $a = 1, h = 1/2$. Here $Z(x)$ is monotonous and therefore we can obtain its inverse $Z^{-1}(x)$ for all x (blue). Using the fact that $Z(x \to \infty) \sim x^{-a}$, we can extrapolate that its inverse has $Z^{-1}(x \to 0) \sim x^{-1/a}$. (b) The nearest neighbor fixed-point activity x_{nn} vs. d_{nn}, as obtained for Regulatory dynamics (4.15) with $a > h$. Following Eq. (2.39), the limit $Z^{-1}(x \to 0)$ captured the active state (blue) in the limit of large d_{nn}, predicting $d_{nn} \sim x_{nn}^{1/a}$. The null-state is also shown (grey). (c) For $a < h$, $Z(x)$ is not monotonous (red) and therefore $Z^{-1}(x)$ is undefined (blue). To treat this we divide $Z(x)$ into two branches: Branch 1 to the left of the maximum point; Branch 2 to its right. (d) In Branch 1 we have $Z_1(x \to 0) \sim x^{h-a}$ (red), providing $Z_1^{-1}(x \to 0) \sim x^{1/(h-a)}$ (light blue). (e) In Branch 2 we have $Z_2(x \to \infty) \sim x^{-a}$ (red), and hence $Z_2^{-1}(x \to 0) \sim x^{-1/a}$ (dark blue). (f) x_{nn} vs. d_{nn} under $a < h$. We observe three states: null-state (grey), active state (dark blue), intermediate state (light blue). Branch 1 has $Z_1^{-1}(x) \to 0$ in the limit of small x, describing a state in which x_{nn} decreases with d_{nn}. This corresponds to the intermediate state, for which we obtain $S > 0$, *i.e.* instability. Branch 2 has $Z_2^{-1}(x) \to \infty$, capturing a positive scaling between d_{nn} and x_{nn}. Therefore Branch 2 is related to the active state, which is asymptotically stable ($S < 0$).

$$M_2\big(Z^{-1}(x)\big) \sim \frac{x^{-\frac{h}{a}}}{1 + x^{-\frac{h}{a}}} \sim 1 - x^{\frac{h}{a}} + \dots, \tag{4.28}$$

in which the leading power is $\Psi_0 = 0$. As a result, we obtain, using (2.68) our final exponent

$$\eta = -\Psi_0(\mu - \nu - \rho) = 0. \tag{4.29}$$

Collecting the other exponents calculated above in (4.27), we derive the stability classifier

$$S = \beta\left(1 + 0 - \frac{h+1}{a} - \frac{a-1}{a} - 0\right) = -\frac{h}{a}\beta < 0, \tag{4.30}$$

indicating that for $a \geq h$ the non-trivial fixed-point is asymptotically stable.

Regulatory dynamics under $a < h$. For $a < h$, the function $Z(x)$ in (4.22) is non-monotonous, its inverse is undefined, and hence the system can potentially reside in multiple fixed-points. As

an example, in Fig. 10c we present $Z(x)$ for a specific choice of $f = 1, a = 3/2, h = 2$ (red), finding that it is, indeed, non-invertible. We therefore divide $Z(x)$ into its two branches, as shown in Fig. 7: Branch 1 - from $x = 0$ upto the maximum point, and Branch 2 - from the maximum point to $x \to \infty$. This allows us to construct the two functions, $Z_1(x)$ (Fig. 10d) and $Z_2(x)$ (Fig. 10e), each of which *is* invertible, and whose inverse function is associated with a distinct fixed-point of the system.

First we analyze $Z_1(x)$ (Fig. 10d, red). As we are interested in the leading power of $M_2(Z_1^{-1}(x))$, we focus on the the behavior around $x \to 0$. Using (4.22) we write

$$Z_1(x \to 0) = x^{h-a} + \dots, \tag{4.31}$$

where we include only the leading term, and, for simplicity, set $f = 1$. We therefore have

$$Z_1^{-1}(x \to 0) = x^{\frac{1}{h-a}} + \dots, \tag{4.32}$$

shown in Fig. 10d (light blue), and consequently

$$M_2\big(Z_1^{-1}(x \to 0)\big) = x^{\frac{h}{h-a}} + \dots. \tag{4.33}$$

This provides, for Branch 1, $\Psi_0 = h/(h-a)$, which, taking μ, ν, ρ from (4.27), predicts

$$\eta = -\Psi_0(\mu - \nu - \rho) = \frac{h(a+h)}{a(a-h)}. \tag{4.34}$$

Collecting all exponents we obtain

$$S = \beta\left(1 + 0 - \frac{h+1}{a} - \frac{a-1}{a} - \frac{h(a+h)}{a(a-h)}\right) = 2\frac{h(a+1)}{a(h-a)}. \tag{4.35}$$

Under the condition $a < h$, S is guaranteed to be positive. Therefore, Branch 1 is asymptotically unstable.

The fixed-point captured by Branch 1 has $Z_1^{-1}(x \to 0) \to 0$. This captures a state in which the nearest neighbor activity x_{nn} tends to zero as d_{nn} is increased. Indeed in Eq. (2.39) we have $x_{\mathrm{nn}} = Z^{-1}(q_{\mathrm{nn}})$, in which $q_{\mathrm{nn}} \sim d_{\mathrm{nn}}^{-1}$ tends to zero in the limit $d_{\mathrm{nn}} \to \infty$, indicating that $Z_1^{-1}(x \to 0)$ captures the asymptotic behavior of x_{nn}. This behavior, links Branch 1 to the intermediate state in the one-dimensional bifurcation diagram of Fig. 10f (light blue), which is, indeed, characterized by $x_{\mathrm{nn}} \to 0$. This state is unstable in the low-dimensional system, and as our formalism now shows, it is also unstable in the asymptotic limit, via our ensemble $\mathbb{E}(A, G, \Omega)$.

Next, we analyze Branch 2, $Z_2(x)$, capturing the part of $Z(x)$ to the right of the maximum point (Fig. 10e, red). Its asymptotic behavior is observed in the limit $x \to \infty$, where we have $Z_2(x) \sim x^{-a}$. Mirroring this behavior to the inverse $Z_2^{-1}(x)$, we have $Z_2^{-1}(x \to 0) \sim x^{-1/a}$ (dark blue), leading to

$$M_2\big(Z^{-1}(x)\big) \sim \frac{x^{-\frac{h}{a}}}{1 + x^{-\frac{h}{a}}} \sim 1 - x^{\frac{h}{a}} + \dots, \tag{4.36}$$

namely $\Psi_0 = 0$. Hence, for Branch 2 we have

$$\eta = -\Psi_0(\mu - \nu - \rho) = 0. \tag{4.37}$$

Together with (4.27) this provides

$$S = \beta\left(1 + 0 - \frac{h+1}{a} - \frac{a-1}{a} - 0\right) = -\frac{h}{a}\beta < 0, \tag{4.38}$$

predicting, for this branch, that it is asymptotically stable.

This branch, in which $Z^{-1}(x \to 0) \to \infty$ captures a state in which x_{nn} increases with d_{nn}, corresponding to the *active* state of Fig. 10f (dark blue). In a low-dimensional system, the stability of this state depends on the system's specific parameters, *i.e.* f_i, g. Yet, our formalism shows that this state becomes asymptotically stable for large heterogeneous networks.

4.3 Population 1 dynamics

We consider mutualistic eco-systems, such as plant-pollinator networks or microbial communities, in which the interacting species exhibit symbiotic relationships. The species populations follow the dynamic equation

$$\frac{\mathrm{d}x_i}{\mathrm{d}t} = b_i x_i(t)\left(1 - \frac{x_i(t)}{c_i}\right) + g\sum_{j=1}^{N} A_{ij}G_{ij}x_i(t)F\big(x_j(t)\big). \tag{4.39}$$

The self-dynamics $M_0(x_i, \mathbf{f}_{0i}) = b_i x_i(1 - x_i/c_i)$ captures logistic growth, driven by parameter b_i, the growth rate, and c_i, the environment carrying capacity. The mutualistic interactions are captured by $M_1(x_i) = x_i$ and $M_2(x_j) = F(x_j)$, where $F(x_j)$ represents the *functional response*, describing the positive impact that species j has on species i. This functional response can take one of several forms, Holling types I - III[13]:

$$F_{\mathrm{I}}(x) = x, \qquad F_{\mathrm{II}}(x) = \frac{x}{1+x}, \qquad F_{\mathrm{III}}(x) = \frac{x^h}{1+x^h}, \tag{4.40}$$

type I featuring a linear response, and types II,III describing a saturating impact of j on i. In our simulations we used Type II interactions, therefore $M_2(x_j) = x_j/(1 + x_j)$.

Null state. Equation (4.39) has a trivial fixed-point $\mathbf{x}^* = (0, \dots, 0)^\top$, in which $M_0(x) = M_1(x) = M_2(x) = 0$. This corresponds to Case III in Table 1, in which the null-state is unstable. This instability, we emphasize, is different from our asymptotic instability of $S > 0$, as it is independent of network size (N) or of degree heterogeneity ($P(d)$). Here, even if we consider the one dimensional version of (4.39)

$$\frac{\mathrm{d}x}{\mathrm{d}t} = b\left(1 - \frac{x}{c}\right) + gxF(x), \tag{4.41}$$

we find that $x = 0$ is unstable, independently of parameters b, c, g. This is despite that fact that the one-dimensional (4.41) is certainly not in the relevant asymptotic regime of $N \to \infty$ and $P(d)$ fat-tailed. Therefore, the null-state instability in this dynamics is unrelated to $\mathbb{E}(A, G, \Omega)$. Fortunately, it be directly analyzed without the need for our more advanced toolbox.

Active state. Next we analyze the non-vanishing fixed-point/s of (4.39) using our formalism. For $R(x), Y(x)$ and $Z(x)$ we have

$$R(x) = -\frac{M_1(x)}{M_0(x)} = \frac{1}{x-1} \tag{4.42}$$

$$Y(x) = M_1(x)R'(x) = -\frac{x}{(x-1)^2} \tag{4.43}$$

$$Z(x) = R(x)M_2(x) = \frac{x}{x^2-1}, \tag{4.44}$$

where for simplicity we set $b_i = c_i = 1$, as indeed these parameters have no effect on the scaling Ω. Inverting $R(x)$ and $Z(x)$, we write

$$R^{-1}(x) = \frac{x+1}{x}, \tag{4.45}$$

$$Z^{-1}(x) = \frac{1}{2x}\left(1 \pm \sqrt{1+4x^2}\right). \tag{4.46}$$

Note that, similar to Regulatory, here too, $Z(x)$ is non-invertible, and hence we have two branches $(\pm)$ for $Z^{-1}(x)$. In this case, however, the *minus* branch corresponds to a purely negative fixed-point, which is physically irrelevant. Therefore, apart from the null fixed-point analyzed above, we are only left with the *plus* branch of (4.46). Taking this branch we construct the Hahn expansions of (2.67) as

$$M_2\left(Z^{-1}(x)\right) = \frac{Z^{-1}(x)}{1+Z^{-1}(x)} = \frac{1+\sqrt{1+4x^2}}{2x+1+\sqrt{1+4x^2}} = 1 - x + \cdots \tag{4.47}$$

$$Y\left(R^{-1}(x)\right) = -\frac{R^{-1}(x)}{\left(R^{-1}(x)-1\right)^2} = x + x^2 \tag{4.48}$$

$$M_1\left(R^{-1}(x)\right) = \frac{x+1}{x} = x^{-1} + 1 \tag{4.49}$$

$$M_2'\left(R^{-1}(x)\right) = \frac{1}{\left(R^{-1}(x)+1\right)^2} = \frac{x^2}{4x^2+4x+1} = x^2 - 4x^3 + \cdots, \tag{4.50}$$

whose leading powers are $\Psi_0 = 0, \Phi_0 = 1, \Pi_0 = -1$ and $\Theta_0 = 2$. Consequently, the dynamic exponents in (2.68) follow

$$\mu = 2 - \Phi_0 = 1; \quad \nu = -\Pi_0 = 1 \quad \rho = -\Theta_0 = -2 \quad \eta = -\Psi_0(\mu - \nu - \rho) = 0. \tag{4.51}$$

As analyzed in Sec. 2.4.1 we have, in Population 1, $\eta = 0$. This is due both to the *Bounded activities* $(0 < x_i < c_i)$ and to the *Saturating* nature of the interaction function. Collecting all exponents we extract the stability classifier from (3.30) as $S = \beta(1 + 1 - 2 - 1 - 0) = -\beta < 0$.

4.4   Biochemical dynamics

As a Biochemical model we consider protein-protein interactions (PPI), which are driven by three processes: $\emptyset \to P_i$, describing the synthesis of the ith protein P_i at a rate f_i; $P_i \to \emptyset$, describing protein degradation at rate b_i; $P_i + P_j \rightleftharpoons P_iP_j$ describing the binding and unbinding of

	Model	Equation	Ω	S
	Epidemic	$\dfrac{\mathrm{d}x_i}{\mathrm{d}t} = -f_i x_i + g\sum_{j=1}^{N} A_{ij}G_{ij}(1-x_i)x_j$	$\Omega = (0,1,-1,0)$	$S = -\beta$
	Regulatory	$\dfrac{\mathrm{d}x_i}{\mathrm{d}t} = -f_i x_i^a + g\sum_{j=1}^{N} A_{ij}G_{ij}\dfrac{x_j^h}{1+x_j^h}$	$\Omega = \left(0,\dfrac{a-1}{a},0,-\dfrac{h+1}{a}\right)$	$S = -\dfrac{h}{a}\beta$
	Population 1	$\dfrac{\mathrm{d}x_i}{\mathrm{d}t} = b_i x_i\left(1-\dfrac{x_i}{c_i}\right) + g\sum_{j=1}^{N} A_{ij}G_{ij}\dfrac{x_i x_j}{1+x_j}$	$\Omega = (0,1,1,-2)$	$S = -\beta$
	Biochemical	$\dfrac{\mathrm{d}x_i}{\mathrm{d}t} = f_i - b_i x_i - g\sum_{j=1}^{N} A_{ij}G_{ij}x_i x_j$	$\Omega = (-1,1,-1,0)$	$S = -\beta$
	Inhibitory	$\dfrac{\mathrm{d}x_i}{\mathrm{d}t} = x_i\left(1-\dfrac{x_i}{f_i}\right)\left(\dfrac{x_i}{b_i}-1\right) + g\sum_{j=1}^{N} A_{ij}G_{ij}\dfrac{x_i}{1+x_j}$	$\Omega = \left(-\dfrac{1}{2},1,\dfrac{1}{2},-1\right)$	$S = -\beta$
	Power	$\dfrac{\mathrm{d}^2 x_i}{\mathrm{d}t^2} = f_i - b_i\dfrac{\mathrm{d}x_i}{\mathrm{d}t} + g\sum_{j=1}^{N} A_{ij}G_{ij}\sin(x_j-x_i)$	$\Omega = (0,1,0,0)$	$S = 0$
	Population 2	$\dfrac{\mathrm{d}x_i}{\mathrm{d}t} = b_i x_i\left(1-\dfrac{x_i}{c_i}\right) + gx_i\dfrac{\sum_{j=1}^{N} A_{ij}G_{ij}x_j}{1+\sum_{j=1}^{N} A_{ij}G_{ij}x_j}$	$\Omega = (0,0,-2,0)$	$S = -\beta$

Table 2: **Dynamic models - summary**. Our seven dynamic models and their associated exponents Ω, as calculated around their active fixed point $\mathbf{x}_1$. For each model we also show the stability classifier S. Parameters (f_i, b_i, etc.) appear in blue and the nonlinear functions themselves in orange. Only the orange terms feed into Ω. The analysis of Power and Population 2, both beyond the scope of Eq. (1.1), appears in Sec. 5.

a pair of interacting proteins at rates B_{ij} and U_{ij} respectively. The hetero-dimer P_iP_j undergoes degradation $P_iP_j \to \emptyset$ at rate Q_{ij}. Using mass-action-kinetics we derive the dynamical equations for this system, providing[12,14]

$$\frac{\mathrm{d}x_i}{\mathrm{d}t} = f_i - b_i x_i(t) + \sum_{j=1}^{N} U_{ij}x_{ij}(t) - \sum_{j=1}^{N} A_{ij}B_{ij}x_i(t)x_j(t) \tag{4.52}$$

$$\frac{\mathrm{d}x_{ij}}{\mathrm{d}t} = B_{ij}A_{ij}x_i(t)x_j(t) - (U_{ij} + Q_{ij})x_{ij}(t), \tag{4.53}$$

where $x_i(t)$ is the concentration of P_i and $x_{ij}(t)$ is the concentration of the hetero-dimer P_iP_j. Under time-scale separation we assume that the hetero-dimer concentration is at steady-state, setting $\mathrm{d}x_{ij}/\mathrm{d}t = 0$ in (4.53). This provides us with

$$\frac{\mathrm{d}x_i}{\mathrm{d}t} = f_i - b_i x_i(t) - g\sum_{j=1}^{N} A_{ij}G_{ij}x_i(t)x_j(t), \tag{4.54}$$

where the effective binding rate is $gG_{ij} = Q_{ij}B_{ij}/(U_{ij} + Q_{ij})$. This has the form of Eq. (1.1), with $M_0(x_i, \mathbf{f}_{0i}) = f_i - b_i x_i$, whose parameters are $\{f_i, b_i\}$, $M_1(x_i) = x_i$ and $M_2(x_j) = x_j$. Denoting the average rates by $f = \langle f\rangle, b = \langle b\rangle$, we write the dynamic functions (2.66) as

$$R(x) = -\frac{M_1(x)}{M_0(x)} = \frac{x}{f - bx} \tag{4.55}$$

$$Y(x) = M_1(x)R'(x) = -\frac{fx}{\left(f - bx\right)^2} \tag{4.56}$$

$$Z(x) = R(x)M_2(x) = \frac{x^2}{f - bx}. \tag{4.57}$$

The inverse functions are, therefore

$$R^{-1}(x) = \frac{fx}{1 + bx} \tag{4.58}$$

$$Z^{-1}(x) = \frac{b}{2}x\left(-1 + \sqrt{1 + \frac{4f}{b^2 x}}\right), \tag{4.59}$$

where in $Z^{-1}(x)$ we choose the positive solution, corresponding to the positive fixed-point of (4.54), as we did in our analysis of Population 1 above. We can now compose the functions in (2.67), obtaining

$$M_2\big(Z^{-1}(x)\big) = Z^{-1}(x) = \sqrt{f}x^{\frac{1}{2}} + \frac{b^2}{8\sqrt{f}}x^{\frac{3}{2}} + \cdots \tag{4.60}$$

$$Y\big(R^{-1}(x)\big) = -\frac{fR^{-1}(x)}{\left(f - bR^{-1}(x)\right)^2} = fx + fbx^2 \tag{4.61}$$

$$M_1\big(R^{-1}(x)\big) = -\frac{fx}{1 + bx} = -fx + fbx^2 + \cdots \tag{4.62}$$

$$M_2'\big(R^{-1}(x)\big) = 1, \tag{4.63}$$

allowing us to extract the leading powers as $\Psi_0 = 1/2, \Phi_0 = 1, \Pi_0 = 1$ and $\Theta_0 = 0$. These powers provide the Biochemical dynamic exponents via (2.68) as

$$\mu = 2 - \Phi_0 = 1; \quad \nu = -\Pi_0 = -1; \quad \rho = -\Theta_0 = 0; \quad \eta = -\Psi_0(\mu - \nu - \rho) = -1 . \tag{4.64}$$

As predicted, these exponents are independent of the parameters f, b, intrinsic to the Biochemical dynamics. Here, since the interactions are adversarial, as indicated by the $-g$ pre-factor preceding the interaction term in (4.54), we have $\mathbf{s} = 0$. Therefore, we use (3.37) to obtain the stability classifier, providing us with $S = \beta(-1 + 0 - 1 + 1) = -\beta$, *i.e.* asymptotically stable.

4.5 Inhibitory dynamics

To model inhibition, *e.g.*, between genes[11] or between hosts and pathogens[15], we use

$$\frac{\mathrm{d}x_i}{\mathrm{d}t} = x_i(t)\left(1 - \frac{x_i(t)}{f_i}\right)\left(\frac{x_i(t)}{b_i} - 1\right) + g\sum_{j=1}^{N} A_{ij}G_{ij}x_i(t)\frac{1}{1 + x_j(t)}. \tag{4.65}$$

The self dynamics captures logistic growth, similar to Population 1, but here, also incorporating

the Allee effect[16], which balances competition with the potentially added benefit of the *tribe*. The competition is expressed in $M_0(x_i)$ through the negative growth occurring when $x_i > f_i$, *i.e.* when x_i exceeds the limited carrying capacity of the environment. This competition, however, is overcome by the enhanced growth at $b_i < x_i < f_i$, capturing the cooperative benefit of i from being surrounded by a greater i population, *e.g.*, hunting in pacts. Hence, Eq. (4.65) is relevant under $b_i \leq f_i$, predicting suppressed growth when $0 < x_i < b_i$ or $x_i > f_i$, and positive growth in the mid-range $b_i < x_i < f_i$. The interaction dynamics describes inhibition: i grows linearly with its own instantaneous population x_i, but at a rate which approaches zero as $x_j \to \infty$. Consequently, the greater is x_j the lower is i's reproduction rate.

Null state. In (4.65) the null state $\mathbf{x}^* = (0, \ldots, 0)^\top$ has $M_0'(0) = -1$ and $M_2(0) = 1$, both non-zero. This adheres to Case I in Sec. 2.5, predicting $W_{ii} \sim -1 + d_i$ and $W_{ij} = 0$. Consequently, as Table 1 indicates, the null state is asymptotically unstable. This is indeed supported by Fig. 5 of the main text, where we show that the active state persists under arbitrary parameter perturbation.

Active state. To analyze the active state of (4.65) we first rewrite its self-dynamics in the Hahn form of Eq. (1.2) as

$$M_0(x_i, \mathbf{f}_i) = -x_i + B_i x_i^2 - Q_i x_i^3, \tag{4.66}$$

where $B_i = (f_i + b_i)/f_i b_i$ and $Q_i = 1/f_i b_i$. Denoting $\langle B \rangle = B$ and $\langle Q \rangle = Q$, we construct the dynamic functions of (2.66), obtaining

$$R(x) = -\frac{M_1(x)}{M_0(x)} = \frac{1}{1 - Bx + Qx^2} \tag{4.67}$$

$$Y(x) = M_1(x)R'(x) = \frac{Bx - 2Qx^2}{\left(1 - Bx + Qx^2\right)^2} \tag{4.68}$$

$$Z(x) = R(x)M_2(x) = \frac{1}{1 + (1 - B)x + (Q - B)x^2 + Qx^3}. \tag{4.69}$$

The inverse function $R^{-1}(x)$ takes the form

$$R^{-1}(x) = \frac{B + \sqrt{B^2 - 4Q + \dfrac{4Q}{x}}}{2Q}, \tag{4.70}$$

where once again, we omit the negative branch, as it represents a negative, and hence irrelevant, fixed-point. In the limit $x \to 0$ we have

$$R^{-1}(x) \approx Q^{-\frac{1}{2}} x^{-\frac{1}{2}}. \tag{4.71}$$

Inverting $Z(x)$ in (4.69) is non-tractable analytically, however, as we only need to evaluate $Z^{-1}(x)$ in the limit of $x \to 0$, we can simplify the calculation, by seeking only the relevant leading terms. In Fig. 11 we show $Z(x)$ (red) and its inverse $Z^{-1}(x)$ (blue). Since $Z(x)$ is non-monotonic, its inverse is undefined, indeed showing several branches (Fig. 11b): Branch 1, the top branch, which diverges in the limit $x \to 0$, Branch 2, intermediate, and Branch 3, for which $Z^{-1}(x) < 0$. Of these, the only relevant branch is Branch 1, as it is the only one covering

the $x \to 0$ regime. The meaning is that, while $Z(x)$ is non-invertible for all $x \in \mathbb{R}$, the limit $Z^{-1}(x \to 0)$ *is* well-defined, as the function is locally invertible around $x = 0$. Examining the corresponding branch in $Z(x)$ we observe that $Z^{-1}(x \to 0)$ is the mirror image of the original function $Z(x)$ in the limit $Z(x \to \infty)$ (Branch 1 in Fig. 11a). Using (4.69) we write $Z(x \to \infty) \sim Q^{-1}x^{-3}$, and therefore we have

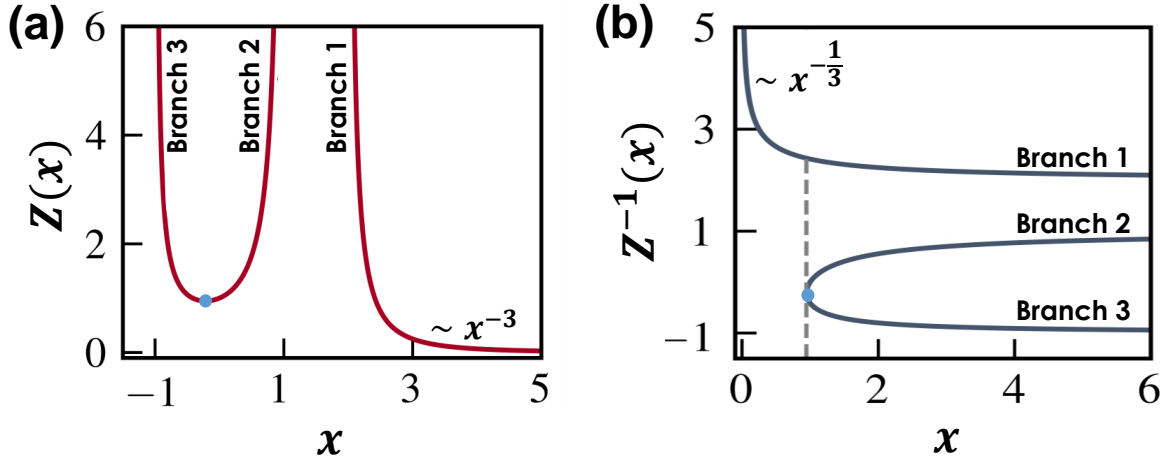$$Z^{-1}(x \to 0) \sim Q^{-\frac{1}{3}} x^{-\frac{1}{3}}. \tag{4.72}$$

Figure 11: **Analyzing $Z(x)$ under Inhibitory dynamics**. (a) $Z(x)$ in (4.69) vs. x. The function is divided into three branches, separated by the minimum point (blue dot) between Branches 3 and 2, and by the asymptotic divergence between Branch 2 and Branch 1. (b) $Z^{-1}(x)$ and its division into the corresponding three branches. To the right of the grey dashed line we observe overlapping solutions, and hence $Z^{-1}(x)$ is undefined. However, the limit $Z^{-1}(x \to 0)$ is well-defined, as in this regime, to the left of the dashed line, only Branch 1 is relevant. The limit $x \to 0$ in $Z^{-1}(x)$ is the mirror image of the limit $x \to \infty$ in $Z(x)$. Therefore, using the fact that $Z(x \to \infty) \sim x^{-3}$ we extrapolate $Z^{-1}(x \to 0) \sim x^{-1/3}$, as appears in Eq. (4.72).

With (4.71) and (4.72) at hand we can now construct the relevant dynamic functions of (2.67), obtaining

$$M_2\big(Z^{-1}(x)\big) = \frac{1}{1 + Z^{-1}(x)} \sim \frac{1}{1 + Q^{-\frac{1}{3}} x^{-\frac{1}{3}}} \sim x^{\frac{1}{3}} + \cdots \tag{4.73}$$

$$Y\big(R^{-1}(x)\big) = \frac{BR^{-1}(x) - 2Q\big(R^{-1}(x)\big)^2}{\Big(1 - BR^{-1}(x) + Q\big(R^{-1}(x)\big)^2\Big)^2}$$

$$\sim \frac{BQ^{-\frac{1}{2}} x^{-\frac{1}{2}} - 2x^{-1}}{\Big(1 - BQ^{-\frac{1}{2}} x^{-\frac{1}{2}} + x^{-1}\Big)^2} \sim x + \cdots \tag{4.74}$$

$$M_1\big(R^{-1}(x)\big) = R^{-1}(x) \sim x^{-\frac{1}{2}} + \cdots \tag{4.75}$$

$$M_2'\big(R^{-1}(x)\big) = -\frac{1}{\big(1 + R^{-1}(x)\big)^2} \sim -\frac{1}{\big(1 + Q^{-\frac{1}{2}} x^{-\frac{1}{2}}\big)^2} \sim x + \cdots . \tag{4.76}$$

From here we extract the leading powers as $\Psi_0 = 1/3, \Phi_0 = 1, \Pi_0 = -1/2$ and $\Theta_0 = 1$, which using (2.68), predicts

$$\mu = 2 - \Phi_0 = 1 \quad \nu = -\Pi_0 = \frac{1}{2} \quad \rho = -\Theta_0 = -1 \quad \eta = -\Psi_0(\mu - \nu - \rho) = -\frac{1}{2}. \quad (4.77)$$

The inhibitory nature of the dynamics is expressed in J through negative off-diagonal weights. This can be observed through (2.51), where the derivative $M_2'(x) < 0$, and hence $\widetilde{W}_{ij}$ is negative. Therefore in Inhibitory we have $\mathbf{s} = 0$, the stability classifier follows (3.37) and, consequently, $S = \beta(1/2 - 1 - 1 + 1/2) = -\beta$, classifying the active state of Inhibitory as asymptotically stable.

Suppressed state. In addition to the null and active states of Inhibitory, this system also exhibits a *suppressed* fixed-point, in which the activities x_i become bimodal: $\sim 50\%$ of the nodes have $x_i \to 0$, and the remaining $\sim 50\%$ have x_i large, positively scaling with d_i. This state emerges as a consequence of the mutual inhibition between neighboring nodes, each pushing its neighbors towards lower activity. To understand this consider a highly active node i with $x_i \gg 1$. This activity in (4.65) suppresses the growth rate of its neighbor j, leading to $x_j \ll 1$. Such suppressed x_j benefits j's neighbors m, who will, consequently, also reach $x_m \gg 1$. As a result the system enters a bifurcated state, in which node i is active, its neighbors are suppressed, its next neighbors are active again and so on. This state breaks our assumed symmetry, in which all neighborhoods are considered similar, and hence cannot be analyzed via our formalism. Accordingly, its associated Jacobian is not covered by the $\mathbb{E}(A, G, \Omega)$ ensemble, therefore beyond the scope of our current analysis.

5 Extended dynamics

Our anaytical framework is centered around Assumptions 1 - 6 of Sec. 1. To examine its applicability beyond these limits, we now examine test cases, each designed to go beyond the scope of Sec. 1.

5.1 Power dynamics - testing Assumption 2

Load balance in power systems requires synchronization between all generators and consumers, often tracked through the phases $x_i(t)$ of all nodes, following[17]

$$\frac{\mathrm{d}^2 x_i}{\mathrm{d}t^2} = f_i - b_i \frac{\mathrm{d}x_i}{\mathrm{d}t} + g \sum_{j=1}^{N} A_{ij} G_{ij} \sin\big(x_j(t) - x_i(t)\big). \quad (5.1)$$

Here f_i is a node's power generation/consumption, depending on whether it is a generator/consumer, b_i is the damping coefficient, and the interaction is designed to synchronize phases x_i and x_j. The interaction strength is mediated by the conductivity of the i, j transmission line, as controlled by g and G_{ij}. Equation (5.1) offers two generalizations to the dynamics of Eq. (2.1) - first, by introducing the second derivative $\mathrm{d}^2 / \mathrm{d}x^2$, and second, through its non-separable interaction mechanism, which cannot be expressed in the form $M_1(x_i)M_2(x_j)$, *i.e.* Assumption 2. Still, as we show below, its perturbative behavior around the synchronized fixed-point continues to be characterized by a Jacobian within the family of $\mathbb{E}(A, G, \Omega)$.

The synchronized state has $x_i(t) = x_j(t)$ for all i, j, which, by shifting to the rotating frame, can be all set to zero, namely $\mathbf{x}^* = (0, \ldots, 0)^\top$. Under a small fixed-point perturbation $\delta \mathbf{x}$ we have

$$\frac{\mathrm{d}^2 \delta x_i}{\mathrm{d}t^2} = -b_i \frac{\mathrm{d}\delta x_i}{\mathrm{d}t} + g \sum_{j=1}^{N} A_{ij} G_{ij} \sin\left(\delta x_j(t) - \delta x_i(t)\right), \tag{5.2}$$

whose linear approximation becomes

$$\frac{\mathrm{d}^2 \delta x_i}{\mathrm{d}t^2} = -b_i \frac{\mathrm{d}\delta x_i}{\mathrm{d}t} + g \sum_{j=1}^{N} A_{ij} G_{ij}\left(\delta x_j(t) - \delta x_i(t)\right) + O(\delta x^2). \tag{5.3}$$

Neglecting the nonlinear terms, Eq. (5.3) can be written as

$$\frac{\mathrm{d}^2 \delta x_i}{\mathrm{d}t^2} = -b_i \frac{\mathrm{d}\delta x_i}{\mathrm{d}t} + J_{ii}\delta x_i(t) + \sum_{\substack{j=1 \\ j\neq i}}^{N} J_{ij}\delta x_j(t), \tag{5.4}$$

where

$$J_{ii} = -g d_i \tag{5.5}$$

$$J_{ij} = A_{ij} G_{ij} \tag{5.6}$$

is the system's Jacobian. The resulting Jacobian is precisely in the form of $J \in \mathbb{E}(A, G, \Omega)$, where $C(\mathbf{f}, g) = g$ and the exponents are $\mu = 1$ and $\eta = \nu = \rho = 0$. It also, incidentally, equals to the graph Laplacian[1] - recovering an already well-known connection. Under these conditions of $\Omega = (0, 1, 0, 0)$, we have S in (3.30) equaling $S = \beta(1 + 0 + 0 - 1 - 0) = 0$, placing Power in the sensitive dynamics class. Here, even if $\lambda > 0$, sufficient damping (b_i) may still stabilize the system. This captures precisely the *sensitivity* under $S = 0$, in which *parameters* govern the value of λ.

Note that in this system, due to the second derivative, J plays a different role as compared to its role in (2.1). Specifically, here J governs not just stability but also the system's potential oscillations around $\mathbf{x}^*$. Still, our main goal is to show that even for this system, not covered by (1.1) we continue to observe $J \in \mathbb{E}(A, G, \Omega)$, further strengthening the importance and relevance of this previously unknown ensemble.

5.2   Non-additive dynamics - testing Assumption 3

In Assumption 3 we take the impact of i's interacting partners on i to be additive, as expressed via Eq. (1.1)'s summation over the nonlinear $M_2(x_j)$, namely $\sum_{j=1}^{N} M_2(x_j)$. To push the limits of this assumption we consider Population 2 dynamics, in which

$$\frac{\mathrm{d}x_i}{\mathrm{d}t} = b_i x_i(t)\left(1 - \frac{x_i(t)}{c_i}\right) + x_i(t)\frac{\sum_{j=1}^{N} A_{ij} G_{ij} x_j(t)}{1 + \sum_{j=1}^{N} A_{ij} G_{ij} x_j(t)}, \tag{5.7}$$

replacing the $\sum_j M_2(x_j)$ structure of (1.1) by $M_2(\sum_j x_j)$, a non-additive form of interaction. Once again, despite violating our analytical assumptions, we can still analyze this system using a dedicated derivation. First, we use (1.8) together with (1.14) to write

$$\sum_{j=1}^{N} A_{ij} G_{ij} x_j = d_i \langle x \rangle_{i,\odot} \approx d_i x_{\mathrm{nn}}, \tag{5.8}$$

substituting the sum by the nearest neighbor average, and already implementing the fact that $f_{M,\odot}(d) \sim 1$, and hence $\langle x \rangle_{i,\odot} \approx x_{\mathrm{nn}}$. This allows us to express the *non-vanishing* fixed-point activity of a node i as

$$1 - x_i + \frac{d_i x_{\mathrm{nn}}}{1 + d_i x_{\mathrm{nn}}} = 0, \tag{5.9}$$

where, for simplicity we have taken $b_i = c_i = 1$, wishing to avoid cumbersome derivations. Extracting x_i from (5.9) we obtain

$$x_i = \frac{1 + 2 d_i x_{\mathrm{nn}}}{1 + d_i x_{\mathrm{nn}}} \sim d_i^0, \tag{5.10}$$

namely that in the limit of large d_i, the fixed-point activities approach a constant and do not scale with degree.

Next, we seek the diagonal Jacobian terms J_{ii}, writing

$$J_{ii} = \frac{\partial}{\partial x_i} \left(x_i (1 - x_i) + x_i \frac{\sum_{j=1}^{N} A_{ij} G_{ij} x_j}{1 + \sum_{j=1}^{N} A_{ij} G_{ij} x_j} \right), \tag{5.11}$$

which, using (5.8), provides us with

$$J_{ii} = 1 - 2 x_i + x_i \frac{d_i x_{\mathrm{nn}}}{1 + d_i x_{\mathrm{nn}}}. \tag{5.12}$$

In (5.12) there are no terms that contribute to the scaling with d_i, as indeed $x_i \sim d_i^0$ and the fraction term on the r.h.s. approaches unity in the limit $d_i \to \infty$. Therefore, we obtain

$$J_{ii} \sim d_i^0, \tag{5.13}$$

predicting $\mu = 0$ in $\mathbb{E}(A, G, \Omega)$.

For the off-diagonal terms we write

$$J_{ij} = \frac{\partial}{\partial x_j} \left(x_i (1 - x_i) + x_i \frac{\sum_{m=1}^{N} A_{im} G_{im} x_m}{1 + \sum_{m=1}^{N} A_{im} G_{im} x_m} \right), \tag{5.14}$$

which we break down into the form

$$J_{ij} = \frac{\partial}{\partial x_j} \left(x_i (1 - x_i) + x_i \frac{A_{ij} G_{ij} x_j + \sum_{\substack{m=1 \\ m \neq j}}^{N} A_{im} G_{im} x_m}{1 + \sum_{m=1}^{N} A_{im} G_{im} x_m} \right). \tag{5.15}$$

44

Extracting the x_j partial derivative we obtain

$$J_{ij} = x_i A_{ij} G_{ij} \left(\frac{1 + \sum_{m=1}^{N} A_{im} G_{im} x_m - A_{ij} G_{ij} x_j - \sum_{\substack{m=1 \\ m \neq j}}^{N} A_{im} G_{im} x_m}{\left(1 + \sum_{m=1}^{N} A_{im} G_{im} x_m\right)^2} \right), \qquad (5.16)$$

which after collecting all terms provides

$$J_{ij} = x_i A_{ij} G_{ij} \frac{1}{\left(1 + \sum_{m=1}^{N} A_{im} G_{im} x_m\right)^2}. \qquad (5.17)$$

In (5.17) the only term that contributes to the scaling with d_i or d_j is the summation in the denominator. Using (5.8) we can express this summation as $\sum_{m=1}^{N} A_{im} G_{im} x_m = d_i x_{\mathrm{nn}}$, leading to

$$J_{ij} = x_i A_{ij} G_{ij} \frac{1}{(1 + d_i x_{\mathrm{nn}})^2}, \qquad (5.18)$$

which in the limit $d_i \to \infty$ provides us with

$$J_{ij} \sim d_i^{-2}, \qquad (5.19)$$

namely, an $\mathbb{E}(A, G, \Omega)$ Jacobian with $\nu = -2$ and $\rho = 0$. Therefore, despite not being within the form of (1.1) our Population 2 dynamics is also part of the broad $\mathbb{E}(A, G, \Omega)$ family with

$$\Omega = (0, 0, -2, 0). \qquad (5.20)$$

This represents an asymptotically stable system with $S = \beta(1 - 2 + 0 - 0 - 0) = -\beta$.

5.3 Extinction dynamics - testing Assumption 4

We consider population dynamics with mixed positive/negative interactions. This represents mutualistic links *a là* Population 1, alongside competitive and predatory interactions. Here, due to the adversarial links, some species populations may reach the absorbing point of $x_i = 0$, and hence a subset of the species may become extinct. The challenge is that this specific subset depends on the initial conditions, and hence the system has no unique fixed-point, having a different set of eliminated species under different initial conditions $\mathbf{x}(t = 0)$.

To test this, we constructed a scale-free A with $N = 6,000$ nodes and $L = 18,000$ links, of which a fraction $0 \leq \phi \leq 1$ are negative ($A_{ij} = -1$), and the remaining $1 - \phi$ are positive ($A_{ij} = 1$). We then implemented Population 1 dynamics as appear in Eq. (4.39), setting, for simplicity, all parameters and link weights to unity, *i.e.* $b_i = c_i = g = G_{ij} = 1$. Starting from an arbitrary initial condition, we allowed the system to naturally reach its fixed-point. During the process, whenever a specific activity reached $x_i(t) \leq \epsilon$ we set it permanently to zero
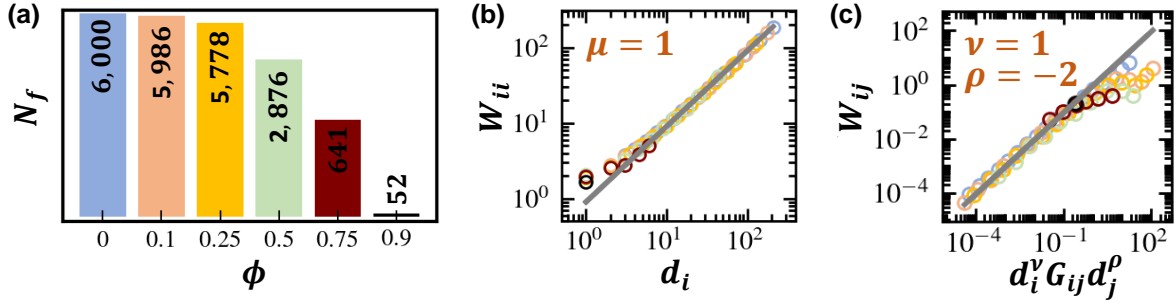
Figure 12: **Emerging stability under mixed interactions**. (a) The number of surviving nodes N_f vs. the fraction of adversarial links ϕ. The more negative interactions the smaller the surviving node set. (b) J_{ii} vs. d_i as obtained from the N_f surviving nodes. (c) J_{ij} vs. $d_i^\nu A_{ij} G_{ij} d_j^\rho$ over the surviving node set. As long as enough nodes survive we continue to observe our predicted scaling patterns. Our prediction only breaks down under large ϕ, where $N_f \ll N$, *i.e.* the majority of nodes are removed.

(extinction), effectively removing it from the network; we used $\epsilon = 10^{-12}$. At its final state the network is reduced to $N_f \leq N$ surviving nodes, upon which we examined our predicted scaling relationships. For example, under $\phi = 0.1$, starting from a randomly selected initial condition, we arrive at a final state of $N_f = 5,986$ surviving nodes, a total of 14 extinctions (Fig. 12a). Increasing ϕ to 25% or 50% the network incurs higher losses, down to $N_f = 5,778$ and $N_f = 2,876$. The crucial point is that the remaining N_f nodes continue to follow the predicted scaling with $\mu = \nu = 1$ and $\rho = -2$ as obtained in Eq. (4.51).

We emphasize that the specific set of surviving nodes is different across the different realizations, and hence the system has no well-defined fixed-point. Still, despite these microscopic differences between the realizations, which depend on the detailed structure of A and on the specific initial condition, the macroscopic scaling patterns remain valid, over the resulting set of surviving nodes in each realization. Of course, as we increase ϕ, extinctions begin to dominate the final state of the system, until at a certain point, the surviving node set becomes too diluted and our predicted Jacobian structure breaks down. Our results in Fig. 12b,c indicate that this breakdown occurs around $\phi = 0.75$ or 0.9, a limit in which the majority of the nodes are lost to extinction.

5.4 Mixed-dynamics - testing Assumption 1

The structure of (1.1) allows for diverse parameters $\mathbf{f}_i$, but at the same time assumes uniform dynamics, as captured via the defined set of powers Γ_{qn} in (1.2). The rationale is that the network components posses specific physical properties that constrain the mechanisms by which they can interact, an assumption mathematically captured by the uniformity of Γ_{qn}. More realistically, however, some systems may comprise 2 or 3 types of nodes/links, in which case (1.1) may incorporate a mixture of few coexisting dynamics. To expressed this we consider the generalization

$$\frac{\mathrm{d}x_i}{\mathrm{d}t} = \sum_{s=1}^{S} B_i^{\{s\}} \left(M_0^{\{s\}}(x_i) + g \sum_{j=1}^{N} \sum_{l=1}^{L} M_1^{\{s\}}(x_i) A_{ij}^{\{l\}} G_{ij} M_2^{\{l\}}(x_j) \right), \qquad (5.21)$$

capturing a coexistence of $s = 1,\ldots,S$ self-dynamics and $l = 1,\ldots,L$ link-dynamics. Here $B_i^{\{s\}} = 1$ if node i has self-dynamics s and zero otherwise; similarly $A_{ij}^{\{l\}} = 1$ in case i and j interact via the lth link-dynamics and zero otherwise. Additionally, $A_{ij}^{\{l\}} \times A_{ij}^{\{l'\}} = 0$ in case

$l \neq l'$, ensuring that i and j can interact through only a single defined mechanism. We focus on cases where the number of coexisting mechanisms is $S, L \sim 1, 2, \ldots$, *i.e.* a limited discrete set of potential competing dynamics.

While we cannot analytically extract J from the generalized (5.21), we can heuristically assume that the coexisting dynamics are manifested in J through an equivalently coexisting exponent set. For example, consider the diagonal weights W_{ii} and their dependence on d_i. Instead of having all terms follow a single scaling relationship μ, we now expect the nodes to partition into S independent scaling functions

$$W_{ii} = W_{ii}(s) \sim B_i^{\{s\}} d_i^{\mu(s)}, \tag{5.22}$$

a set of S scaling functions, in which each node follows its s-dependent exponent $\mu(s)$.

For the off-diagonal weights W_{ij}, we expect such partition to be dictated by i's self-dynamics s, j's self-dynamics s' and the i, j link dynamics l. Therefore W_{ij} will be divided into a potential of $S^2 \times L$ coexisting scaling functions, capturing the potential number of s, s', l combinations. We can express this as

$$W_{ij} = W_{ij}(s, s', l) \sim d_i^{\nu(s,l)} B_i^{\{s\}} A_{ij}^{\{l\}} G_{ij} B_j^{\{s'\}} d_j^{\rho(s',l)}, \tag{5.23}$$

in which $\nu(s, l)$ is the exponent ν derived under self/link-dynamics s and l, and $\rho(s', l)$ is the exponent ρ matching the combination s' and l, *i.e.* using j's self-dynamics.

Together, this provides a straightforward generalization in which each of the Jacobian weights follows one of the potential $S^2 \times L$ scaling relationships with the exponent sets
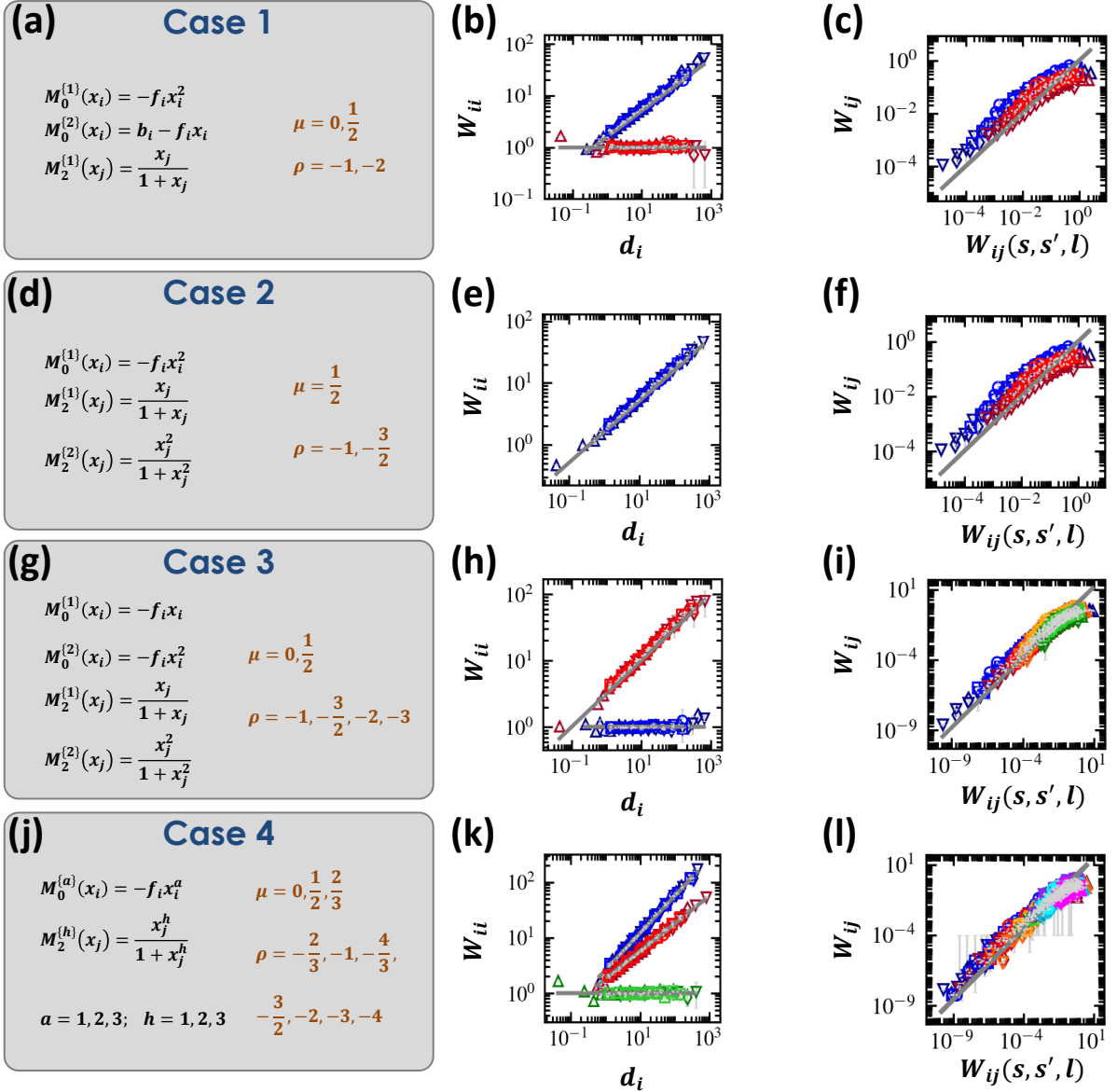
(a) Case 1

$M_0^{\{1\}}(x_i) = -f_i x_i^2$

$M_0^{\{2\}}(x_i) = b_i - f_i x_i$ $\qquad \mu = 0, \frac{1}{2}$

$M_2^{\{1\}}(x_j) = \frac{x_j}{1+x_j}$ $\qquad \rho = -1, -2$

(b) W_{ii} vs. d_i

(c) W_{ij} vs. $W_{ij}(s, s', l)$

(d) Case 2

$M_0^{\{1\}}(x_i) = -f_i x_i^2$

$M_2^{\{1\}}(x_j) = \frac{x_j}{1+x_j}$ $\qquad \mu = \frac{1}{2}$

$M_2^{\{2\}}(x_j) = \frac{x_j^2}{1+x_j^2}$ $\qquad \rho = -1, -\frac{3}{2}$

(e) W_{ii} vs. d_i

(f) W_{ij} vs. $W_{ij}(s, s', l)$

(g) Case 3

$M_0^{\{1\}}(x_i) = -f_i x_i$

$M_0^{\{2\}}(x_i) = -f_i x_i^2$ $\qquad \mu = 0, \frac{1}{2}$

$M_2^{\{1\}}(x_j) = \frac{x_j}{1+x_j}$ $\qquad \rho = -1, -\frac{3}{2}, -2, -3$

$M_2^{\{2\}}(x_j) = \frac{x_j^2}{1+x_j^2}$

(h) W_{ii} vs. d_i

(i) W_{ij} vs. $W_{ij}(s, s', l)$

(j) Case 4

$M_0^{\{a\}}(x_i) = -f_i x_i^a$ $\qquad \mu = 0, \frac{1}{2}, \frac{2}{3}$

$M_2^{\{h\}}(x_j) = \frac{x_j^h}{1+x_j^h}$ $\qquad \rho = -\frac{2}{3}, -1, -\frac{4}{3},$

$a = 1, 2, 3; \quad h = 1, 2, 3$ $\qquad -\frac{3}{2}, -2, -3, -4$

(k) W_{ii} vs. d_i

(l) W_{ij} vs. $W_{ij}(s, s', l)$

Figure 13: **The dynamic Jacobian ensemble under mixed dynamics**. We consider four examples of increasing complexity. (a) **Case 1**. Two competing self-dynamics and a single interaction dynamics distributed randomly across all nodes (left, black). The resulting coexisting values of μ and ρ are listed on the right (orange). (b) The diagonal weights W_{ii} vs. degree d_i. Nodes belonging to $M_0^{\{1\}}(x_i)$ have $\mu(1) = 1/2$ (blue), whereas those following $M_0^{\{2\}}(x_i)$ have $\mu(2) = 0$ (red). (c) The off-diagonal terms W_{ij} vs. the theoretically predicted $W_{ij}(s, s', l)$ in Eq. (5.23). We observe the two coexisting scaling relationships (red, blue), precisely as predicted - the red data points having $\nu(1, 1) = 0, \rho(1, 1) = -1$, the blue data points having $\nu(2, 1) = 0, \rho(2, 1) = -2$. (d)-(f) **Case 2**. A similar partition into independent scaling relationships is also observed under mixed link-dynamics. (g)-(i) **Case 3**. Incorporating both mixed self and link-dynamics, we observe the diagonal W_{ii} split into two scaling rules, and the off-diagonal W_{ij} into four independently observed scaling relationships, all in accordance with predictions (5.22) and (5.23). (j)-(l) **Case 4**. We randomly assign three different forms of self ($a = 1, 2, 3$) and interaction ($h = 1, 2, 3$) dynamics. This system is predicted to exhibit 3 distinct scaling relationships for W_{ii} (panel j, μ, orange) and seven for W_{ij} (panel j, ρ, orange). Each panel includes results from five networks (ER, SF, SF1, PPI1 and PPI2), whose nodes/links were divided into logarithmic bins $\mathbb{B}(b), b = 1, \ldots, B$ (Supplementary Sec. 7.3). The number of bins ranges from $B = 10$ to 20 for the nodes (panels b,e,h,k), and $B = 20$ to 30 for the links (panels c,f,i,l). Therefore, the sample size within each bin is $|\mathbb{B}(b)| \in (300, 600)$ for nodes and $|\mathbb{B}(b)| \in (1,200, 1,800)$ for links. The error bars represent 95% confidence intervals within each bin.

$$\Omega^{\{s,s',l\}} = \Big(\eta(s,s',l), \mu(s), \nu(s,l), \rho(s',l)\Big). \tag{5.24}$$

Each individual exponent is calculated via our formalism, by selecting the appropriate $M_0(x)$, $M_1(x)$ and $M_2(x)$. We emphasize that this is a heuristic expansion of our formalism, and hence, to validate it we examine it below, numerically, for a set of four dynamic combinations of varying complexity (Fig. 13a,d,g,j). We also note that one may consider other potential forms of mixed-dynamics generalization, some more complex to analyze than our proposed (5.21). However, we reserve the full analysis of mixed-dynamics for future works on the topic.

Case 1. Mixed self-dynamics (Fig. 13a-c). We consider a system with $S = 2$ self-dynamics and a single ($L = 1$) link-dynamics. The diagonal weights W_{ii} have $\mu(1) = 1/2$ (blue) and $\mu(2) = 0$ (red). For W_{ij} we observe $\nu(1,1) = \nu(2,1) = 0$ and $\rho(1,1) = -1, \rho(2,1) = -2$. In principle, while this system has four potential scaling combinations, it reduces to just two, thanks to the shared value of ν. Hence, $W_{ij}(s,s',l)$ splits between a scaling $W_{ij}(s,1,1) \sim d_i^0 G_{ij} d_j^{-1}$ in case j has self-dynamics $s' = 1$ (blue) and $W_{ij}(s,2,1) \sim d_i^0 G_{ij} d_j^{-2}$ under j in self-dynamics $s' = 2$ (red); the value of s, denoting i's self-dynamics plays no role in $W_{ij}(s,s',l)$.

Case 2. Mixed interaction-dynamics (Fig. 13d-f). Here we have $L = 2$ forms of link-dynamics, predicting a single scaling for W_{ii} of $\mu(1) = 1/2$, and two potential scaling rules for W_{ij}: $\nu(1,1) = 0, \rho(1,1) = -1$ (red) and $\nu(1,2) = 0, \rho(1,2) = -3/2$ (blue).

Case 3. Mixed self/interaction-dynamics (Fig. 13g-i). We now incorporate a mixture of both self and link-dynamics, *i.e.* $S = L = 2$. This leads to $\mu(1) = 0$ (blue) and $\mu(2) = 1/2$ (red); $\nu(s,l) = 0$ for all s,l; and $\rho(1,1) = -2$ (red), $\rho(1,2) = -3$ (blue), $\rho(2,1) = -1$ (green), $\rho(2,2) = -3/2$ (orange).

Case 4. Mixed self/interaction-dynamics (Fig. 13j-l). To increase the challenge we consider $M_0^{\{a\}}(x_i) = -f_i x_i^a$ and $M_2^{\{h\}}(x_j) = x_j^h/(1 + x_j^h)$ for $a, h = 1, 2, 3$. This represents a mixture of three independently distributed self and interaction dynamics, 9 combinations altogether. We predict three coexisting exponents $\mu(s)$ and seven (distinct) coexisting $\rho(s',l)$, all fully corroborated in Fig. 13k,l.

5.5 Distributed powers - testing Assumption 1

Another potential generalization of Assumption 1 is to have the powers Γ_{qn} in the expansion (1.2) of $M_q(x)$ drawn from a continuous distribution. When this is the case, our analysis captures the scaling patterns extracted from the *average* powers. This naturally prompts us to test its robustness against potential power-variability. To examine this we consider Regulatory dynamics of the form of Eq. (4.15), only this time we extract the powers a, characterizing the nodes, and h, characterizing the links, from a continuous distribution. Specifically, we use $h \sim U(10^{-3}, 3)$, a uniform distribution ranging from $h = 10^{-3}$ to $h = 3$; we set the bottom limit just slightly above zero to ensure no link has $h = 0$, a limit in which $M_2(x)$ becomes independent of x. This sets the average link-dynamics at $\langle h \rangle = 1.5$ with a standard deviation of $\sigma_h \approx 0.87$.

For the self-dynamic power a we examine three scenarios ● Low variability, where $a \sim U(1.8, 2.2)$ ● Medium variability, where $a \sim U(1.5, 2.5)$ ● High variability, where $a \sim U(1, 3)$. In all three cases we have $\langle a \rangle = 2$, but with a gradually increasing standard deviation $\sigma_a = 0.11, 0.30$ and 0.60 across the different settings.

Using the analysis of Sec. 4.2 we extract the Jacobian scaling from the average powers, writing
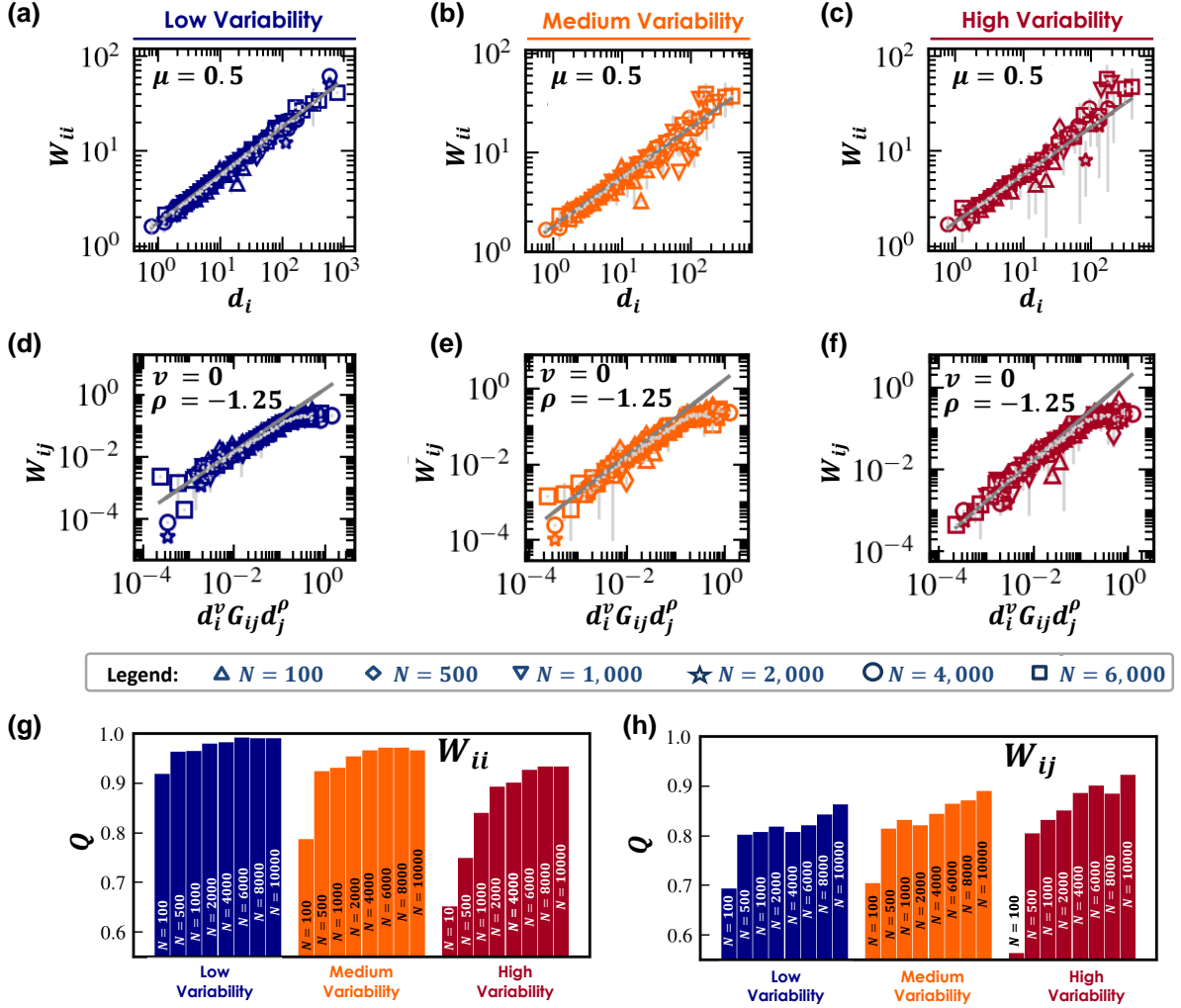
Figure 14: **Our Jacobian scaling patterns under distributed powers**. (a)-(c) The diagonal weights W_{ii} vs. d_i as obtained from Regulatory dynamics on networks of size $N = 100, \ldots, 6,000$ (symbols) under distributed a, h. The data is well-approximated by our analytically predicted scaling $\mu = 0.5$ (grey), which is extracted from $\langle a \rangle, \langle h \rangle$. We implemented three scenarios - low (blue), medium (orange) and high (red) variability. Here the data are logarithmically binned (Sec. 7.3), and the error bars (grey) capture the noise within each bin. As expected under high variability we observe higher noise levels. (d)-(f) Similar results for the off-diagonal weights W_{ij}. (g)-(h) The quality of the linear fit Q for W_{ii} and W_{ij}, as obtained from networks of size $N = 10^2, \ldots, 10^4$, under the three variability levels (low - blue; medium - orange; high - red). As the system size N is increased the quality of the predicted scaling is improved, indicating that our analysis is asymptotically robust against power variability. Each panel includes results from networks of size $N = 100, 500, 1,000, 2,000, 4,000$ and $6,000$ nodes with $\langle k \rangle = 6$. In panels a-f we divided all nodes/links into logarithmic bins $\mathbb{B}(b), b = 1, \ldots, B$ (Supplementary Sec. 7.3). The number of node bins ranges from $B = 10$ for the smallest network to $B = 24$ for the largest. For the links the range is $B = 12$ to 26. Therefore, the sample size within each bin is $|\mathbb{B}(b)| \in (50, 250)$ for nodes and $|\mathbb{B}(b)| \in (250, 1,400)$ for links. The error bars represent 95% confidence intervals within each bin.

$$\mu = \frac{\langle a \rangle - 1}{\langle a \rangle} = 0.5; \quad \nu = 0; \quad \rho = -\frac{\langle h \rangle + 1}{\langle a \rangle} = -1.25. \tag{5.25}$$

In Fig. 14 we display the numerically obtained Jacobian weights, W_{ii} and W_{ij}, finding that, indeed, they can be well approximated by our predicted scaling with the averaged exponents in (5.25). Under low variability (blue) the plots are rather clean, as expected, and as we increase the variability (orange, red) we observe increasing levels of noise, expressed via the growing error bars (grey), that are designed to quantify the scaling uncertainty.

50

In our analysis, we examined networks with $N = 100$ to $N = 6{,}000$ nodes (symbols, Fig. 14 legend). As we increase the network size we observe a convergence to the mean. This means that the confounding effect of the a, h variability is exacerbated by finite size, and as we approach the asymptotic limit $N \to \infty$, our analysis becomes robust against such variability in the powers.

To systematically quantify this asymptotic convergence we used the mean-square-error R^2 to assess the deviation between the observed numerical results and our theoretically predicted scaling. To understand this, consider our scaling predictions, taking the form $Y \sim X^\alpha$. They can be expressed in log-space as linear functions, namely $y = \alpha x + \beta$ where $y = \log Y$ and $x = \log X$. Here the slope α captures the exponential scaling, which we *predict*, and hence treat as fixed. The constant β, on the other hand, can be set arbitrarily. Upon measuring y we obtain N data-points (x_i, y_i), $i = 1, \ldots, N$, which we fit to a linear function with our fixed slope α, then select β to attain the best fit, *i.e.* minimizing R^2. The quality of the resulting fit is then captured by $Q = 1 - R^2$, such that $Q \to 0$ represents a failed fitting and $Q \to 1$ is a perfect fit. In Fig. 14g,h we show Q vs. N, finding that, indeed, the greater is N the better is the quality of our analytical prediction in (5.25). Hence, for a sufficiently large network, our results are robust against such deviations from Assumption 1, conforming to the average powers *a là* Eq. (5.25).

Taken together, Secs. 5.1 - 5.5 exemplify that real-world Jacobians, under rather broad conditions, follow the scaling patterns predicted for $\mathbb{E}(A, G, \Omega)$. We wish to emphasize that we do not claim that this ensemble covers *all* network dynamics, as indeed, these sections provide just a few anecdotal examples beyond the coverage of our original Eq. (1.1) under Assumptions 1-6. Still, these examples do indicate the potential merit in further studying this Jacobian ensemble and its relevance to a potentially vast range of real-world dynamic applications.

6   Local vs. global stability

Our asymptotically stable class ($S < 0$) represents a robust stability, that remains unaffected by microscopic discrepancies, such as parameter or topological perturbations. But what if we explicitly form an unstable motif and introduce it *brute force* into the network. Can such a local intervention destabilize the system? Here, we demonstrate that an asymptotically stable system remains insensitive to such local instabilities, whose impact on the network becomes negligible as $N \to \infty$.

To examine this we implemented Population 1 dynamics, as in (4.39), on a scale-free network of size N. We denote this system by P_N. We also constructed a two node exclusion motif P_2, whose dynamics is given by

$$
\begin{aligned}
\frac{\mathrm{d}y_1}{\mathrm{d}t} &= y_1(1 - y_1) - gy_1y_2 \\
\frac{\mathrm{d}y_2}{\mathrm{d}t} &= y_2(1 - y_2) - gy_1y_2.
\end{aligned}
\tag{6.1}
$$

The motif P_2 exhibits three fixed-points: two stable *exclusion* states, in which only one of the species survives, *i.e.* $y_1 > 0$ *or* $y_2 > 0$, and a single unstable *coexisting* state, in which both $y_1 = y_2 > 0$. We now directionally couple $P_2 \to P_N$, by adding the terms $\cdots + Cy_1$ and $\cdots + Cy_2$ to the equations of two randomly selected nodes in P_N. Under such coupling the activities y_1, y_2
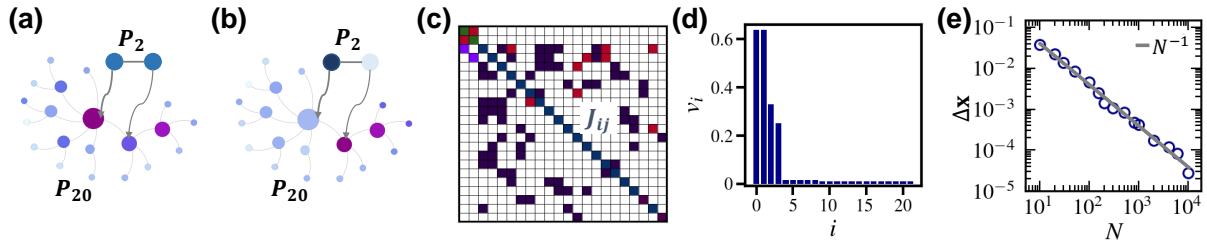
Figure 15: **Local vs. global instability**. (a) The system P_N (here $N = 20$), an asymptotically stable network of N nodes is coupled with P_2 of Eq. (6.1), an exclusion motif, set at the unstable coexisting state $y_1 = y_2 > 0$. The global state of the two systems together is denoted by $\mathbf{x}_0$. (b) Following perturbation P_2 transitions to the exclusion state, thus affecting its neighboring nodes in P_N. The system settles at the new state $\mathbf{x}_1$. Therefore, in principle, $\mathbf{x}_0$ is unstable. This indicates that a microscopic intervention, here coupling $P_2 \to P_N$, can destabilize an otherwise asymptotically unstable system. (c) The Jacobian J, as obtained from the coupled $P_2 \to P_N$ system. The nodes in P_2 are represented by the entries at the top-left corner (red, green), and their immediate neighborhood directly below (purple). (d) The principal eigenvector entries v_i are highly localized around P_2 ($i = 1, 2$) and its immediate neighborhood ($i = 3, 4, 5$). Therefore, the instability of $\mathbf{x}_0$ is strictly localized and has no discernible effect on the majority of the nodes. (e) The global response $\Delta\mathbf{x}$ vs. the size of P_N (circles). Indeed, $\Delta\mathbf{x} \to 0$, scaling with N^{-1} (grey solid line). This asserts P_N's asymptotic stability.

of P_2 affect the state of P_N, but not vice versa, as no coupling exists in the opposite direction. Hence, P_2's fixed-points remain unaffected by this coupling.

We next set P_2 at its unstable coexisting state and allow the coupled system $P_2 \to P_N$ to reach its global fixed-point $\mathbf{x}_0$. This state $\mathbf{x}_0$, the fixed-point of the $N+2$ nodes of P_N and P_2 combined is, by definition, unstable. Indeed, even the slightest perturbation to y_1 or y_2 will drive P_2 into its exclusion state. Then, through the coupling C this change in state of P_2 will spillover to affect the activities of the nodes in P_N, driving them towards a new state $\mathbf{x}_1$. Consequently, while the original P_N had an asymptotically stable $\mathbf{x}_0$ state, the coupling with P_2, a microscopic perturbation, caused it to no longer be stable. To demonstrate this, we extracted J from the complete $N + 2$ node system, and, as expected, found that the principal eigenvalue λ is, indeed, positive (Fig. 15c).

The crucial point is that $\mathbf{x}_0$'s instability remains strictly local. To observe this we examine the principal eigenvector $\mathbf{v}$, associated with λ. In Fig. 15d we observe that $\mathbf{v}$ is highly localized, with most its mass condensed on P_2, and a small fraction on the nearby nodes of P_N, directly neighboring P_2. Therefore, while $\mathbf{x}_0$ is, indeed, unstable, the final state $\mathbf{x}_1$ reached by the system is, for the most part, identical to $\mathbf{x}_0$, barring a localized discrepancy on P_2 and its immediate vicinity. For a sufficiently large system, such local instability, becomes asymptotically negligible.

To observe this we measure the global response

$$\Delta\mathbf{x} = \frac{1}{N} \sum_{j=1}^{N} |x_{1j} - x_{0j}|, \tag{6.2}$$

capturing the average long-term shift in the state of all nodes, as a result of the perturbation to $\mathbf{x}_0$. Obtaining $\Delta\mathbf{x}$ from networks P_N of different size, ranging from $N = 10$ to $N = 10^4$ we observe that $\Delta\mathbf{x} \sim N^{-1}$, approaching $\Delta\mathbf{x} \to 0$ in the limit $N \to \infty$. Under these conditions $\mathbf{x}_0$, our initial *unstable* state, is asymptotically identical to $\mathbf{x}_1$, the system's perturbed state. Therefore, if $\mathbf{x}_0 \to \mathbf{x}_1$, we can say that x_0 it *is* stable, as it is robust against perturbation. This captures precisely the local nature of the instability, as it remains confined to a bounded neighborhood around P_2, and hence, when averaged over the entire system vanishes as $1/N$.

More broadly, it demonstrates the notion of asymptotic stability, that under $N \to \infty$ the system becomes insensitive to perturbation, here withstanding the forced coupling with the unstable motif P_2.

7   Methods and data analysis

7.1   Numerical integration

To numerically test our predictions we constructed Eq. (1.1) for each of the systems in Sec. 4, using the appropriate network A, G (Scale-free, Erdős-Rényi, empirical, etc.). We then used a fourth-order Runge-Kutta stepper (Matlab's ode45) to numerically solve the resulting equations. Starting from an arbitrary initial condition $x_i(t = 0)$, $i = 1, \ldots, N$, we allowed the system to reach steady-state by waiting for $\dot{x}_i \to 0$. To numerically realize this limit we implemented the termination condition

$$\max_{i=1}^{N} \left| \frac{x_i(t_n) - x_i(t_{n-1})}{x_i(t_n)\Delta t_n} \right| < \varepsilon, \tag{7.1}$$

where t_n is the time stamp of the nth Runge-Kutta step and $\Delta t_n = t_n - t_{n-1}$. As the system approaches a steady-state, the activities $x_i(t_n)$ become almost independent of time, and the numerical derivative $\dot{x}_i = (x_i(t_n) - x_i(t_{n-1}))/\Delta t_n$ becomes small compared to $x_i(t_n)$. The condition (7.1) guarantees that the maximum of $\dot{x}_i/x_i$ over all activities $x_i(t_n)$ is smaller than the pre-defined termination variable ε. In our simulations, across the different dynamics we tested, we set $\varepsilon \le 10^{-12}$, a rather strict condition, to ensure that our system is sufficiently close to the *true* steady-state.

7.1.1   Numerical analysis of Power dynamics

To analyze Power dynamics we used the Newton-Raphson method to extract the roots of

$$0 = f_i + g \sum_{j=1}^{N} A_{ij} G_{ij} \sin\left(x_j(t) - x_i(t)\right), \tag{7.2}$$

providing the fixed-point of (5.1), under $\ddot{x}_i = \dot{x}_i = 0$. For a system with n_{gen} generators and n_{load} loads, we set $f_i = -1$ for load nodes and $f_i = n_{\text{load}}/n_{\text{gen}}$ for generators. This ensures a global balance of power generation vs. demand. The global weight was set to $g = 1$, and the link weights were also set uniformly to $G_{ij} = 1$, *i.e.* a binary network. In our empirical power-networks (Sec. 7.4) the number of loads n_{load} vs. generators n_{gen} is specified in the data. For the model networks we used a balanced network with 50% generators and 50% loads, assigned at random. As our initial condition we extracted x_i from a uniform distribution, seeking a starting point from which the system converges to a fully positive solution. This was satisfied for $x_i \sim U(0.8, 1.5)$ for the model networks and for $x_i \sim U(3.5, 4.5)$ for the empirical ones. Using the obtained roots $\mathbf{x} = (x_1, \ldots, x_N)^{\top}$ we constructed the relevant Jacobian matrix as explained below in Sec. 7.2.

7.2 Numerically estimating J

Once the steady state $\mathbf{x} = (x_1, \ldots, x_N)^\top$ is reached we construct the *numerical* Jacobian by substituting the numerically obtained states x_i into (2.11) and (2.51). This represents the system's *actual* stability matrix, as obtained for each dynamics on its relevant networks. For example, consider our Epidemic model in Eq. (4.3), where $M_0(x) = -f_i x_i$, $M_1(x_i) = 1 - x_i$ and $M_2(x) = x_j$, and hence $M_0'(x) = -f_i$, $M_1' = -1$ and $M_2' = 1$. Once we obtain $\mathbf{x}$ we introduce all numerically calculated x_i into W_{ii} and W_{ij}, which for Epidemic take the form

$$W_{ii} = -f - g \sum_{j=1}^{N} A_{ij} G_{ij} x_j \tag{7.3}$$

and

$$W_{ij} = g A_{ij} G_{ij} (1 - x_i). \tag{7.4}$$

This construction, directly from the numerically obtained fixed-point $\mathbf{x}^*$ is *exact*, incorporating all the potential confounding factors of the specific system, from the fine-structure and potential degree-correlations in A, to the random distribution of $\mathbf{f}_{qi}$ and G_{ij}, or the varying interaction strength g. In Fig. 3 of the main text we compare the scaling of these numerically estimated W_{ii} and W_{ij} vs. the theoretically predicted ensemble $\mathbb{E}(A, G, \Omega)$, as provided by (2.69) and (2.70).

7.3 Logarithmic binning

Our main theoretical prediction focuses on scaling relationships, such as $W(d) \sim d^\mu$, which we observe by their linear slope in a log-log plot (*e.g.*, Fig. 3 of main text). To construct such plots we employed logarithmic binning[18]. First we divide all nodes into B bins

$$\mathbb{B}(b) = \left\{ i \in \{1, \ldots, N\} \,\middle|\, c^{b-1} < \frac{d_i}{d_{\min}} \leq c^b \right\}, \tag{7.5}$$

where $b = 1, \ldots, B$, c is a constant and $d_{\min} = \min_{i=1}^{N} d_i$ is the minimal weighted degree in $A \otimes G$. In (7.5) the bth bin includes all nodes i whose weighted degree d_i is between $d_{\min} c^{b-1}$ and $d_{\min} c^b$. The parameter c is selected such that the unity of all bins $\cup_{b=1}^{B} \mathbb{B}(b)$ includes all nodes, hence we set $c^B = d_{\max}/d_{\min}$. Therefore, the first bin $b = 1$ is bounded from below by $d_{\min}$, and the final bin bounded from above by $d_{\max}$. Dividing the nodes according to (7.5) generates exponentially growing bins in d_i, which are *linear* in $\log d_i$, allowing to naturally observe the scaling in the logarithmic plots.

After dividing all nodes into bins, we plot the average degree of the nodes in each bin

$$d_b = \langle d_i \rangle_{i \in \mathbb{B}(b)} = \frac{1}{|\mathbb{B}(b)|} \sum_{i \in \mathbb{B}(b)} d_i \tag{7.6}$$

versus the average $W(d)$ term of nodes in that bin

$$W(d_b) = \langle W_{ii} \rangle_{i \in \mathbb{B}(b)} = \frac{1}{|\mathbb{B}(b)|} \sum_{i \in \mathbb{B}(b)} W_{ii}. \tag{7.7}$$

In a similar fashion we plot $W_{ij} \sim d_i^\nu G_{ij} d_j^\rho$, this time applying the binning to $W_{ij}^{\text{Theory}} = d_i^\nu G_{ij} d_j^\rho$, instead of to d_i. Therefore, the bins are defined as

$$\mathbb{B}(b) = \left\{ (i,j) \big| A_{ij} = 1, c^{b-1} < \frac{W_{ij}^{\text{Theory}}}{W_{\min}} \leq c^b \right\}, \tag{7.8}$$

such that in each bin we include all node pairs whose product $d_i^\nu G_{ij} d_j^\rho$ is within a given range. Similarly to (7.5) we set $W_{\min} = \min(W_{ij}^{\text{Theory}})$, and select c such that the entire range of W_{ij}^{Theory} is covered. As above, we then plot the average *real* W_{ij} in each bin vs. the theoretically predicted W_{ij}^{Theory}. Specifically, these averages take the form

$$W^{\text{Real}}(b) = \langle W_{ij} \rangle_{(i,j) \in \mathbb{B}(b)} = \frac{1}{|\mathbb{B}(b)|} \sum_{(i,j) \in \mathbb{B}(b)} W_{ij} \tag{7.9}$$

$$W^{\text{Theory}}(b) = \langle d_i^\nu G_{ij} d_j^\rho \rangle_{(i,j) \in \mathbb{B}(b)} = \frac{1}{|\mathbb{B}(b)|} \sum_{(i,j) \in \mathbb{B}(b)} W_{ij}^{\text{Theory}}, \tag{7.10}$$

where W_{ij} in (7.9) is constructed via Sec. 7.2.

7.4   Model and empirical networks

To test our predictions we used model and empirical networks, as summarized below:

ER. An Erdős-Rényi random network with $N = 6,000$ nodes and an average degree of $\langle k \rangle = 6$. Weights were added using $G_{ij} \sim \mathcal{N}(1.0, 0.1)$, a normal distribution function with mean $\mu = 1.0$ and variance $\sigma^2 = 0.1$. Note that this weight distribution allows for a small number of negative weights, hence, in practice, it test out predictions under a coexistence of a majority positive along side a small minority of negative links.

SF. A binary scale-free network with $N = 6,000$ nodes, average degree $\langle k \rangle = 6$, and degree distribution following $P(k) \sim k^{-\gamma}$ with $\gamma = 2.5$. Under this distribution we have $d_{\text{nn}} \sim N^\beta$ with $\beta = 0.6$, allowing us to examine our asymptotic limits (which require $\beta > 0$).

SF1. Using the underlying topology of SF we added weights G_{ij}, extracted from a normal distribution with mean $\mu = 1.0$ and variance $\sigma^2 = 0.1$, *i.e.* $G_{ij} \sim \mathcal{N}(1.0, 0.1)$. Also here we did not limit the weights from becoming negative.

SF2. Using the underlying topology of SF we added weights G_{ij}, from a scale-free probability density function $P(G) \sim G^{-\alpha}$ with $\alpha = 3$. Hence, SF2 represents an extremely heterogeneous network, featuring both scale-free topology and scale-free weights.

UCIonline. An instant messaging network from the University of California Irvine [19], capturing $61,040$ transactions between $1,893$ users during a $T = 218$ day period. Connecting all individuals who exchanged messages throughout the period, we obtain a network of $1,893$ nodes with $27,670$ links, exhibiting a fat-tailed degree distribution. Here weights G_{ij} are taken from a scale-free probability density function $P(G) \sim G^{-\alpha}$ with $\alpha = 3$, once again examining conditions of extreme heterogeneity.

Email Epoch. This dataset monitors $\sim 3 \times 10^5$ emails exchanged between $3,185$ individuals over the course of ~ 6 months [20], giving rise to a scale-free social network with $31,885$ binary links. Here too weights G_{ij} were extracted from a scale-free probability density function $P(G) \sim G^{-\alpha}$

Epidemic	$\mathbf{f}_i = \{f_i\}$	$f_i \sim \mathcal{N}(\mu, \sigma^2), \mu = 1.0, \sigma^2 = 0.1, f_i \geq 0.1$	
Regulatory	$\mathbf{f}_i = \{f_i\}$	$f_i \sim \mathcal{N}(\mu, \sigma^2), \mu = 1.0, \sigma^2 = 0.1, f_i \geq 0.1$	
Population 1	$\mathbf{f}_i = \{b_i, c_i\}$	$b_i = 1, c_i \sim \mathcal{N}(\mu, \sigma^2), \mu = 1.0, \sigma^2 = 0.1, c_i \geq 0.1$	
Biochemical	$\mathbf{f}_i = \{f_i, b_i\}$	$f_i, b_i \sim \mathcal{N}(\mu, \sigma^2), \mu = 1.0, \sigma^2 = 0.1, f_i, b_i \geq 0.1$	
Inhibitory	$\mathbf{f}_i = \{f_i, b_i\}$	$b_i \sim \mathcal{N}(\mu, \sigma^2), \mu = 1.0, \sigma^2 = 0.1, b_i \geq 0.1, f_i = 2b_i$	
Power	$\mathbf{f}_i = \{f_i, b_i\}$	$f_i = \begin{cases} -1 & \text{For consumers} \\ \dfrac{n_{\text{load}}}{n_{\text{gen}}} & \text{For generators} \end{cases}, \quad b_i = 1$	
Population 2	$\mathbf{f}_i = \{b_i, c_i\}$	$b_i = 1, c_i \sim \mathcal{N}(\mu, \sigma^2), \mu = 1.0, \sigma^2 = 0.1, c_i \geq 0.1$	

Table 3: **Model parameters**. For each of our dynamic models we summarize the dynamic parameters used in our simulations. For example, in Epidemic the recovery rate was extracted from a truncated normal distribution with mean $\mu = 1.0$ and variance $\sigma^2 = 0.1$. To avoid the irrelevant scenraio of a negative recovery rate we truncated this distribution at $f_i \geq 0.1$. Biochemical, Inhibitory and Power have two parameters $\mathbf{f}_i = (f_i, b_i)$. In Inhibitory the Alee effect required $f_i > b_i$ for all species. To ensure this we extracted b_i from a truncated normal distribution, then set $f_i = 2b_i$. In Power the loads were set to -1 for consumer nodes, then the generation was gauged to ensure a balanced network.

with $\alpha = 3$.

PPI1. The yeast scale-free protein-protein interaction network, consisting of $1,647$ nodes (proteins) and $5,036$ undirected links, representing chemical interactions between proteins [21]. Weights were assigned via $G_{ij} \sim \mathcal{N}(1.0, 0.1)$.

PPI2. The human protein-protein interaction network, a scale-free network, consisting of $N = 2,035$ nodes (proteins) and $L = 13,806$ protein-protein interaction links [22]. Here too, weights were assigned via $G_{ij} \sim \mathcal{N}(1.0, 0.1)$.

Microbial 1. To construct microbial networks we collected data on 844 microbial species and 283 associated metabolites [23]. This allowed us to construct an 844×283 directed bipartite network B whose links capture the production and consumption of metabolites among the microbial species: $B_{im} = 1$ if species i *produces* metabolite m; $B_{mi} = 1$ if species i *consumes* metabolite m $(i = 1, \dots, 844; m = 1, \dots, 283)$. We then used

$$K_{ij} = \frac{\sum_{m=1}^{283} B_{mi} B_{mj}}{\sum_{m=1}^{283} B_{mi}} \tag{7.11}$$

to construct a weighted directed complemnetarity network. In this network the links connect species that compete over the same metabolites. The link weights capture the strength of the competition, quantifying the fraction of i's consumed matebolites (denominator) over which it must compete with j (numerator). The resulting K has a small fraction of isolated species, hence we consider only its giant connected components, which includes $N = 737$ microbial species linked through $L = 113,350$ competitive interactions.

Microbial 2. Using B above we now construct a mutualistic network via

$$K_{ij} = \frac{\sum_{m=1}^{283} B_{jm}B_{mi}}{\sum_{m=1}^{283} B_{mi}}, \qquad (7.12)$$

now describing the fraction of i's total consumption (denominator) that is produced by j (numerator). Here, the connected component remains with $N = 496$ nodes and $L = 43,964$ links.

The two networks are of different nature: Microbial 1 is adversarial, relevant *e.g.*, for Inhibitory, while Microbial 2 is cooperative, naturally fitting our Population 1/2 dynamics. Still, for the purpose of examining our theoretical predictions, and mainly for confronting them with empirically observed networks, we applied our Population 1/2 dynamics on both Microbial 1 and 2, despite the fact that the former, is, perhaps, less relevant.

Power 1. Mapping a segment from the power network of Great Britain, consisting of $N = 2,224$ nodes and $L = 2,804$ links. The nodes are split into 394 generators and 1,830 consumer loads. The network data can be downloaded from *http://www.nationalgrid.com*

Power 2. A segment of the Polish power network, typically referred to as "case2383"[24–26]. The network has $N = 2,383$ nodes, 327 of which are generators and the remaining 2,056 are consumer loads. These loads and generators are linked through $L = 2,886$ transmission lines. This data can be downloaded from *roman.korabat@polsl.pl*.

References

[1] M.E.J. Newman. *Networks - an introduction.* Oxford University Press, New York, 2010.

[2] J. Gao, B. Barzel and A.-L. Barabási. Universal resilience patterns in complex networks. *Nature*, 530:307–312, 2016.

[3] G. Caldarelli. *Scale-free networks: complex webs in nature and technology.* Oxfrod University Press, New York, 2007.

[4] S. Boccaletti, V. Latora, Y. Moreno, M. Chavez and D.-U. Hwang. Complex networks: Structure and dynamics. *Physics Reports*, 424:175–308, 2006.

[5] L. Schmetterer and K. Sigmund (Eds.). *Hans Hahn Gesammelte Abhandlungen Band 1/Hans Hahn Collected Works Volume 1.* Springer, Vienna, Austria, 1995.

[6] R. Pastor-Satorras and A. Vespignani. Epidemic spreading in scale-free networks. *Phys. Rev. Lett.*, 86:3200–3203, 2001.

[7] H.I. Schreier, Y. Soen and N. Brenner. Exploratory adaptation in large random networks. *Nature Communications*, 8:14826, 2017.

[8] R.M. May. Will a large complex system be stable? *Nature*, 238:413 – 414, 1972.

[9] R. Pastor-Satorras, C. Castellano, P. Van Mieghem and A. Vespignani. Epidemic processes in complex networks. *Rev. Mod. Phys.*, 87:925–958, 2015.

[10] P.S. Dodds and D.J. Watts. A generalized model of social and biological contagion. *Journal of Theoretical Biology*, 232:587–604, 2005.

[11] G. Karlebach and R. Shamir. Modelling and analysis of gene regulatory networks. *Nature Reviews*, 9:770–780, 2008.

[12] B. Barzel and O. Biham. Binomial moment equations for stochastic reaction systems. *Phys. Rev. Lett.*, 106:150602–5, 2011.

[13] C.S. Holling. Some characteristics of simple types of predation and parasitism. *The Canadian Entomologist*, 91:385–398, 1959.

[14] E.O. Voit. *Computational Analysis of Biochemical Systems.* Cambridge University Press, New York, NY, 2000.

[15] D. Wodarz, J.P. Christensen and A.R. Thomsen. The importance of lytic and nonlytic immune responses in viral infections. *Trends in Immunology*, 23:194–200, 2002.

[16] W.C. Allee and E.S. Bowen. Studies in animal aggregations: Mass protection against colloidal silver among goldfishes. *Journal of Experimental Zoology*, 61:185–207, 1932.

[17] G. Filatrella, A. Nielsen and N. Pedersen. Analysis of a power grid using a Kuramoto-like model. *Eur. Phys. J. B*, 61:485–491, 2008.

[18] S. Milojević. Power-law distributions in information science: making the case for logarithmic binning. *Journal of the American Society for Information Science and Technology*, 61:2417–2425, 2010.

[19] T. Opsahl and P. Panzarasa. Clustering in weighted networks. *Social Networks*, 31:155–163, 2009.

[20] J.-P. Eckmann, E. Moses and D. Sergi. Entropy of dialogues creates coherent structures in e-mail traffic. *Proc. Natl. Acad. Sci. USA*, 101:14333–7, 2004.

[21] H. Yu *et al.* High-quality binary protein interaction map of the yeast interactome network. *Science*, 322:104–110, 2008.

[22] J.F. Rual *et al.* Towards a proteome-scale map of the human protein-–protein interaction network. *Nature*, 437:1173–1178, 2005.

[23] R. Lim, J.J.T. Cabatbat, T.L.P. Martin, H. Kim, S. Kim, J. Sung, C.-M. Ghim and P.-J. Kim. Large-scale metabolic interaction network of the mouse and human gut microbiota. *Scientific Data*, 7:1–8, 2020.

[24] R.D. Zimmerman, C.E. Murillo-Sánchez and R.J. Thomas. MATPOWER: Steady-state operations, planning, and analysis tools for power systems research and education. *IEEE Transactions on power systems*, 26:12–19, 2010.

[25] A.E. Motter, S.A. Myers, M. Anghel and T. Nishikawa. Spontaneous synchrony in power-grid networks. *Nature Physics*, 9:191–197, 2013.

[26] T. Nishikawa and A.E. Motter. Comparative analysis of existing models for power-grid synchronization. *New Journal of Physics*, 17:015012, 2015.